

# Geochronology of gneisses adjacent to the Mylonite Zone in southwestern Sweden: evidence of a tectonic window?

***James Davies***

Dissertations in Geology at Lund University,  
Master's thesis, no 584  
(45 hp/ECTS credits)

---



Department of Geology  
Lund University  
2020



# **Geochronology of gneisses adjacent to the Mylonite Zone in southwestern Sweden: evidence of a tectonic window?**

Master thesis  
James Davies

Department of Geology  
Lund University  
2020

# Contents

<b>1 Introduction</b> .....	<b>7</b>
<b>2 Geological setting</b> .....	<b>9</b>
2.1 The geology of southwestern Sweden	9
2.1.1 The Sveconorwegian Province	9
2.1.1.1 The Eastern Segment	10
2.1.1.2 The Mylonite Zone	10
2.1.1.3 Idefjorden terrane	11
2.2 'B-Bulan'	12
<b>3 Fieldwork and methodology</b> .....	<b>12</b>
3.1 Field area	12
3.2 Field methods	16
3.3 Preparation	16
3.3.1 Zircon separation	16
3.3.2 SEM analysis	16
3.3.3 Why zircon?	16
3.4 U-Pb dating	17
3.4.1 LA-ICP-MS	17
3.4.2 Why LA-ICP-MS?	17
3.5 Data processing and quality control	17
3.5.1 Quality control—91500	19
3.5.2 Error expansion	20
3.5.3 Pb correction	20
3.5.4 Discordance filtering	20
3.5.5 Pb-Pb vs U-Pb	20
<b>4 Samples and results</b> .....	<b>21</b>
4.1 Sample analyses	21
4.1.1 Sample 4.5a-i: 'Brobacka' (N57°58.840', E012°26.142')	21
4.1.2 Sample 2.5j-i (N57°58.759', E012°25.035')	21
4.1.3 Sample 2.5j-iv (N57°58.759', E012°25.035')	21
4.1.4 Sample 4f-i (N57°59.579', E012°22.793')	21
4.1.5 Sample 4g-i (N57°59.568', E012°22.796')	24
4.1.6 Sample 3m-ii (N57°59.420', E012°22.776')	24
4.1.7 Sample 3b-i (N57°58.711', E012°21.858')	24
4.1.8 Sample 3a-v (N57°58.703', E012°21.843')	24
4.1.9 Sample 3a-iii (N57°58.703', E012°21.843')	25
4.1.10 Sample 3a-i (N57°58.703', E012°21.843')	25
4.2 Summary of results	28
<b>5 Discussion</b> .....	<b>38</b>
5.1 Validity of the results	38
5.2 Interpretation of the results	38
5.3 A window into the Eastern Segment?	41
5.4 Evidence of a common pre-Sveconorwegian history?	41
<b>6 Conclusions</b> .....	<b>41</b>
<b>7 Future studies</b> .....	<b>41</b>
<b>Acknowledgements</b> .....	<b>42</b>
<b>References</b> .....	<b>42</b>
<b>Appendix</b> .....	<b>46</b>

**Cover Picture:** A view of the Ålandasjön, close to Brobacka Nature Reserve, taken from location 2.5a. Picture credit: James Davies.

# Geochronology of gneisses adjacent to the Mylonite Zone in southwestern Sweden: evidence of a tectonic window?

JAMES DAVIES

Davies, J.R., 2020: Geochronology of gneisses adjacent to the Mylonite Zone in SW Sweden: evidence of a tectonic window?. Dissertations in Geology at Lund University, No. 584, 59 pp. 45 hp (45 ECTS credits).

**Abstract:** The relationship between the Eastern Segment and Idefjorden terrane prior to the Sveconorwegian orogeny has long been debated. Evidence of a common history is minimal and localised; at the same time, the notion that the Sveconorwegian orogeny formed as a result of a collisional event is also disputed. In this thesis, I analyse a region of the Idefjorden terrane, colloquially known as 'B-Bulan', close to the boundary with the Eastern Segment, which shows evidence of Eastern Segment-age (1.81-1.65 Ga) signatures and possibly Hallandian-age (1.47-1.38 Ga) signatures previously unseen in the Idefjorden terrane. Ages were determined using U-Pb spot dating of zircon using Laser Ablation Inductively-Coupled Mass Spectrometry (LA-ICP-MS). The  $^{207}\text{Pb}/^{206}\text{Pb}$  ages of samples analysed shows the presence of Idefjorden and Eastern Segment signatures, as well as a potential Hallandian signature in a small number of samples. Idefjorden signatures are recorded in three samples at three locations (4f-i, 4g-i and 3m-ii). They show weighted mean  $^{207}\text{Pb}/^{206}\text{Pb}$  ages of  $1625 \pm 5$  Ma (4f-i),  $1603 \pm 4$  Ma (4g-i) and  $1641 \pm 11$  Ma (3m-ii). Eastern Segment protolith ages are recorded in five samples at two locations (2.5j and 3a). At location 3a, samples show weighted mean  $^{207}\text{Pb}/^{206}\text{Pb}$  ages of  $1693 \pm 12$  Ma (3a-v),  $1692 \pm 3$  Ma (3a-iii) and  $1705 \pm 3$  Ma (3a-i). At location 2.5j, zircon populations of Eastern Segment age are observed between 1850 and 1650 Ma (2.5j-i) and around 1685 Ma (2.5j-iv). Both samples show multiple zircon populations (including Hallandian signatures) and complex field relationships which require closer examination. This study shows the presence of Eastern Segment-aged units and Hallandian signatures within B-Bulan, further west than previously acknowledged.

**Keywords:** Geochronology, Hallandian orogeny, Mylonite Zone, Sveconorwegian orogeny, U-Pb, Idefjorden terrane, Eastern Segment, B-Bulan, Brobacka

**Supervisor(s):** Anders Scherstén

**Subject:** Bedrock Geology

*James Davies, Department of Geology, Lund University, Sölvegatan 12, SE-223 62 Lund, Sweden.  
Email: jamesdavies010@hotmail.co.uk*

# Åldersdatering av gnejser längs Mylonitzonen i sydvästra Sverige: bevis på ett tektoniskt fönster?

JAMES DAVIES

Davies, J.R., 2020: Geokronologi av gnejser intill Mylonitzonen i sydvästra Sverige: bevis på ett tektoniskt fönster? *Examensarbeten i geologi vid Lunds universitet*, Nr. 584, 59 sid. 45 hp.

**Sammanfattning:** Förhållandet mellan Östra Segmentet och Idefjorden terrane före Sveconorwegian orogeny har länge diskuterats. Bevis på en gemensam historia är minimal och lokaliserad; samtidigt bestrider man också tanken på att Sveconorwegian orogeny bildades till följd av en kollisionshändelse. I den här avhandlingen analyserar jag en region i Idefjorden terrane, i allmänhet känd som 'B-Bulan', nära gränsen till det Östra Segmentet, som visar bevis på östliga segmentets ålder (1,81-1,65 Ga) underskrifter och eventuellt Hallandian- ålder (1,47-1,38 Ga) signaturer som tidigare inte har setts i Idefjorden terrane. Åldrarna bestämdes med användning av U-Pb-fläckdatering av zirkon med användning av Laser Ablation induktiv-kopplad massspektrometri (LA-ICP-MS). Åldrarna  $^{207}\text{Pb} / ^{206}\text{Pb}$  för analyserade prover visar närvaron av Idefjorden- och Östra Segmentet-signaturer, samt en potentiell Hallandian-signatur i ett litet antal prover. Idefjorden-signaturer registreras i tre prover på tre platser (4f-i, 4g-i och 3m-ii). De visar viktat medelvärde  $^{207}\text{Pb} / ^{206}\text{Pb}$  i åldrarna  $1625 \pm 5$  Ma (4f-i),  $1603 \pm 4$  Ma (4g-i) och  $1641 \pm 11$  Ma (3m-ii). Protolithåldrar i östra segmentet registreras i fem prover på två platser (2,5j och 3a). På plats 3a visar prover vägat medelvärde  $^{207}\text{Pb} / ^{206}\text{Pb}$  åldrar av  $1693 \pm 12$  Ma (3a-v),  $1692 \pm 3$  Ma (3a-iii) och  $1705 \pm 3$  Ma (3a-i). På plats 2,5j observeras zirkonpopulationer i östra segmentets ålder mellan 1850 och 1650 Ma (2,5j-i) och omkring 1685 Ma (2,5j-iv). Båda proverna visar flera zirkonpopulationer (inklusive hallandiska signaturer) och komplexa fältförhållanden som kräver närmare undersökning. Denna studie visar närvaron av enheter i det östra segmentet och Hallandian-signaturer inom B-Bulan, längre västerut än tidigare erkänt.

**Nyckelord:** Geochronology, Hallandian orogeny, Mylonite Zone, Sveconorwegian orogeny, U-Pb, Idefjorden terrane, Eastern Segment, B-Bulan, Brobacka

**Handledare:** Anders Scherstén

**Ämnesinriktning:** Berggrundsgeologi

*James Davies, Geologiska institutionen, Lunds Universitet, Sölvegatan 12, 223 62 Lund, Sverige.*

*E-post: jamesdavies010@hotmail.co.uk*

# 1 Introduction

The geology of southwestern Sweden is defined by two major lithotectonic units, the Eastern Segment and the Idefjorden terrane, bounded by a major plastic shear zone, the Mylonite Zone. The Eastern Segment and Idefjorden terrane are distinct from each other in a number of ways:

- 1) The **protolith ages** in the southern part of the Eastern Segment are between 1.81 and 1.66 Ga (Söderlund et al. 1999; Söderlund et al. 2002; Möller et al. 2007; Petersson et al. 2013; Möller et al. 2015), with no evidence of younger protoliths, while in the Idefjorden terrane the oldest dated protoliths are the 1.66 Ga Mjösjö dacite and the 1.64 Ga Härsjön gneiss (Schersten et al. 2000; Åhäll & Connelly 2008; Petersson et al. 2015). Protilith ages in the Idefjorden terrane are between 1.66 and 1.52 Ga (Åhäll et al. 1995; Brewer et al. 1998; Schersten et al. 2000; Schersten et al. 2004; Åhäll & Connelly, 2008; Petersson et al. 2015; see Figure 1).
- 2) The **metamorphic grade**, on the whole, is higher in the Eastern Segment, with evidence of localised eclogite-facies metamorphism at 0.97 Ga (Möller et al. 2015) that is not recorded in the Idefjorden terrane. The highest grade of metamorphism recorded in the Idefjorden terrane is granulite facies, immediately west of the Mylonite Zone (Bingen et al. 2008b; Söderlund et al. 2008).
- 3) The **timing of peak metamorphism** in the Idefjorden terrane is recorded in high-pressure amphibolite- to granulite-facies metamorphism between 1.05 and 1.02 Ga (Austin Hegardt et al. 2007; Bingen et al. 2008b; Söderlund et al. 2008), almost 60 million years before the onset of metamorphism in the Eastern Segment. Metamorphism is first recorded in the Eastern Segment at 0.99 Ga and peaks with high-pressure granulite- and eclogite-facies metamorphism at 0.97 Ga (Johansson et al. 1991; Möller 1998; Larson et al. 1999; Möller 1999; Johansson et al. 2001; Andersson et al. 2002; Austin Hegardt 2010; Möller et al. 2015). While the Eastern Segment was undergoing high-pressure metamorphism, the Idefjorden terrane was undergoing low- to mid-amphibolite-facies reworking (Andersson et al. 2002).
- 4) Concrete evidence of **Hallandian metamorphism** is limited to the Eastern Segment. Previous studies, with the exception of Lundqvist et al. (2005), have found no evidence of Hallandian-age (1.47-1.38 Ga; Ulmius et al. 2015) metamorphism west of the Mylonite Zone. Other evidence, such as bimodal magmatism between 1.34 and 1.30 Ga, and older, Gothian-age veining, is not observed east of the Mylonite Zone in the Eastern Segment (Åhäll & Connelly 1998; Austin Hegardt et al. 2007; Åhäll & Connelly 2008).

As Figure 1 shows, evidence of correlation prior to

the onset of the Sveconorwegian orogeny is minimal and localised<sup>1</sup>. Magmatism dated between 1.28 and 1.20 Ga are recorded in the Idefjorden terrane and in the Transscandinavian Igneous Belt (TIB), along and east of the Sveconorwegian Frontal Deformation Zone (SFDZ; the eastern boundary of the Eastern Segment; see Fig 2) (Welin et al. 1981; Persson et al. 1983; Welin & Samuelsson 1987; Söderlund et al. 2005; Åhäll & Connelly 2008; Brander et al. 2012). While the evidence is lacking in the Eastern Segment, it is possible that evidence could have been overprinted by later Sveconorwegian deformation. Further, a mafic dyke swarm is recorded in the westernmost region of the Idefjorden terrane at 1.46 Ga, in the same time frame as Hallandian metamorphism in the Eastern Segment (Åhäll & Connelly 1998).

Nevertheless, despite only minimal correlation between the terranes, there is no conclusive evidence of a major collision event – such as ophiolite suites, subduction-related Sveconorwegian magmatism in the vicinity of the Mylonite Zone, or oceanic or continental-margin deposits (Åhäll & Connelly, 2008) – so the debate about the nature of the relationship between the Idefjorden terrane and the Eastern Segment prior to the Sveconorwegian orogeny is far from settled.

Further, the presence of Hallandian signatures west of the tentatively-defined Mylonite Zone (Lundqvist et al. 2005) in a relatively unexplored area colloquially known as ‘B-Bulan’ (see Figure 3), has opened up the possibility of identifying Hallandian signatures in the Idefjorden terrane. At the same time, B-Bulan is bounded by shear zones, so its relationship to the surrounding Idefjorden terrane is also unclear, and could instead be a part of the Eastern Segment west of the Mylonite Zone.

In this thesis I aim to answer the following:

- 1) Is it possible to trace Hallandian-age signatures into B-Bulan?
- 2) Is it possible to trace Eastern Segment protoliths into B-Bulan?
- 3) If Hallandian-age signatures are present, is there evidence of Idefjorden units associated with Hallandian signatures? If so, what could that tell us about the history of southwestern Sweden? If not, could B-Bulan be a window into the Eastern Segment?

<sup>1</sup>It is important to consider that absence of evidence is not evidence of absence. On the other hand, age correlation can be coincidence, rather than evidence of a common history.

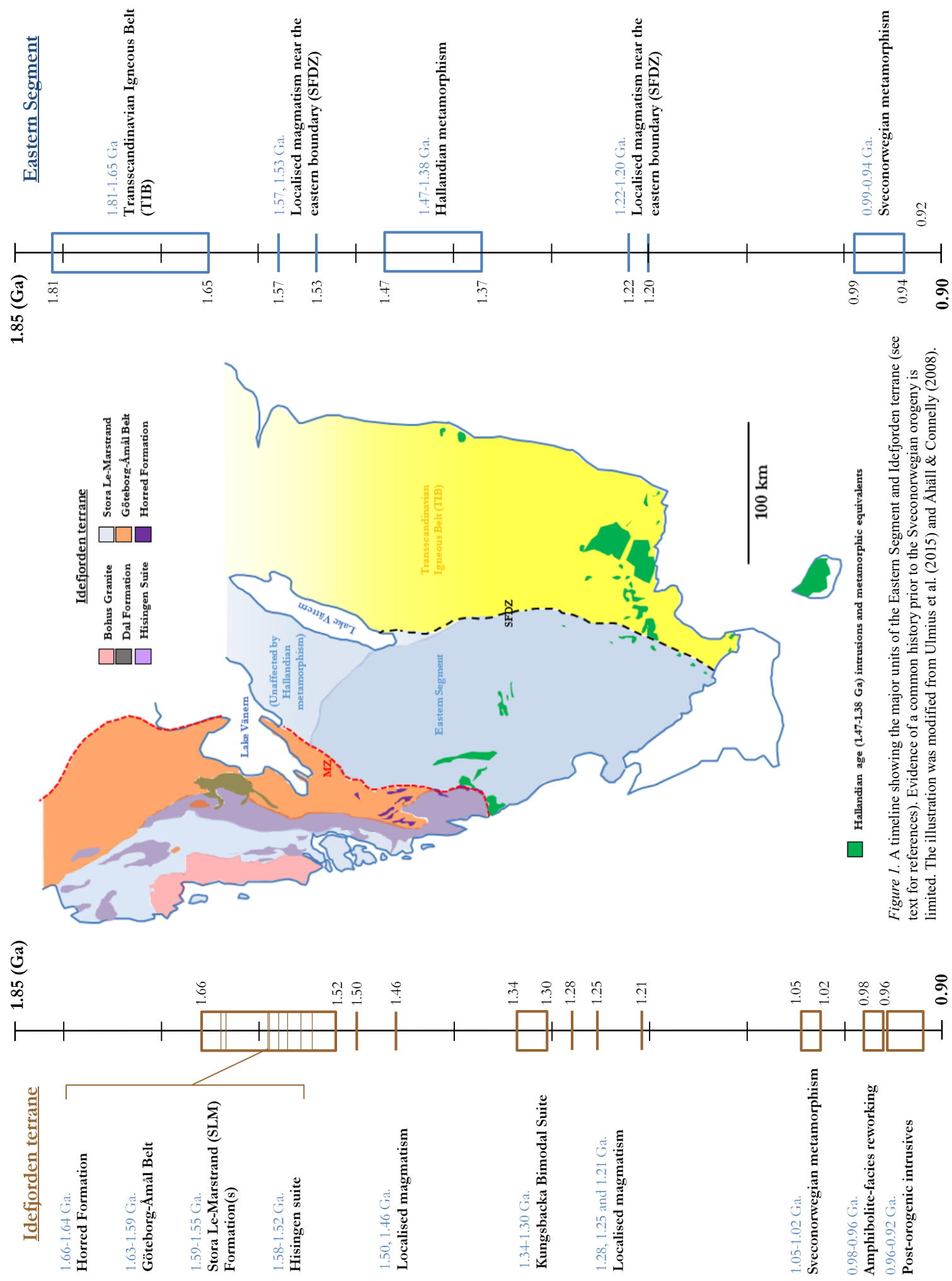


Figure 1. A timeline showing the major units of the Eastern Segment and Idefjorden terrane (see text for references). Evidence of a common history prior to the Sveconorwegian orogeny is limited. The illustration was modified from Ulmius et al. (2015) and Åhäll & Connelly (2008).



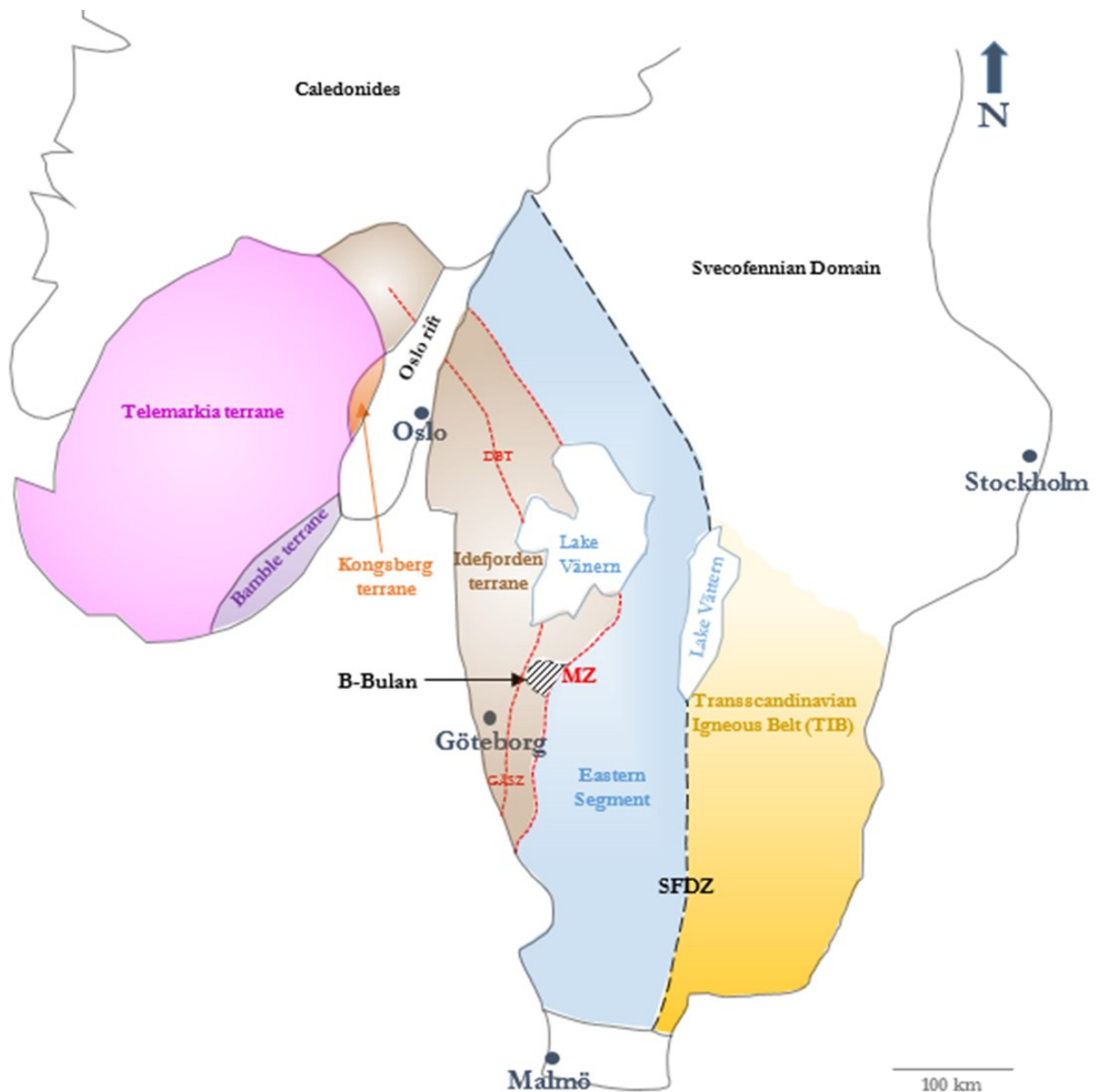


Figure 2. A summary of the geology of SW Sweden showing the main lithotectonic units and shear zones in the Sveconorwegian Province. SFDZ = Sveconorwegian Frontal Deformation Zone, MZ = Mylonite Zone, GÄSZ = Göta Älv Shear Zone, DBT = Dalsland Boundary Thrust. Modified from Bingen et al. (2008b).

## 2 Geological setting

### 2.1 The geology of SW Sweden

The geology of SW Sweden is made up of a succession of Precambrian provinces that show a younging trend from east to west. The shield area is divided into two parts by a N-S striking deformation zone known as the Sveconorwegian Frontal Deformation Zone (Wahlgren et al. 1994; other authors, such as Bethelsen (1980) and Jarl (2002) refer to the boundary as the Sveconorwegian Front and Protogine Zone, respectively), which separates rocks relatively unaffected by the Sveconorwegian orogeny to the east from those affected by Sveconorwegian metamorphism to the west.

To the east of the Sveconorwegian Frontal

Deformation Zone (SFDZ) and untouched by Sveconorwegian metamorphism is the ca. 1.81-1.65 Ga Transscandinavian Igneous Belt (TIB), a large, N-S trending belt dominated by granitoids which are partially affected by Sveconorwegian metamorphism in the west (Larson et al. 1998; Söderlund et al. 1999; Gorbatshev 2004). All rocks to the west of the Sveconorwegian Frontal Deformation Zone are part of the Sveconorwegian Province.

#### 2.1.1 The Sveconorwegian Province

The Sveconorwegian Province is an orogenic belt extending more than 500 kilometres across the southwestern area of the Fennoscandian Shield (Möller et al. 2015), which has been reworked during processes associated with the 1.14-0.92 Ga Sveconorwegian orogeny (Bingen et al. 2008b) and is

characterised by five lithotectonic segments: Telemarkia, Bamble, Kongsberg, Idefjorden and Eastern Segment (see Bingen et al. 2008b for more detailed descriptions). The eastern part of the Sveconorwegian Province, where my field area lies, is defined by two of these: the Eastern Segment in the east and the Idefjorden terrane in the west. The boundary between the Eastern Segment and the Idefjorden terrane is defined by a major ductile shear zone, the Mylonite Zone, which is shallowly west-dipping in the south and subvertical in the north (Stephens et al. 1996; Viola et al. 2011; Petersson et al. 2013).

#### 2.1.1.1 *The Eastern Segment*

The Eastern Segment is a 50-100 km wide north-south-trending belt consisting predominantly of orthogneisses with minor mafic suites of different generations. Their protolith ages and compositions suggest that they are equivalent to the 1.81-1.66 Ga granitic-monzonitic-syenitic intrusions of the Trans-Scandinavian Igneous Belt (TIB) to the east of the Sveconorwegian Frontal Deformation Zone (Söderlund et al. 1999; Söderlund et al. 2002; Möller et al. 2007; Petersson et al. 2013; Möller et al. 2015).

Widespread igneous activity is largely absent from the Eastern Segment between 1.66 and 1.47 Ga, aside from minor dolerite intrusions in the east, near the Sveconorwegian Frontal Deformation Zone (SFDZ), between 1.57 and 1.53 Ga (Wahlgren et al. 1996; Söderlund et al. 2004; Söderlund et al. 2005; Söderlund & Ask, 2006; Bingen et al. 2008b).

Hallandian metamorphism, defined by high-grade metamorphism, partial melting and magmatism between 1.47 and 1.38 Ga, is present in the southern section of the Eastern Segment (Christoffel et al. 1999; Johansson et al. 2001; Andersson et al. 2002; Söderlund et al. 2002). Most evidence of Hallandian metamorphism has been overprinted by high-grade Sveconorwegian metamorphism; however, partial melting and metamorphic zircon growth have preserved Hallandian-age signatures in zircons (Ulmius et al. 2015). The Hallandian metamorphic event is believed to have terminated with the emplacement of granite-norite-charnockite suites around 1.38-1.37 Ga (Åhäll et al. 1997; Andersson et al. 1999; Christoffel et al. 1999; Andersson et al. 2002; Ulmius et al. 2015). Record of Hallandian-age metamorphism is lacking in the Idefjorden terrane to the west (see Figure 1). Post-dating the Hallandian orogeny, dyke swarms from 1.22 to 1.20 Ga are recorded in the east of the Eastern Segment, at the boundary of the SFDZ (Söderlund et al. 2005; Söderlund & Ask, 2006; Bingen et al. 2008b).

Sveconorwegian high-grade metamorphism is first recorded in the Eastern Segment at 0.99-0.98 Ga, significantly later than in the Idefjorden terrane. High-pressure granulite- and eclogite-facies metamorphism is recorded, with peak metamorphism estimated to have occurred at around 0.97 Ga (Johansson et al. 1991; Möller 1998; Larson et al. 1999; Möller 1999; Andersson et al. 2002; Austin Hegardt 2010; Johansson et al. 2001; Möller et al. 2015). Partial melting took place between 0.98 and 0.96 Ga, and

granitic pegmatitic intrusions were emplaced between 0.96 and 0.94 Ga (Andersson et al. 1999; Möller & Söderlund 1997; Möller et al. 2007). Evidence of Sveconorwegian metamorphism prior to 0.99 Ga is absent in the Eastern Segment (Möller et al. 2015).

The Eastern Segment is defined by Sveconorwegian metamorphism and overprinting, and has been divided into three compartments by Möller et al. (2015). The frontal wedge (upper) is the least metamorphosed section of the Eastern Segment, with non-penetratively deformed bedrock (Wahlgren et al. 1994) and greenschist- to amphibolite-facies metamorphism associated with the Sveconorwegian orogeny. The transitional (middle) section shows penetrative, gneissic deformation but no migmatisation, with deformation occurring under amphibolite-facies conditions (Söderlund et al. 2004) during the Sveconorwegian orogeny. Mafic rocks are amphibolite and garnet amphibolite, and relict igneous textures are preserved (Möller et al. 2015). The lower (internal) section is the most metamorphosed section of the Eastern Segment, with a predominantly highly-metamorphosed orthogneiss bedrock showing high-P granulite- and upper-amphibolite-facies metamorphism, with localised retrogressed eclogite-facies metamorphism. (Johansson et al. 1991; Möller 1998; Möller 1999; Austin Hegardt et al. 2005; Möller et al. 2015).

#### 2.1.1.2 *The Mylonite Zone*

The Mylonite Zone is a less-than-10-km-wide and more-than-450-km-long ductile high-strain zone that separates the Eastern Segment from units west of the zone, such as the Idefjorden terrane; it marks the eastern boundary of the Idefjorden terrane. The location of the Mylonite Zone is not always clear (as Figure 4 demonstrates), but is crudely defined on the magnetic anomaly map (Figure 4) by a banded pattern indicating a change in magnetic signature at the boundary between the Eastern Segment and Idefjorden lithological units.

The strike direction varies from north-northeasterly in the southern part (with local variations near my field area), to northerly in the central part and northwesterly in the northern part (Stephens et al. 1996), while the dip varies from gently westward-dipping in the south to moderately westward-dipping in the central part and steeply dipping or sub-vertical in the north, although this may vary locally. The westerly dip is interpreted to be a result of the tilting of the Mylonite Zone under either oblique or inclined transpressional conditions (Robin & Cruden 1994; Viola & Henderson 2010).

Syn-deformational melting in the southern part of the Mylonite Zone records high-grade metamorphism, while greenschist-facies in the north is interpreted to record retrograde metamorphism (Stephens et al. 1996). Kinematic variations are observed along the length of the Mylonite Zone (Robin & Cruden 1994; Stephens et al. 1996; Viola & Henderson 2010; Viola et al. 2011). In the north, sinistral strike-slip dominates locally with duplexes showing compressional, dip-slip structures. Top-to-the-east, reverse shearing and sinistral strike-slip movement is recorded in the south, close to Vänern, while dextral, strike-slip movement has been inferred in the southernmost part of the

Mylonite Zone (Viola & Henderson 2010). This is overprinted by top-to-the-east-southeast displacement followed by top-to-the-west extension during the late-Sveconorwegian orogeny (Stephens et al. 1996; Berglund, 1997; Viola et al. 2011; Möller et al. 2015).

Some areas in the southern Mylonite Zone record migmatitisation at 0.98-0.97 Ga (Andersson et al. 2002), which is coeval with high-grade metamorphism in the Eastern Segment (Möller et al. 2007; Möller et al. 2015); U-Pb ages of 0.92 Ga in titanite and zircon have also been recorded, indicating late-stage metamorphism and ductile deformation (Johansson & Johansson 1993; Schersten et al. 2004).

The Mylonite Zone is believed to have initially formed as a result of crustal shortening, either WNW-ESE or NW-SE, oblique to the pre-Sveconorwegian continental margin (Stephens et al. 1996; Viola & Henderson 2010). The differences in pre-Sveconorwegian history between the Eastern Segment and Idefjorden terrane has led to suggestions that the zone formed as a Sveconorwegian suture (e.g. Austin Hegardt 2010); in other words, the Mylonite Zone formed as a result of the event that formed the Sveconorwegian orogeny. This interpretation is disputed, however, with critics suggesting a lack of supporting evidence, such as ophiolite suites, subduction-related Sveconorwegian magmatism in the vicinity of the Mylonite Zone, oceanic deposits and/or continental-margin deposits (Åhäll & Connelly 2008).

#### 2.1.1.3 Idefjorden terrane

The Idefjorden terrane lies to the west of the Mylonite Zone and extends approximately 400 km long and 140 km wide ( Petersson et al. 2015). The Idefjorden terrane is bounded to the west by the Telemarkia and Kongsberg terranes and to the east by the Eastern Segment (see Bingen et al. 2008b).

The dominant lithological units in the Idefjorden terrane are 1.66-1.52 Ga metagranitoids, gneisses and metasediments, formed and assembled during the Gothian orogeny (see Bingen et al. 2005); evidence for older geological units are lacking (Åhäll et al. 1995; Brewer et al. 1998; Schersten et al. 2000; Schersten et al. 2004; Åhäll & Connelly, 2008; Petersson et al. 2015). The magmatic protoliths are generally granite to tonalite (Bingen et al. 2005; Åhäll & Connelly, 2008; Petersson et al. 2013), the oldest of which are the Mjösjö dacite (1.66 Ga) and the Hårsjön gneiss (1.64 Ga) of the Horred formation ( Schersten et al. 2000; Åhäll & Connelly 2008; Petersson et al. 2015).

The 1.63-1.59 Ga Göteborg-Åmål Belt is composed of supracrustal rocks (volcanics, volcaniclastics and sediments) of the Åmål formation that have been metamorphosed to greenschist- and amphibolite-facies gneisses. The Göteborg suite, of a similar age, consists of granitic and mafic bodies that have intruded into supracrustal rocks of the Horred and Åmål formations (Brewer et al. 1998; Åhäll & Connelly 2008; Petersson et al. 2015).

The 1.59-1.55 Ga Stora Le-Marstrand (SLM) formation(s) consists of migmatitised metasediments and metabasalts that post-date the Göteborg-Åmål Belt (Åhäll & Daly 1989; Åhäll & Connelly 2008). The youngest protoliths attributed to the Gothian orogeny

are from the 1.58-1.52 Ga Hisingen suite, which are intermediate granitoids and mafic-felsic suites that intrude the Horred, Åmål and SLM formations. Deformation varies from migmatitised to undeformed (Åhäll & Connelly 2008), with the southern part of the Göta Alv Shear Zone (GASZ) roughly defining the boundary between greenschist-facies granites west of the shear zone and veined amphibolite-facies rocks east of the shear zone (Austin Hegardt 2010).

Suites that post-date the Gothian orogeny and pre-date the Sveconorwegian orogeny occur as variably deformed and metamorphosed lithological units, including the 1.50 Ga Brevik gabbro and Stigfjorden granite (Åhäll & Connelly 1998), the 1.46 Ga Orust dyke swarm, the 1.34-1.30 Ga Kungsbacka Bimodal Suite of granitic and gabbroic bodies, the 1.28 Ga Bunketorp granite, the 1.25 Ga Segmon granite and the 1.21 Ga Sandsjön granite gneiss (Welin et al. 1981; Persson et al. 1983; Welin & Samuelsson 1987; Åhäll & Connelly 1998; Austin Hegardt et al. 2007; Åhäll & Connelly 2008). Concrete evidence of Hallandian metamorphism in the Idefjorden terrane is yet to be recorded.

The pre-Sveconorwegian evolution of the Idefjorden terrane appears to be distinct from the pre-Sveconorwegian shield in the Eastern Segment and foreland region east of the Sveconorwegian Province, which is also reflected in the variable timing and conditions of Sveconorwegian deformation and metamorphism (Andersson et al. 2002; Bingen et al. 2008b; Petersson et al. 2013). This has led some to suggest that the Idefjorden terrane was displaced from its original tectonic position during the Sveconorwegian orogeny (Andersson et al. 2002; Bingen et al. 2008b) and transported eastward relative to the Eastern Segment (Stephens et al. 1996; Viola et al. 2011).

During the Sveconorwegian orogeny, the Idefjorden terrane records 1.05-1.02 Ga high-pressure amphibolite- to granulite-facies metamorphism immediately west of the Mylonite Zone (Austin Hegardt et al. 2007; Bingen et al. 2008b; Söderlund et al. 2008). Metamorphism within the Idefjorden terrane is heterogeneous, ranging from greenschist- to locally-granulite-facies conditions (Petersson et al. 2015). Metamorphism in the Idefjorden terrane is around 30 million years older than high-pressure metamorphism in the Eastern Segment (Bingen et al. 2008a; Austin Hegardt 2010; Petersson et al. 2015).

At 0.98-0.96 Ga, around the time when the Eastern Segment underwent high-pressure metamorphism, the Idefjorden terrane was undergoing low- to mid-amphibolite-facies reworking (Andersson et al. 2002). However, movement along the Göta Alv Shear Zone within the Idefjorden terrane at 0.97 Ga suggests that this was active after the general 1.05-1.02 Ga event (Austin Hegardt 2010).

Evidence of the Sveconorwegian orogeny is last recorded with the post-orogenic emplacement of 0.96-0.92 Ga intrusives such as the Vinga porphyry (Åhäll & Schoberg 1999), Bohus granite-pegmatite (Eliasson & Schöberg 1991), Hakefjorden norite (Schersten et al. 2000) and Blomskog granite-pegmatite (Bingen et al. 2006), among others (see Bingen et al. 2008b for a comprehensive list).



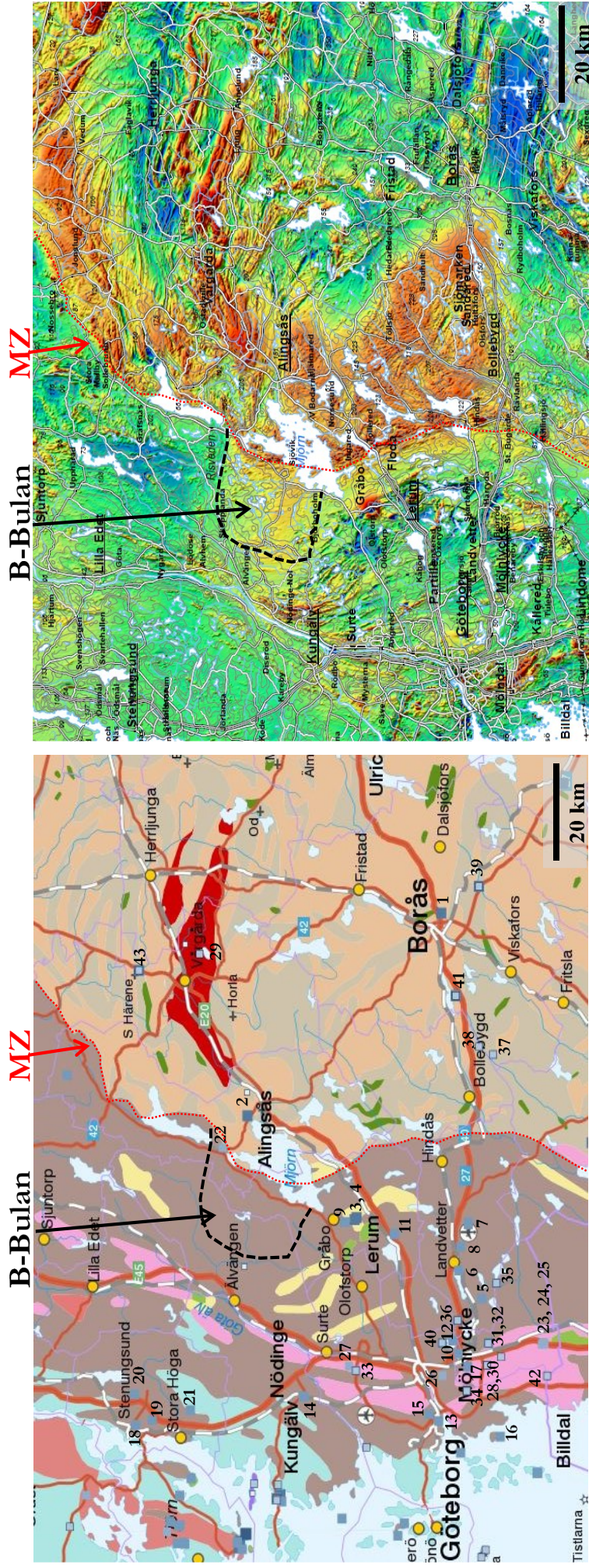


Figure 4. (Left) Bedrock map of the area surrounding B-Bulan from the Swedish Geological Survey's online database (source: Swedish Geological Survey). Modified to include the B-Bulan area (which, according to this map, is indistinguishable from the surrounding bedrock). Numbers correspond to samples dated in the region, as shown in Table 1. (Right) Airborne magnetic anomaly map of the region (source: Swedish Geological Survey). Red represents areas of high magnetic field strength, while blue represents areas of low magnetic field strength. B-Bulan is clearly distinct from the surrounding Idefforden terrane.

Table 1. A summary of dated samples in the vicinity of B-Bulan, according to the Swedish Geological Survey's database (accessed in May 2018).

#	Region	Age (Ma)	+/- (Ma)	Lithotectonic Unit	Comments	Source
1	Borås	1674	8	Eastern Segment	U-Pb; tonalite	Schersten et al. 2000
2	Alingsås	1666	23	Eastern Segment	Granitic migmatitic gneiss	Lundqvist et al. 2012
3	Gråbo-Floda	1640	9	Idefjorden terrane	Pb-Pb; Härsjö gneiss (Horred Fm)	Petersson et al. 2015
4	Gråbo-Floda	1624	6	Idefjorden terrane	Pb-Pb; granite vein	Schersten et al. 2000
5	Mölnadal-Mölnlycke-Lindome	1616	10	Idefjorden terrane	U-Pb; Granitic veined gneiss; Göteborg suite	Austin Hegardt & Cornell 2010
6	Landvetter	1614	5	Idefjorden terrane	Delsjön augen granite-gneiss	Ahlin et al. 2006
7	Landvetter	1608	12	Idefjorden terrane	U-Pb; Landvetter intrusion; Göteborg suite	Österlund 2015
8	Landvetter	1607	20	Idefjorden terrane	U-Pb; Gneiss (granodiorite), foliated, pegmatitic veins (migmatitic)	Österlund 2015
9	Gråbo-Floda	1605	10	Idefjorden terrane	Pb-Pb age; Göteborg suite	Schersten et al. 2004
10	Mölnadal-Mölnlycke-Lindome	1605	9	Idefjorden terrane	U-Pb; Kallebäck orthogneiss; Göteborg suite	Åhäll & Connelly 2008
11	Lerum	1603	40	Idefjorden terrane	U-Pb; Lerum granite	Welin & Samuelsson 1987
12	Mölnadal-Mölnlycke-Lindome	1585	4	Idefjorden terrane	U-Pb; Felsic vein; Hisingen suite	Ahlin et al 2006
13	Mölnadal-Mölnlycke-Lindome	1563	2	Idefjorden terrane	U-Pb; Rya granodiorite; Hisingen suite	Åhäll & Connelly 2008
14	Kungälv	1561	10	Idefjorden terrane	U-Pb, Pb-Pb; Ytterby granodioritic gneiss; Hisingen suite	Petersson et al 2015
15	Mölnadal-Mölnlycke-Lindome	1559	2	Idefjorden terrane	U-Pb; Biskopsgården granite; Hisingen suite	Åhäll & Connelly 2008
16	Mölnadal-Mölnlycke-Lindome	1558	2	Idefjorden terrane	U-Pb; Förö dyke; Hisingen suite	Åhäll & Connelly 2008
17	Mölnadal-Mölnlycke-Lindome	1547	5	Idefjorden terrane	U-Pb; Bifrost tonalite; Hisingen suite	Åhäll & Connelly 2008
18	Stenungsund	1543	6	Idefjorden terrane	U-Pb, Pb-Pb; Stenungsund granodioritic gneiss; migmatitic	Petersson et al. 2015
19	Stenungsund	1530	18	Idefjorden terrane	U-Pb; Stenungsund granite	Åhäll 1991
20	Stenungsund	1530	6	Idefjorden terrane	U-Pb; Hällungen granodiorite; Hisingen suite	Åhäll & Connelly 2008
21	Stora Höga	1526	15	Idefjorden terrane	Rb-Sr; Stenungsund granite	Åhäll 1991
22	Brobacka	1450	N/A	Undefined	U-Pb; Gneiss	Lundqvist et al. 2005
23	Mölnadal-Mölnlycke-Lindome	1362	9	Idefjorden terrane	U-Pb; Askim granite	Welin & Samuelsson 1987
24	Mölnadal-Mölnlycke-Lindome	1343	7	Idefjorden terrane	U-Pb; Askim granite; Kungsbacka bimodal suite	Austin Hegardt et al 2007
25	Mölnadal-Mölnlycke-Lindome	1336	10	Idefjorden terrane	U-Pb; Askim granite; Kungsbacka bimodal suite	Austin Hegardt et al 2007
26	Mölnadal-Mölnlycke-Lindome	1333	8	Idefjorden terrane	U-Pb; Chalmers gabbro; Kungsbacka bimodal suite	Kiel et al 2003
27	Surte-Kärre	1311	8	Idefjorden terrane	U-Pb; Kärre Granite; Kungsbacka bimodal suite	Austin Hegardt et al 2007
28	Mölnadal-Mölnlycke-Lindome	1279	69	Idefjorden terrane	Rb-Sr; Bunketorp granite	Welin & Samuelsson 1987
29	Södra Härene-Vårgårda	1224	8	Eastern Segment	U-Pb; syenite	Berglund 1997
30	Mölnadal-Mölnlycke-Lindome	1192	7	Idefjorden terrane	Rb-Sr; Bunketorp granite	Welin & Samuelsson 1987
31	Mölnadal-Mölnlycke-Lindome	1178	16	Idefjorden terrane	U-Pb; Pegmatite dyke crosscutting migmatite	Haeggman 2015
32	Mölnadal-Mölnlycke-Lindome	1060	77	Idefjorden terrane	U-Pb, Pb-Pb; Migmatitic orthogneiss; Göteborg suite	Haeggman 2015
33	Surte-Kärre	1043	11	Idefjorden terrane	U-Pb; Pegmatite	Austin Hegardt et al 2007
34	Mölnadal-Mölnlycke-Lindome	1038	10	Idefjorden terrane	U-Pb (on columbite-tantalite); Högsbo pegmatite	Jonason 2016
35	Mölnadal-Mölnlycke-Lindome	1028	50	Idefjorden terrane	U-Pb; Granitic veined gneiss; Göteborg suite	Austin Hegardt & Cornell 2010
36	Mölnadal-Mölnlycke-Lindome	1017	17	Idefjorden terrane	U-Pb; Granitic veined gneiss; Göteborg suite	Austin Hegardt & Cornell 2010
37	Bollebygd	985	4	Eastern Segment	U-Pb; eclogite	Möller et al. 2015
38	Bollebygd	978	7	Eastern Segment	U-Pb; eclogite	Möller et al. 2015
39	Borås	976	6	Eastern Segment	U-Pb; orthogneiss, migmatitic	Möller et al. 2015
40	Mölnadal-Mölnlycke-Lindome	974	22	Idefjorden terrane	U-Pb; Delsjön augen granite-gneiss; migmatitic	Ahlin et al 2006
41	Bollebygd	957	4	Eastern Segment	Re-Os; felsic vein in mafic boudin (HP granulite-eclogite)	Austin Hegardt et al 2005
42	Mölnadal-Mölnlycke-Lindome	950	2	Idefjorden terrane	U-Pb, Pb-Pb (on baddelyite); Heden dyke; Göteborg dolerite	Hellström & Persson 2009
43	Södra Härene-Vårgårda	932	10	Eastern Segment	U-Pb (on titanite); granodiorite palaeosome	Connelly et al 1996

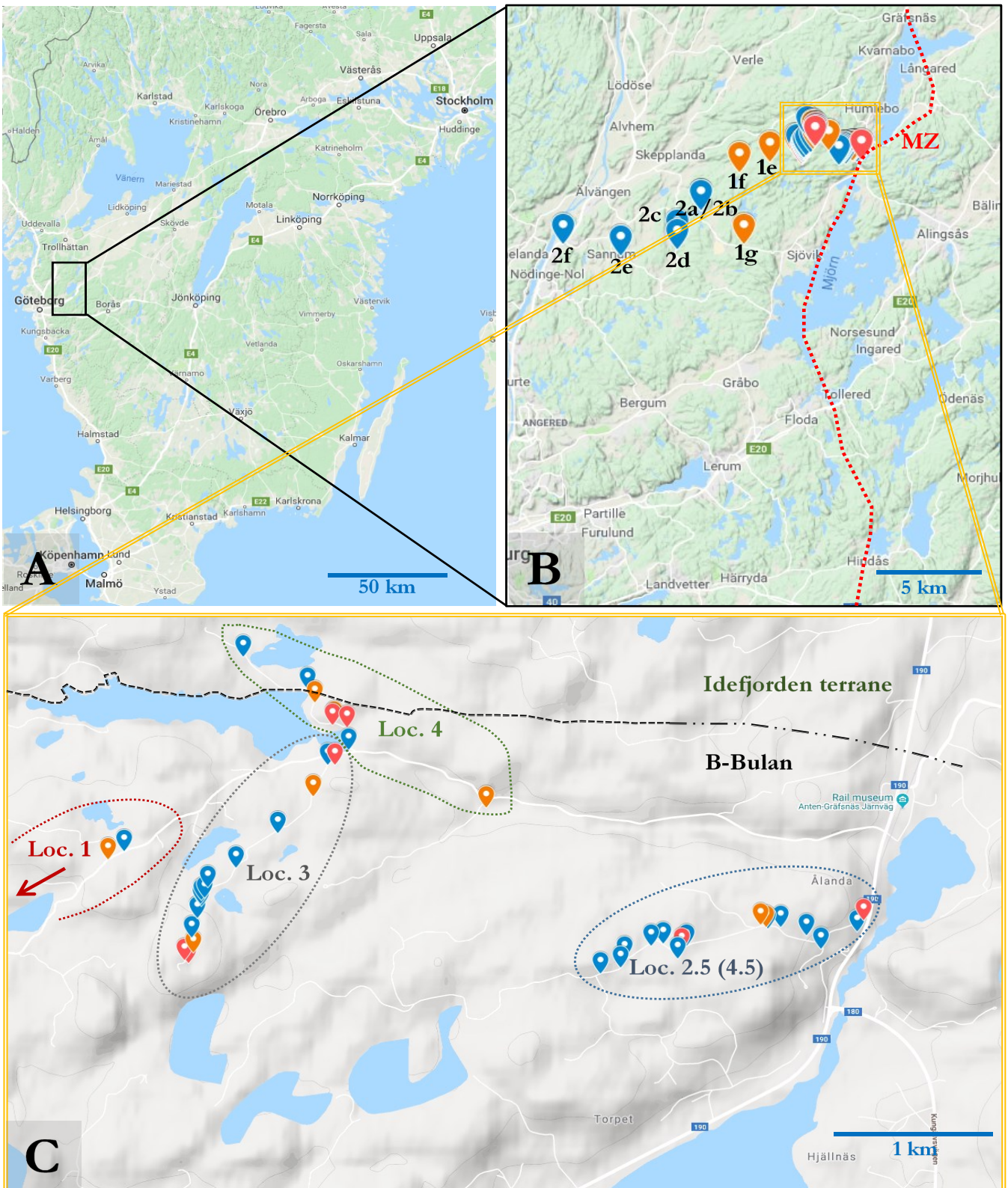


Figure 5. A) Terrain map of southwestern Sweden, with the rectangle referring to my field area. B) Terrain map of my field area with locations marked. Red marker indicates a location where a sample was taken and dated, orange marker indicates a location where a sample was taken, while blue is a location where no sample was taken (see Appendix 1). C) A closer look at my field area. The black line marks the boundary between B-Bulan and the surrounding area. Map data © 2019 Google.

magmatism nearby, in the border area between the Eastern Segment and the Idefjorden terrane. Given the absence of evidence for Hallandian metamorphism in the Idefjorden terrane, the potential to find a link between the Idefjorden terrane and Eastern Segment prior to the Sveconorwegian orogeny also made the area very suitable for study.

The Swedish Geological Survey (SGU) identifies a granitic gneiss in Brobacka – an area on the outer boundary of B-Bulan, lying fractionally to the west of the Mylonite Zone – with an interesting, unpublished age of 1.45 Ga (Lundqvist et al. 2005), which correlates with the Hallandian orogeny (Ulmius et al. 2015). The other side of the road from this location was my starting point, marked in Appendix 2 as location 2.5a/4.5a.

When deciding the areas to analyse, I had three aims: 1) to follow the Hallandian-age unit known as Brobacka gneiss, that Lundqvist et al. (2005) had identified, westwards in order to determine how far west it extended and whether there were any interesting field relationships between units below and above this; 2) to follow the boundary between B-Bulan and the surrounding rocks from north to south, aiming to find either a contact or at least a notable difference between lithological units within and outside B-Bulan; 3) to note and sample a variety of rocks to determine whether Eastern Segment units are present within B-Bulan, based on determined protolith ages.

## 3.2 Field methods

I spent four days in the field. For the first day-and-a-half I was guided around the area to get an overview. I marked each location on the map (see Figure 5) and took samples for reference. As almost every location that I had visited on the first day had been previously dated and described, I decided not to date any of these samples. I started my individual fieldwork on the afternoon of the second day at location 2.5a (revisited on day four to collect a better sample – sample 4.5a), near to the location that had been previously identified as having Hallandian-age signatures, and took samples that were to be my type locality, ‘Brobacka’ (named after the nearby nature reserve). From location 2.5a, I followed the path westwards and took samples where possible. I was particularly interested in finding more evidence of Hallandian-age signatures as far west as possible and noting field relationships with other units. When sampling I tried to take representative samples from a variety of units, but with a bias towards those that resembled the Brobacka type locality – K-feldspar-rich augen gneiss (texture dependent on the degree of deformation) – and surrounding units. On days three and four I sampled further west than I had walked the day before, following north-south trending trails to determine whether the Brobacka type-locality could be traced further into B-Bulan, and to compare the rocks from within B-Bulan to those located further north, in known Idefjorden terrane.

Samples collected from the four days were taken back and stored as a reference (see Appendix 1). Some were cut to make thin sections, while others were crushed and prepared for zircon separation.

## 3.3 Preparation

### 3.3.1 Zircon separation

Zircon was separated by crushing samples on a steel plate before milling the crushed chips in a Cr-steel swing mill. Fine-grained material was washed and panned to separate heavy mineral fractions. Magnetic minerals were removed using a handheld magnet before zircon grains were hand-picked from the heavy mineral residue under a binocular microscope.

Zircon grains were extracted for analysis from 10 samples. Between 40 and 50 grains were picked from more fertile samples; less than 10 grains were picked from more sparsely-populated samples. Picked zircon grains were then cast into one-inch cylindrical epoxy mounts. The epoxy mounts were polished to expose the surface of each crystal (adapted from Linders 2016).

### 3.3.2 SEM analysis

The epoxy mounts were coated with carbon and placed in the TESCAN Mira3 scanning electron microscope (SEM) at the Department of Geology, Lund University for high-magnification imaging of zircons. An SEM scans a high-energy electron beam at a sample, producing a wide range of secondary features that can be used to determine the composition and surface topography (Egerton 2005).

The settings used for the analysis were the following: an acceleration voltage of 10 kV or 15 kV (depending on the sample), a working distance of between 10.0 and 11.0 mm (depending on the sample) and a beam current of 18 nA.

Back-scattered electron (BSE) imaging and cathodoluminescence (CL) imaging were used to characterise the internal structure and zoning patterns as well as the presence of inclusions and fractures in individual crystals. These images were used to decide where to place spots that would be analysed by the LA-ICP-MS (laser ablation inductively-coupled plasma mass spectrometer). BSE-imaging illuminates heavy elements more than light ones, which is especially useful when trying to find inclusions or uranium-rich/poor domains in zircons. CL imaging uses light emitted during electron bombardment of the sample, which is almost only produced by trace elements such as rare earth elements, to highlight compositional contrasts (Long 1995; Lewerentz 2011). Fractures and inclusions were to be avoided, while zoning patterns helped identify crystals that may have experienced multiple phases of growth.

### 3.3.3 Why zircon?

As Linders (2016) explains, zircon is often used in geochronology because: 1) you find it in many different rocks (both metamorphic and igneous, and even sediments); 2) it takes in uranium and thorium, but not lead; 3) it has a high closure temperature (>900°C); and 4) it is very chemically and physically resistant – nearly indestructible (Lee et al. 1997; Finch & Hanchar 2003; Faure & Mensing 2005).



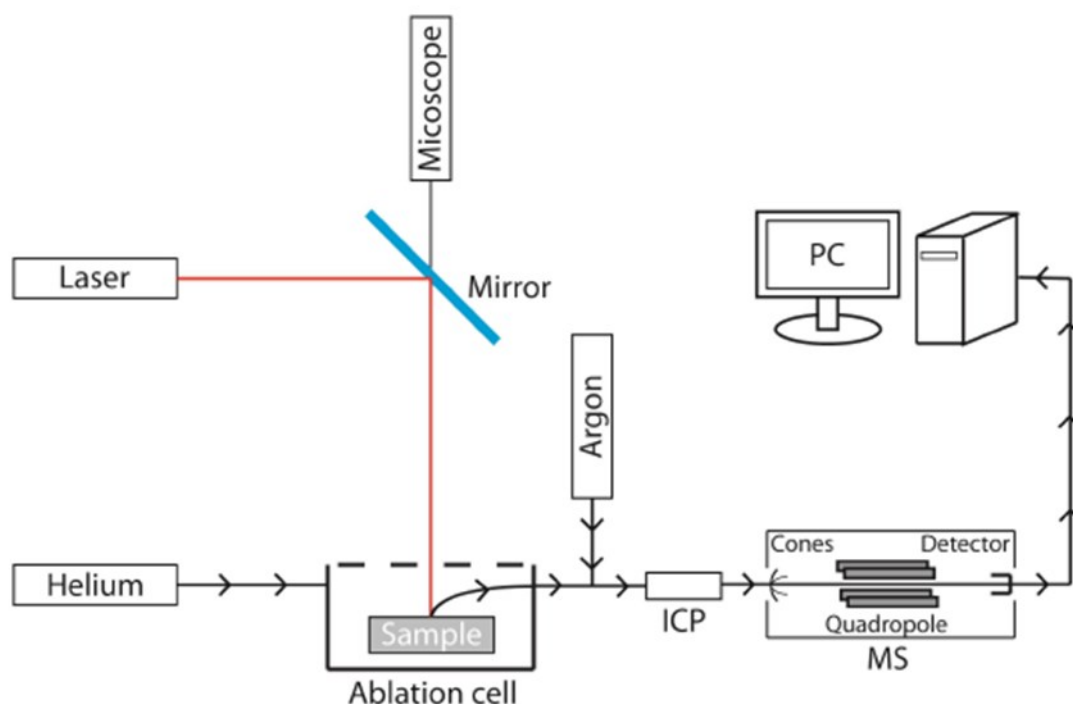


Figure 6. Illustration of the main components of an LA-ICP-MS instrument (Olsson, 2016; modified from Richter, 2013).

### 3.4 U-Pb dating

Spots were placed on selected grains that were then analysed, along with reference zircons (GTJ-1 and 91500) using the LA-ICP-MS. The following isotopes were analysed using the mass spectrometer:  $^{202}\text{Hg}$ ,  $^{204}\text{Hg}$ ,  $^{206}\text{Pb}$ ,  $^{207}\text{Pb}$ ,  $^{208}\text{Pb}$ ,  $^{232}\text{Th}$  and  $^{238}\text{U}$ . The laser ablation system used was the Teledyne Photon Machines Analyte G2, while the ICP-MS instrument was the Bruker Aurora M90, both located at the Biology Building of Lund University.

The dimensions of the spots were adapted according to the degree of zoning, presence of inclusions and size of the crystal;  $20\mu\text{m} \times 20\mu\text{m}$  was the standard, but was adjusted to  $24\mu\text{m} \times 17\mu\text{m}$  and  $29\mu\text{m} \times 14\mu\text{m}$  when necessary. The laser had a wavelength of 193 nm, a pulse width of 10 Hz and an energy intensity of  $3.5\text{ J/cm}^2$ .

Analytical conditions are specified in Appendix 3.

#### 3.4.1 LA-ICP-MS

As mentioned above, U-Pb dating was performed on selected grains using LA-ICP-MS (laser ablation inductively-coupled mass spectrometry). The laser is used to ablate the surface of the crystal, which produces an aerosol of nanometre-scale particles. A carrier gas (usually a noble gas, Ar or He) is flushed through the ablation cell, which picks up and transports the aerosol particles into the inductively-coupled plasma. A different gas flow (Ar) is heated to  $10,000^\circ\text{K}$  (forming a plasma), which then breaks down and ionises the aerosols (Primer 2005; Olsson 2016).

The ionised particles then enter the mass spectrometer (MS), which is held at a low pressure through a set of metal cones. The mass spectrometer

consists of an ion lens, mass analyser and an ion counter (detector). Ions are accelerated and separated from photons and neutral material through electrostatic lenses (ion lenses) before reaching the mass spectrometer. The mass analyser focuses ions of specific mass to charge ratios into the detector, which counts electrical pulses and produces a mass spectrum (Primer 2005; Olsson 2016).

#### 3.4.2 Why LA-ICP-MS?

The LA-ICP-MS method has a number of advantages: 1) it is capable of measuring a wide array of elements; 2) it can detect elements down to the parts-per-trillion (ppt) scale; 3) it works with a variety of spot sizes (from around  $5\text{-}750\mu\text{m}$ , depending on the instrument); and 4) it has a short analysis time compared with other instruments (Richter 2013; Olsson 2016).

Some problems associated with the LA-ICP-MS method are the mass discrimination of isotopes and elemental fractionation between lead and uranium during analysis (Horn et al. 2000). These error sources are mitigated by the application of external and internal corrections using a standard, where the age and isotopic ratios are known (Jackson et al. 1997; Kosler & Sylvester 2003; Olsson 2016).

### 3.5 Data processing and quality control

Zircon samples were analysed in five LA-ICP-MS sessions, and the data was normalised using the zircon GJ-1 as primary standard. Zircon 91500 was used as a secondary reference for quality control.

The data from the LA-ICP-MS analysis was processed using Iolite software. A baseline correction was made to filter out background radiation and

flawed data was rejected. The data was then processed in Microsoft Excel, and represented in plots using IsoplotR software (Vermeesch 2018).

Tera-Wasserburg concordia diagrams have been used to illustrate the  $^{238}\text{U}/^{206}\text{Pb}$  and  $^{207}\text{Pb}/^{206}\text{Pb}$  ratios using ellipses that correspond to  $2\sigma$  standard error (see Figure 17 and Figure 18). If the ellipse overlaps the concordia curve, the datum is considered to be concordant (and reliable). If the ellipse does not overlap the concordia curve, the datum is discordant and should be interpreted with caution. Discordance can occur due to calibration errors in the analytical instrument (in this case, the LA-ICP-MS machine), as well as geological factors such as Pb loss, common Pb (as demonstrated in Figure 7) or a blend of age domains (Schoene 2014).

The presence of common Pb is indicated by analyses that plot above the concordia, with high  $^{207}\text{Pb}$  levels relative to  $^{206}\text{Pb}$  during the formation (or growth) of the mineral. The long half-life of  $^{238}\text{U}$  to  $^{206}\text{Pb}$  compared with  $^{235}\text{U}$  to  $^{207}\text{Pb}$  indicates that some common Pb was present at formation to account for the discrepancy. Common Pb may also be confused with Hg interference, due to its similar atomic mass.

Pb loss can be indicated by an analysis that plots to the right of the concordia, with a low  $^{206}\text{Pb}$  count relative to  $^{238}\text{U}$  (represented as a high  $^{238}\text{U}/^{206}\text{Pb}$  ratio on Figure 7). Pb loss can occur during metamorphism

above a mineral's closure temperature or through recent weathering. In this case, Pb loss may represent a problem with the U-Pb calibration of the analysing instrument, as there is significant discordance in two of the 91500 sessions (see Figure 7). I concluded that the Pb-Pb results were more reliable than the U-Pb results, and this was corroborated by the appearance of a systematic offset to the right in all sessions (see Figure 7).

A measurement of how well the data is in line with the age model can be described by the Mean Square of Weighted Deviates (MSWD; this is discussed further in Chapter 3.5.1). An MSWD of approximately 1 indicates a good fit of the data with the model. If the MSWD is considerably greater than 1, this suggests either an underestimation of uncertainties, incorrect error propagation, or geological uncertainty that hasn't been accounted for; an MSWD of less than 1 suggests overestimated errors or uncertainties (Ludwig 2012; Schoene 2014).

Each sample was filtered to remove any analysis with a discordance of greater than 10%. Analyses with greater than 10% discordance were deemed to be unrepresentative – either due to calibration error, common Pb or Pb loss – and therefore were discounted.

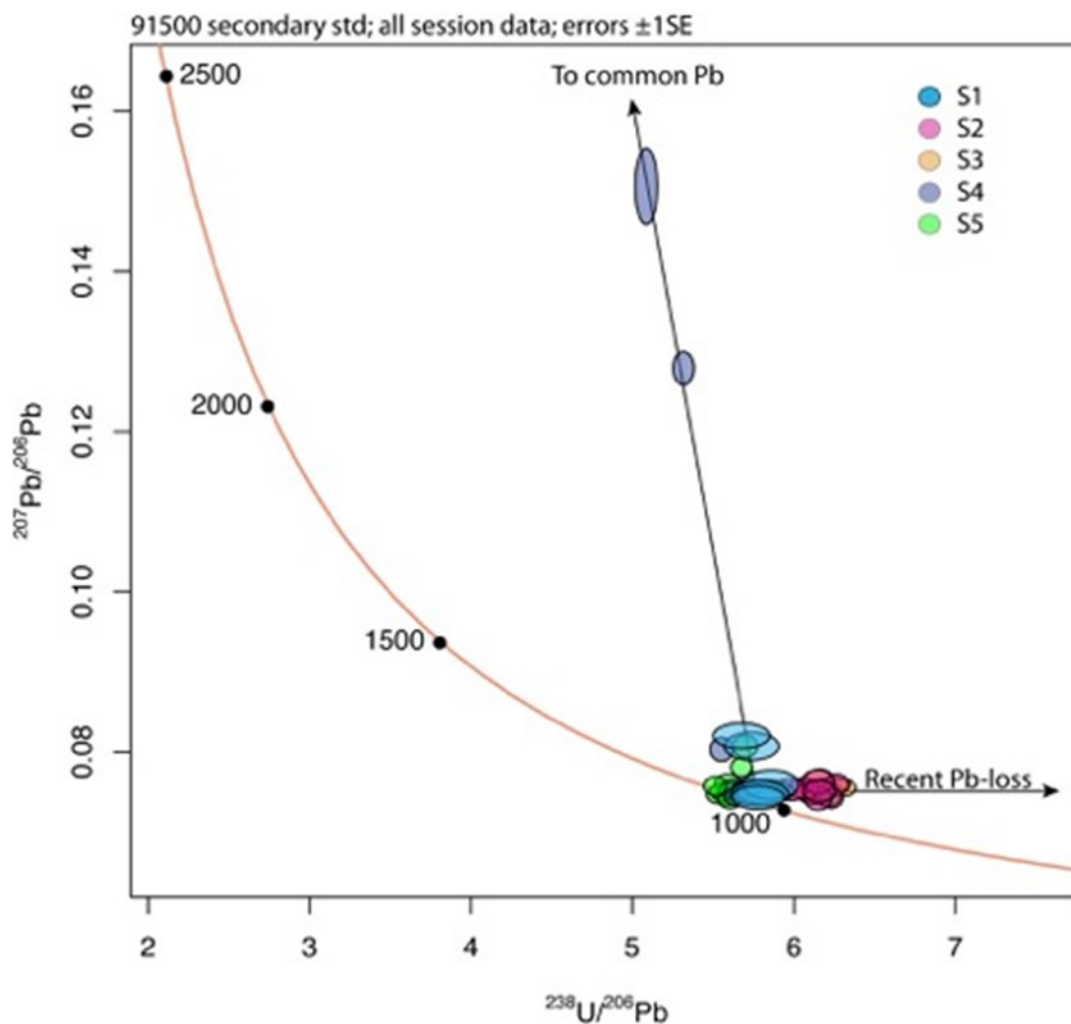


Figure 7. Summary of 91500 analyses from all sessions with no discordance filtering. As the graph shows, two samples from S4 show strong tendencies to common Pb, recording Pb-Pb ages of more than 1000 million years older than expected. It is not clear whether this is due to Pb loss in the sample or a calibration error with the LA-ICP-MS. Other analyses show recent Pb-loss trends to the right of the concordia. All values are to 1 standard error (SE).

91500 secondary std; data <10% discordance; error expansion factor 1.6  
 Mean = 1066.5 ±5.4 Ma (±2s; MSWD = 1.6)

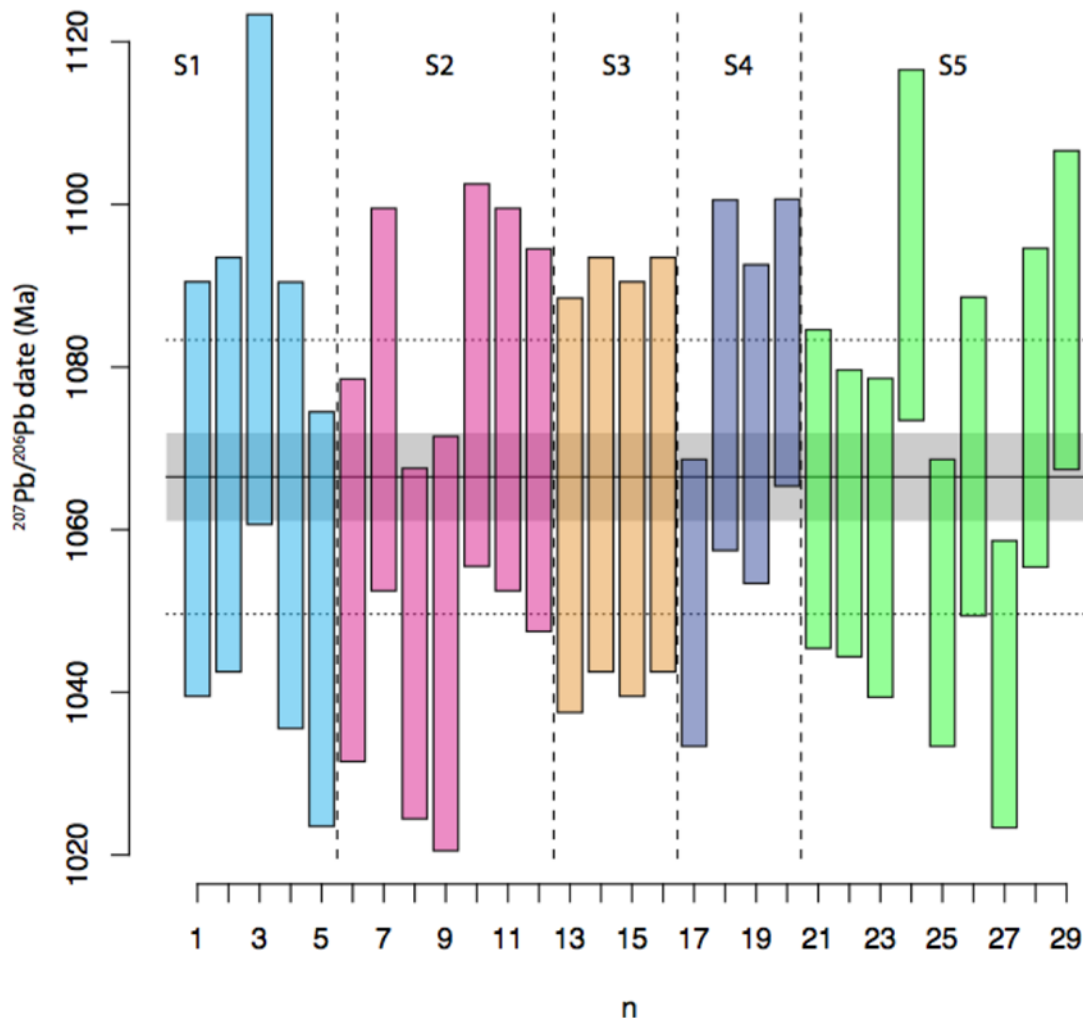


Figure 8. Pb-Pb ages of all 91500 sessions, filtered to remove samples greater than or equal to 10% discordance. Error expansion was increased to 1.6x to reduce dispersion. Ages are not Pb corrected.

### 3.5.1 Quality control—91500

Zircon 91500 is a commonly used reference material in zircon geochronology and geochemistry due to its homogeneity and reliability across a broad range of elements and their isotopes. The accepted weighted mean reference values for  $^{207}\text{Pb}/^{206}\text{Pb} = 0.07488$  ( $\pm 0.00001$ ,  $1\sigma$ ) and  $^{206}\text{Pb}/^{238}\text{U} = 0.17917$  ( $\pm 0.00008$ ,  $1\sigma$ ), corresponding to apparent  $^{207}\text{Pb}/^{206}\text{Pb}$  and  $^{206}\text{Pb}/^{238}\text{U}$  ages of  $1065.4 \pm 0.3$  Ma and  $1062.4 \pm 0.4$  Ma respectively (Wiedenbeck et al. 1995). 91500 was used as a secondary standard for data quality control, i.e. it was analysed periodically within each analytical session and treated as an unknown. Error magnification of 1.6x was done to account for the excess scatter; this has the effect of bringing the MSWD down by magnifying the error, while having a minimal effect on the result.

In this analysis the spot data from zircon 91500 shows very mixed results. A reliable analysis would

cluster around 1065 Ma, within error, but as Figure 7 shows, results from 91500 tests from all sessions show a variety of ages, some with errors of nearly 100 million years (two data points from Session 4 recorded Pb-Pb ages around 1000 Ma older than expected). This is significant, because if the accuracy of the test sample is disputed, it is very possible that later results from the same session are also incorrect. On the other hand, the U and Pb concentrations were considerably lower in the 91500 than in my samples. The 91500 would therefore be much more sensitive to common Pb corrections than my samples, and the associated errors would also be much greater.

Whether these results indicate a problem with the calibration of the measuring instrument, the LA-ICP-MS, or an irregularity in the 91500 sample is not clear. But given similar discordance challenges in many of the analysed samples, the calibration of the measuring instrument seems the most plausible.

Similarly the mean standard weighted deviation (MSWD), which is a good measure of the uncertainty attached to each datum, is abnormally high. In an ideal situation, the analysis would produce results that cluster closely around the mean, so that any differences and errors associated with each result would be due to analytical discrepancies (such as counting anomalies in the mass spectrometer). In isotope geochronology, however, there are often lots of sources of uncertainty – both analytical and non-analytical – which could range from an uncertainty about the level of background noise (low impact) to the degree of lead loss in a sample (higher impact).

MSWD is inversely proportionate to the reproducibility of the data when accounting for the analytical uncertainty in each datum. So in order to increase the likelihood of repeating these results, the spread from the mean has to be reduced by increasing the error bar associated with each result, and therefore the degree of overlap between results. In other words, if the MSWD falls outside of the accepted number, then another source of unmeasured uncertainty is not being accounted for. By increasing the size of the error, it is more likely to capture the unaccounted uncertainty.

### 3.5.2 Error expansion

As Figure 8 shows, in order to bring down MSWD to a reasonably reliable level the degree of uncertainty was expanded to 1.6x its measured value to account for unidentified analytical or geological errors. The question, then, is whether to apply the recalibration used on 91500 to make similar adjustments to the sample data. Are all the data grossly underestimating the level of uncertainty unaccounted for, or is it likely that by recalibrating the data, the degree of uncertainty is overestimated, leaving the results ambiguous?

I decided not to expand the errors on all of my data, as the concentrations of U and Pb were significantly higher in the samples than the 91500 standard, and would therefore be less sensitive to small changes in U and Pb counts. Secondly, each sample had a different number of analyses, which would have required error expansions of different amounts for each sample. This would have added great confusion and introduced the possibility of further error compared to leaving the results unexpanded. Further, expanding the errors may give a false impression of the spread being lower than it is due to overestimated errors. By not expanding the error, the MSWD is larger, but the data itself are hardly affected.

### 3.5.3 Pb correction

A Pb correction may be necessary in samples that contain large amounts of common Pb. The assumption is made that some Pb is present in the zircon sample at the time of formation (common Pb), which, if left unaccounted for, would give an older date than the true age. As zircon allows U but not Pb into its mineral structure, the only Pb that a zircon should contain is radiogenic Pb (ie.  $^{206}\text{Pb}$  or  $^{207}\text{Pb}$ ). Common Pb is represented by  $^{204}\text{Pb}$  – the stable isotope – which crystallises in a relatively fixed ratio to the radiogenic  $^{206}\text{Pb}$  and  $^{207}\text{Pb}$  isotopes. Therefore the amount of  $^{204}\text{Pb}$  in a sample can give a good estimate of the initial

amount of radiogenic Pb at the time of formation, which can then be recalculated (or ‘reset’) to avoid overestimating the amount of radiogenic Pb, and therefore the age, of the sample.

However, this leaves room for error because: a) the ratio of  $^{207}\text{Pb}$  to  $^{204}\text{Pb}$  varies with the age of the Pb source, and b)  $^{204}\text{Pb}$  has an isobaric interference due to  $^{204}\text{Hg}$ , which can compromise the amount of  $^{204}\text{Pb}$  in the mass spectrometer, leading to overcompensation in the recalculation.

Given the difficulty in distinguishing  $^{204}\text{Pb}$  from  $^{204}\text{Hg}$  in the LA-ICP-MS and the potential for overcorrection, not to mention the added complexity of comparing samples with different degrees of Pb correction, I decided not to apply a Pb correction to my results.

### 3.5.4 Discordance filtering

Given the discordance of some data points observed in the 91500 standard, measured by the distance from the concordia, it was inevitable to expect that some data points from the samples in corresponding sessions would also show high degrees of discordance, and as such would more than likely be unrepresentative of the true age. In order to take into account the possibility that some results had been affected by analytical or calibration error, I decided to compromise and filter out all results with greater than 10% discordance.

### 3.5.5 Pb-Pb vs U-Pb

In an ideal world, U-Pb and Pb-Pb dating would complement one another by recording similar ages that plot on, or very near to, the concordia. Unfortunately, the systematic offset of U-Pb ages to the right of the concordia suggests a problem with the U-Pb calibration in the measuring instrument. As a result, the MSWDs of U-Pb analyses were off the charts, and completely unreliable. If there is a calibration error, either in the U count or between U and Pb, Pb-Pb is likely to be more reliable, as it deals only with the relationship between radiogenic Pb isotopes, and is unaffected by the U count.

## 4 Samples and results

### 4.1 Sample analyses

#### 4.1.1 Sample 4.5a-i: 'Brobacka' (N57°58.840', E012°26.142')

Sample 4.5a-i is a medium- to coarse-grained gneiss recognised by Lundqvist et al. (2005). It has an abundance of deformed, ~3-5 cm K-feldspar porphyroclasts surrounded by quartz, plagioclase and abundant biotite. The sample is heavily deformed in places, with sigmoidal structures, subgrain recrystallisation of quartz and a pronounced foliation defined by altered biotite. Secondary muscovite is also present. The zircon grains are <250 µm along their c-axis, mostly subhedral and show some zoning patterns.

A sample of Brobacka gneiss has been dated by Lundqvist et al. (2005) to 1450 Ma. I dated a separate sample from nearby. Of 62 analyses, 31 analyses have a discordance of less than or equal to 10%. These analyses have a weighted mean  $^{207}\text{Pb}/^{206}\text{Pb}$  age of  $1481 \pm 3$  Ma, with an MSWD of 5.8 ( $1481 \pm 8$  Ma to 95% confidence;  $\text{MSWD} \times 2\sigma$ ). One outlier of  $1598 \pm 16$  Ma is excluded from the age calculation

#### 4.1.2 Sample 2.5j-i (N57°58.759', E012°25.035')

Sample 2.5j-i is a medium-grained granitic gneiss made up of K-feldspar, plagioclase and quartz with abundant biotite. K-feldspar porphyroclasts are surrounded by finer-grained quartz and plagioclase. The sample is less deformed than other samples in the area. Biotite defines a weak fabric. Hornblende, titanite and zircon are also present. The zircon grains are up to 200 µm along their c-axis, vary from anhedral to subhedral and show minor zoning.

Of 65 analyses, 27 analyses have a discordance of less than 10%, with distinct clusters of interest. The oldest cluster has a Pb-Pb signature of between 1850 to 1700 Ma (Eastern Segment, upper limit), while the other clusters show ages of around 1680 to 1650 Ma

(Eastern Segment), 1590 to 1520 Ma (either Idefjorden or an Eastern Segment and Hallandian mixed age) and 1500 to 1450 Ma (lower limit falls within the Hallandian age, but upper limit is difficult to interpret). Considering the distinct populations (see Figure 18), the weighted mean ages are unlikely to be representative of the sample.

#### 4.1.3 Sample 2.5j-iv (N57°58.759', E012°25.035')

Sample 2.5j-iv is a medium- to coarse-grained granitic gneiss consisting of K-feldspar, quartz, minor plagioclase and biotite. It is very micaceous in some areas – but less so in others – and contains K-feldspar megacrysts. The thin section shows subgrain recrystallisation in quartz and a lack of fine-grained matrix. Biotite defines a weak fabric. This sample is less deformed and altered than other samples in the area. The zircon grains are up to 100 µm along their c-axis, anhedral to subhedral and show some zoning at the rims.

Of 29 analyses, 16 have a discordance of less than 10% with distinct populations of interest. Aside from two samples that are older than 1850 Ma (also observed in sample 2.5j-i), two samples dated to around 1685 Ma, four dated to between 1540 and 1510 Ma, and several falling between 1480 and 1430 Ma.

#### 4.1.4 Sample 4f-i (N57°59.579', E012°22.793')

Sample 4f-i is a medium-grained granitic gneiss rich in plagioclase; it has notable quantities of quartz and K-feldspar. Epidote and chlorite are present, probably a result of biotite recrystallisation. Plagioclase shows alteration on the surface. The zircon grains analysed are <250 µm along their c-axis, subhedral and show some zoning patterns.

Of 69 analyses, 27 analyses have a discordance of less than or equal to 10%. These analyses have a weighted mean  $^{207}\text{Pb}/^{206}\text{Pb}$  age of  $1625 \pm 5$  Ma, with an MSWD of 4.6 ( $1625 \pm 10$  Ma to 95% confidence;  $\text{MSWD} \times 2\sigma$ ).



Figure 9. Sample 4.5a-i. A medium-coarse grained gneiss with an abundance of deformed K-feldspar surrounded by quartz, plagioclase and biotite. Localised pegmatites were also observed.



Figure 10. An overview of location 2.5j, looking NW. This location shows a transition from K-feldspar-rich augen gneiss. Each letter is analysed in Figure 11.



Figure 11. A detailed look at Location 2.5j. A: Gradational change from granodiorite into K-feldspar-rich granite with augen. It is difficult to determine whether this is the same unit seen at Location 2.5a (4.5a; Brobacka type locality). B: Tight recumbent folding in a granodiorite-rich unit. C: Recumbent folding of a pegmatite close to Sample 2.5j-iii, a granodiorite. Photo B and D are also marked. D: Folded and foliated granodiorite. E: Folded K-feldspar-rich augen gneiss (Sample 2.5j-i). It is not clear whether this is the same as the Brobacka type locality, or whether it is just a K-feldspar-rich augen gneiss. F: K-feldspar-rich gneiss, micaceous. This is the unit above Sample 2.5j-i, and the transition is gradational, rather than sharp. The highest unit at Location 2.5j, strongly banded and foliated; K-feldspar like a pancake.

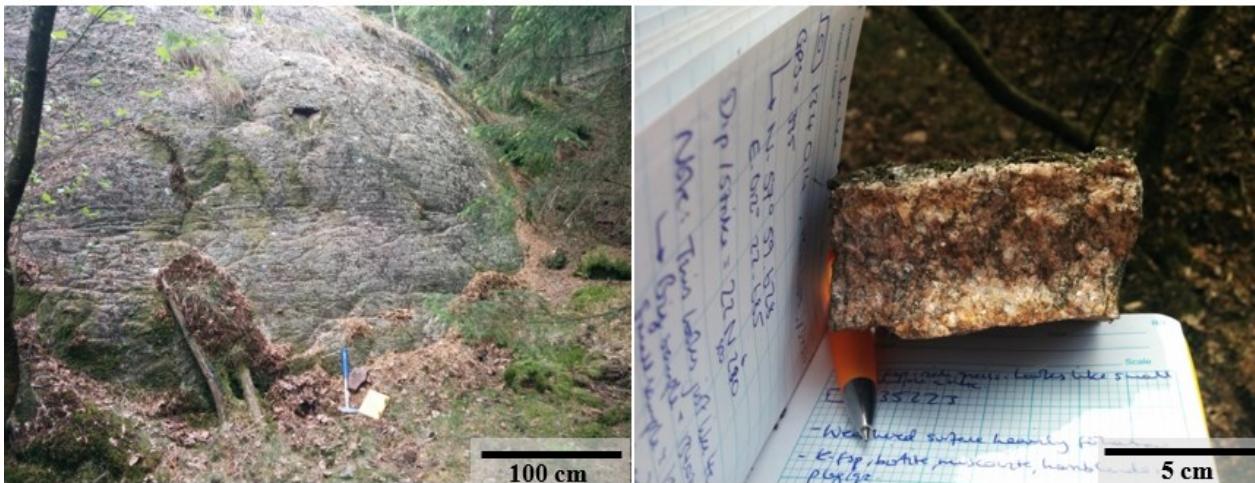


Figure 12. Sample 4f-i is a medium-grained granitic gneiss rich in plagioclase, with notable quantities of quartz and K-feldspar. Epidote and chlorite are also present.

#### 4.1.5 Sample 4g-i (N57°59.568', E012°22.796')

Sample 4g-i is a medium-grained granitic gneiss, consisting of plagioclase, quartz and K-feldspar with abundant biotite. Titanite, epidote and muscovite are minor minerals. Plagioclase grains have a dusty appearance while biotite grains show alteration. The sample is quite strongly deformed, with biotite and minor minerals defining the foliation. The zircon grains are <100  $\mu\text{m}$  along their c-axis, subhedral and show variable zoning.

Of 28 analyses, 20 have a discordance of less than 10%. These analyses have a weighted mean  $^{207}\text{Pb}/^{206}\text{Pb}$  age of  $1603 \pm 4$  Ma, with an MSWD of 2.2 ( $1603 \pm 6$  Ma to 95% confidence; MSWD  $\times 2\sigma$ ).



Figure 13. Sample 4g-i is a medium-grained granitic gneiss consisting of plagioclase, quartz and feldspar with abundant biotite.

#### 4.1.6 Sample 3m-ii (N57°59.420', E012°22.776')

Sample 3m-ii is a fine- to medium-grained granodioritic gneiss rich in plagioclase, with quartz and K-feldspar. It contains epidote, and chlorite, which probably would have formed during retrograde metamorphism, as well as hornblende, muscovite, and titanite that orientate parallel to the foliation. The fabric is pronounced, and plagioclase crystals shows considerable alteration, suggesting strong deformation and recrystallisation. The zircon grains analysed are  $\sim 100$   $\mu\text{m}$  along their c-axis, subhedral and show notable zoning patterns.

Of 13 analyses, 5 have a discordance of less than or equal to 10%. These analyses have a weighted mean  $^{207}\text{Pb}/^{206}\text{Pb}$  age of  $1641 \pm 11$  Ma, with an MSWD of 4.9 ( $1641 \pm 25$  Ma to 95% confidence; MSWD  $\times 2\sigma$ ).

#### 4.1.7 Sample 3b-i (N57°58.711', E012°21.858')

Sample 3b-i is a medium-grained granitic-granodioritic gneiss. Aside from plagioclase and quartz with minor K-feldspar, it has abundant biotite. Rutile is present, with a coronitic texture, which may suggest high-pressure, high-temperature metamorphism. Plagioclase is dusty, while quartz has a ribboned texture, suggesting strong deformation. The zircon grains are up to 150  $\mu\text{m}$  along their c-axis, subhedral and show very little zoning.

#### 4.1.8 Sample 3a-v (N57°58.703', E012°21.843')

Sample 3a-v is a fine- to medium-grained granitic gneiss consisting of quartz, plagioclase and K-feldspar in similar quantities. Porphyroclasts of K-feldspar and abundant biotite are apparent from the hand specimen. It is not dissimilar to the Brobacka type locality (4.5a-i), but has less K-feldspar and appears to be more strongly metamorphosed. The weathered surface appears more foliated, with a higher composition of mica. This could be interpreted either as metamorphic



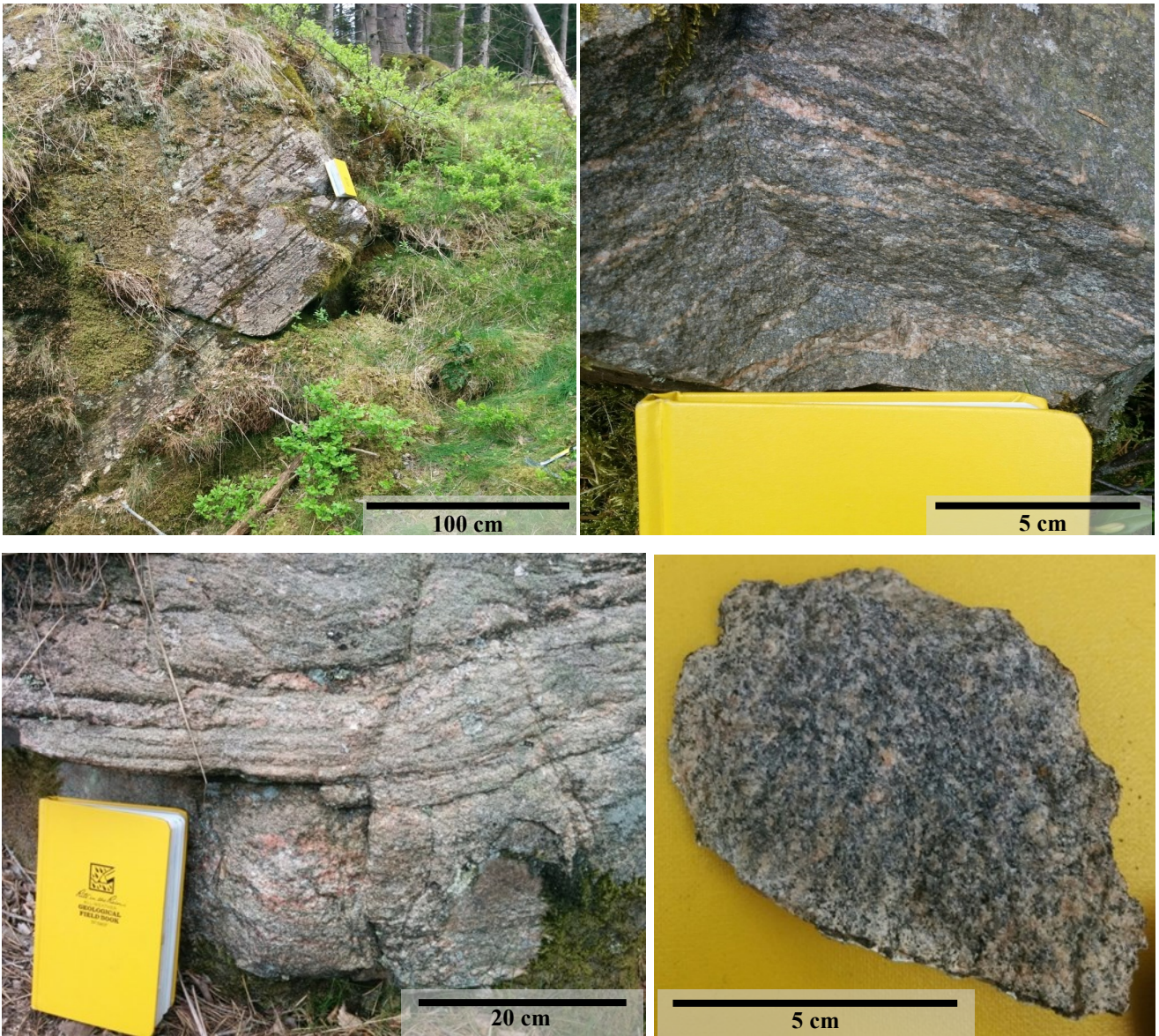


Figure 14. (Above): Sample 3m-ii is a granodioritic gneiss rich in plagioclase, with quartz and K-feldspar. (Below): Sample 3m-ii is a granodioritic gneiss rich in plagioclase, with quartz and K-feldspar.

biotite or a reflection of the protolith composition. No thin section is available for this sample. The zircon grains are up to 200  $\mu\text{m}$  along their c-axis, anhedral to subhedral with inclusions, and show varying amounts of zoning.

Of 6 analyses, 5 have a discordance of less than 10%. These analyses have a weighted mean  $^{207}\text{Pb}/^{206}\text{Pb}$  age of  $1693 \pm 12$  Ma, with an MSWD of 0.25.

#### 4.1.9 Sample 3a-iii (N57°58.703', E012°21.843')

Sample 3a-iii is a fine- to medium-grained granitic gneiss consisting of K-feldspar, abundant mafic minerals, quartz and maybe plagioclase. It is not dissimilar to the Brobacka type locality (4.5a-i), but has less K-feldspar and appears to be more strongly metamorphosed. No thin section is available for this sample. The zircon grains are around 100  $\mu\text{m}$  along their c-axis, subhedral and show varying amounts of zoning.

Of 37 analyses, 25 have a discordance of less than 10%. These analyses have a weighted mean

$^{207}\text{Pb}/^{206}\text{Pb}$  age of  $1692 \pm 3$  Ma, with an MSWD of 15 ( $1692 \pm 12$  Ma to 95% confidence;  $\text{MSWD} \times 2\sigma$ ). One analysis was discounted as an outlier (marked in red on Figure 17).

#### 4.1.10 Sample 3a-i (N57°58.703', E012°21.843')

Sample 3a-i is a fine- to medium-grained granitic gneiss consisting of K-feldspar porphyroclasts with a dark, sugary matrix of quartz. The thin section shows strongly altered and deformed feldspars, quartz ribbons and bands of aphanitic ground mass. Biotite and epidote are also present and orientate parallel to the foliation. The zircon grains are around 150  $\mu\text{m}$  along their c-axis, anhedral to subhedral and show varying amounts of zoning.

Of 32 analyses, 25 have a discordance of less than 10%. These analyses have a weighted mean  $^{207}\text{Pb}/^{206}\text{Pb}$  age of  $1705 \pm 3$  Ma, with an MSWD of 8.9 ( $1705 \pm 9$  Ma to 95% confidence;  $\text{MSWD} \times 2\sigma$ ). One analysis was discounted as an outlier (marked in red on Figure 17).



**Legend**

- A** Sample 3a-i
- B** Sample 3a-ii
- C** Sample 3a-iii
- D** Sample 3a-v
- E** Notable deformation
- \* Sample 3a-iv

\* Sample 3a-iv was not photographed. It is a thin, K-feldspar-poor horizon.

Figure 15. An overview of location 3a. Each letter is analysed in Figure 16.



Figure 16. A) Sample 3a-i. K-feldspar porphyroclasts with a dark matrix. B, Bii) Sample 3a-ii shows distinct surface banding and a more granodioritic composition than sample 3a-i or 3a-iii. C) Sample 3a-iii resembles Sample 3a-i and is dominated by K-feldspar. Sample 3a-iii resembles the sample taken from the Brobacka type locality at 2.5a (4.5a), but appears to be more strongly metamorphosed. D) Sample 3a-v, like Sample 3a-ii, is more granodioritic in composition, and does not resemble the sample from the Brobacka type locality. E) Strong folding and banding near Sample 3a-v, which requires further study.

## 4.2 Summary of results

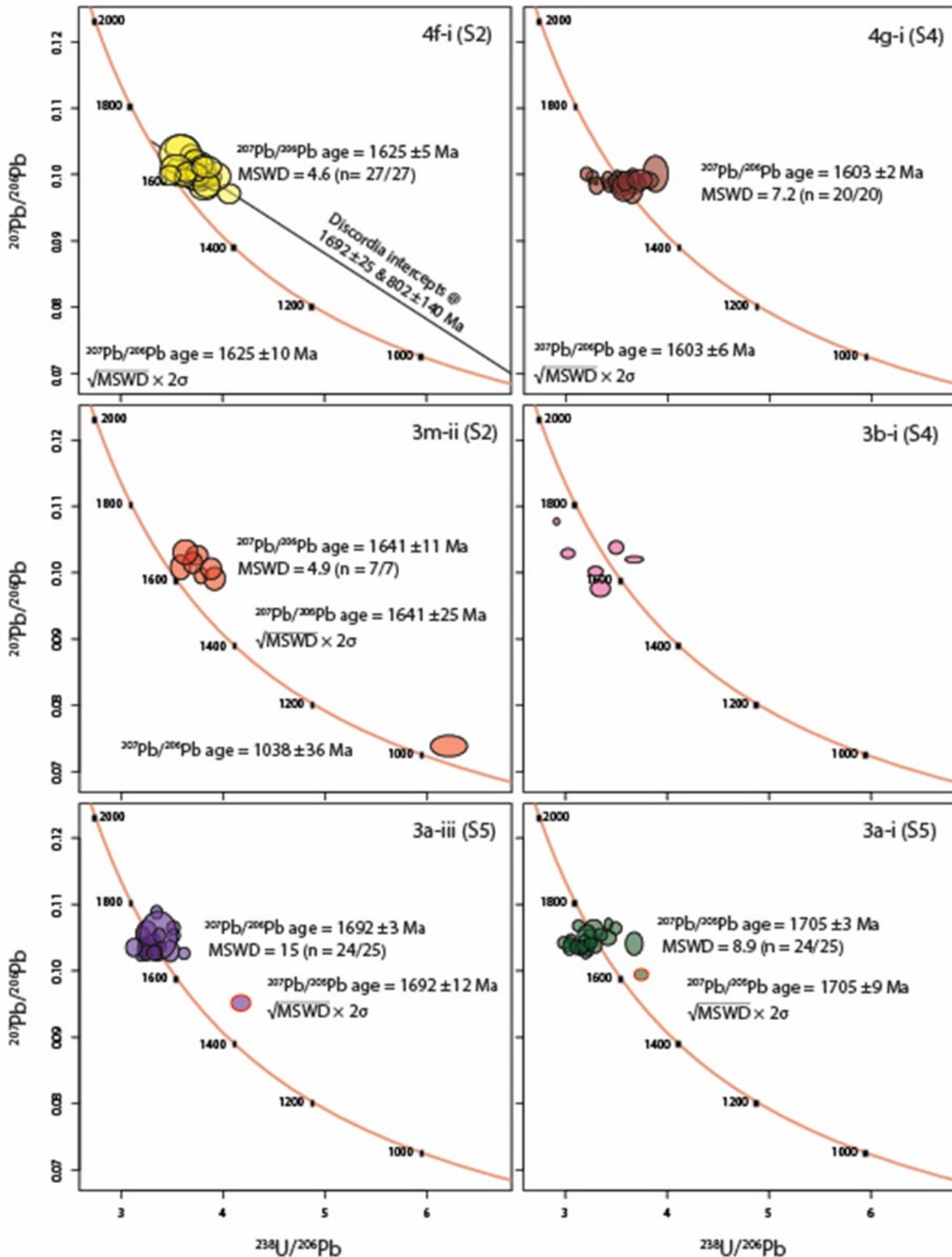


Figure 17. Tera-Wasserburg concordia diagrams showing all data points with  $\leq 10\%$  discordance. The data are not Pb corrected. MSWD = mean standard weighted deviation; n = number of samples considered in the age calculation. Where MSWD is very high, the age uncertainty is increased by multiplying  $\sqrt{\text{MSWD}}$  by  $2\sigma$ . Data points outlined in red were not considered in the age calculations. An arbitrary discordia intercept was produced for sample 4f-i to analyse the possibility that the upper intercept of  $1692 \pm 25$  Ma could be relevant. Given systematic discordance in the U-Pb system, the general Idefjorden signature of Pb-Pb ages, and the less plausible lower intercept age, it is likely that the discordia intercept is irrelevant.

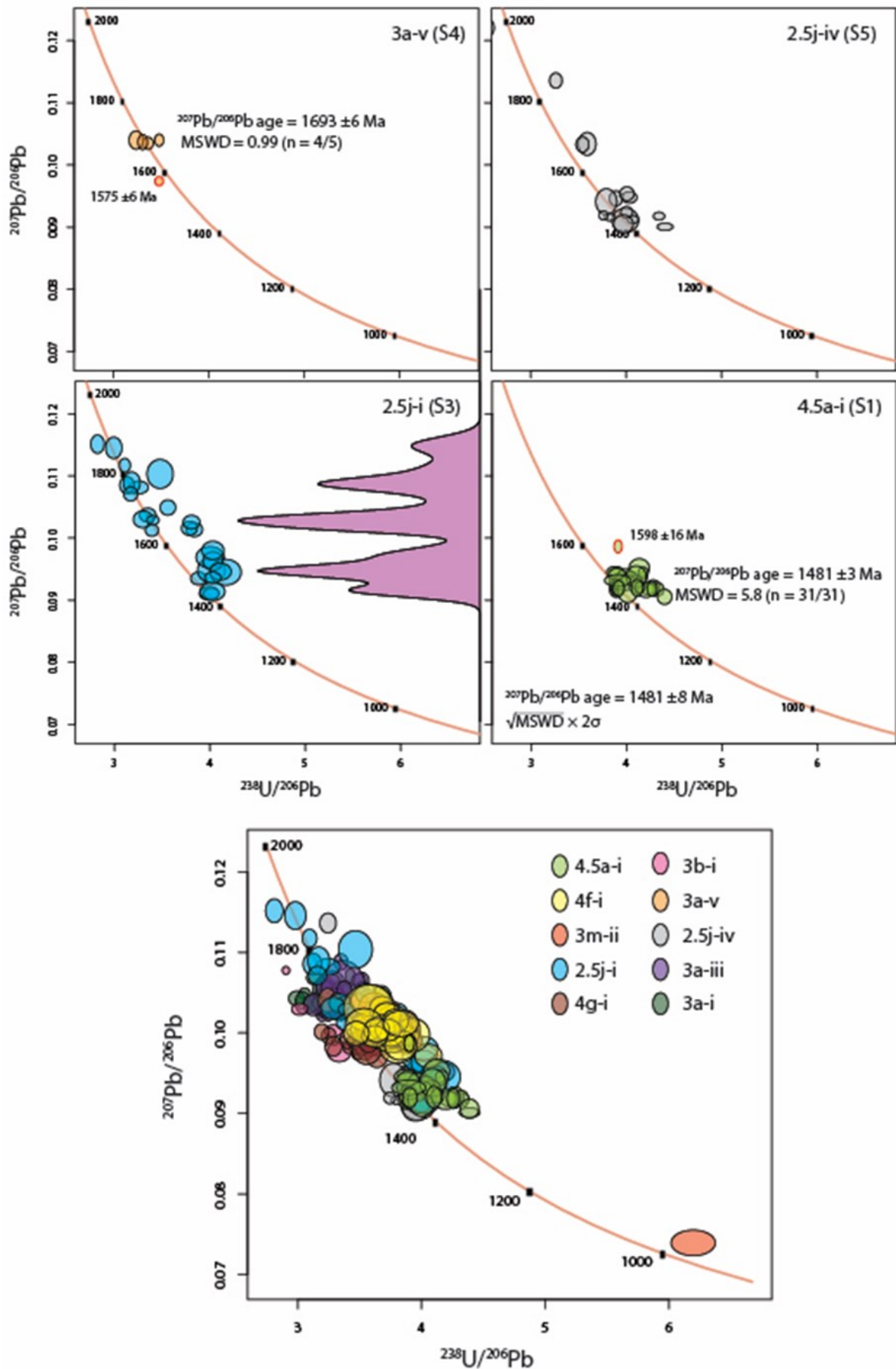


Figure 18. (Above): Tera-Wasserburg concordia diagrams showing all data points with  $\leq 10\%$  discordance. The data are not Pb corrected. MSWD = mean standard weighted deviation; n = number of samples considered in the age calculation. Where MSWD is very high, the age uncertainty is increased by multiplying  $\sqrt{\text{MSWD}}$  by  $2\sigma$ . Data points outlined in red were not considered in the age calculations. (Below): Combined Tera-Wasserburg Concordia diagram showing the data points of all samples. Eastern Segment and Idefjorden protolith signatures are visible, as are Hallandian-age signatures; almost no record of Sveconorwegian zircon growth is visible.

Table 2. An LA-ICP-MS data for all analysed zircons with a discordance of  $\leq 10\%$ .

Sample / Spot I.D.	Grain #	U (ppm)	Th (ppm)	Th/U	$^{206}\text{Pb}/^{204}\text{Pb}$	$^{238}\text{U}/^{206}\text{Pb}$	$^{207}\text{Pb}/^{206}\text{Pb} \pm \sigma$	$^{238}\text{U}/^{206}\text{Pb} \pm \sigma$	$^{207}\text{Pb}/^{206}\text{Pb} \pm \sigma$	Disc. %
<b>Sample 4.5a-i</b>										
Spot 01	1	202	240	1.188	169	3.909	0.017	0.0004	0.0986	8.1
Spot 02	1	424	243	0.574	313	4.137	0.016	0.0005	0.0905	5.3
Spot 03	3	446	85	0.191	349	3.882	0.026	0.0005	0.0926	0.8
Spot 04	3	247	203	0.822	195	3.900	0.017	0.0005	0.0929	-1.1
Spot 05	2	488	384	0.787	347	4.333	0.023	0.0005	0.0918	8.4
Spot 06	4	417	487	1.168	273	3.880	0.037	0.0006	0.0922	2.6
Spot 11	8	506	243	0.480	388	4.174	0.017	0.0003	0.0923	7.8
Spot 12	8	86	129	1.493	81	4.396	0.031	0.0004	0.0918	8.0
Spot 15	11	337	70	0.207	257	3.896	0.021	0.0005	0.0917	0.4
Spot 16	12	320	620	1.936	236	4.105	0.024	0.0007	0.0933	5.4
Spot 17	13	412	266	0.644	333	4.275	0.022	0.0009	0.0931	7.4
Spot 21	18	1444	176	0.122	929	3.906	0.031	0.0003	0.0925	0.1
Spot 22	19	181	124	0.685	144	4.223	0.028	0.0004	0.0944	6.4
Spot 25	22	318	192	0.604	239	3.887	0.027	0.0004	0.0915	-1.0
Spot 35	30	256	79	0.309	216	3.989	0.041	0.0005	0.0925	3.4
Spot 39	33	894	190	0.212	657	3.915	0.025	0.0005	0.0929	0.7
Spot 42	36	215	97	0.452	160	4.172	0.021	0.0004	0.0942	8.6
Spot 43	37	323	104	0.321	284	4.078	0.025	0.0004	0.0937	4.2
Spot 45	38	388	586	1.510	274	4.092	0.028	0.0005	0.0921	5.1
Spot 46	38	250	134	0.535	188	3.896	0.036	0.0009	0.0918	2.6
Spot 47	39	183	184	1.003	166	4.049	0.023	0.0005	0.0917	5.2
Spot 48	40	448	253	0.565	331	4.277	0.030	0.0004	0.0918	7.7
Spot 49	41	495	193	0.390	351	4.010	0.045	0.0007	0.0938	1.9

Sample / Spot I.D.	Grain #	U (ppm)	Th (ppm)	Th/U	$^{206}\text{Pb}/^{204}\text{Pb}$	$^{238}\text{U}/^{206}\text{Pb}$	$^{207}\text{Pb}/^{206}\text{Pb} \pm \sigma$	$^{207}\text{Pb}/^{206}\text{Pb} \pm \sigma$	$^{238}\text{U}/^{206}\text{Pb}$ (Ma)	$\pm \sigma$	$^{207}\text{Pb}/^{206}\text{Pb}$ (Ma)	$\pm \sigma$	Disc. %	
Spot 50	41	695	87	0.125	522	4.202	0.044	0.0921	0.0004	1376	13	1461	10	5.8
Spot 51	42	178	152	0.852	152	4.098	0.043	0.0932	0.0004	1407	13	1504	14	6.4
Spot 53	43	451	177	0.392	333	4.136	0.021	0.0920	0.0006	1396	6	1469	8	5.0
Spot 54	44	361	117	0.325	290	3.905	0.056	0.0918	0.0005	1470	19	1491	8	1.4
Spot 56	45	628	218	0.347	479	4.108	0.025	0.0911	0.0006	1404	8	1467	11	4.3
Spot 57	46	626	38	0.060	474	4.266	0.021	0.0919	0.0005	1358	6	1463	10	7.2
Spot 58	46	113	124	1.093	88	4.318	0.040	0.0952	0.0006	1343	11	1448	12	7.3
Spot 59	47	1365	42	0.031	916	3.914	0.024	0.1044	0.0010	1467	8	1465	10	-0.1
Spot 61	49	274	220	0.801	224	4.131	0.043	0.0945	0.0004	1398	13	1532	12	8.8
<b>Sample 4f-i</b>														
Spot 04	3	903	18	0.020		3.820	0.057	0.09780	0.00065	1499	20	1582	13	5.2
Spot 06	4	203	193	0.947		3.700	0.034	0.09890	0.00047	1542	13	1603	9	3.8
Spot 08	5	179	138	0.771		3.631	0.038	0.10040	0.00060	1568	15	1631	11	3.9
Spot 11	8	127	98	0.776		3.857	0.042	0.09940	0.00060	1486	14	1612	12	7.8
Spot 16	11	145	104	0.715		3.798	0.044	0.10030	0.00060	1507	16	1629	11	7.5
Spot 21	15	315	334	1.060		3.766	0.045	0.09930	0.00055	1518	16	1611	10	5.8
Spot 22	16	208	170	0.817		4.065	0.045	0.09710	0.00060	1418	14	1569	12	9.6
Spot 27	18	138	118	0.855		3.768	0.055	0.09920	0.00070	1517	20	1609	13	5.7
Spot 28	19	612	661	1.080		3.593	0.064	0.10050	0.00085	1583	25	1633	16	3.1
Spot 29	20	244	87	0.357		3.597	0.065	0.10400	0.00080	1581	25	1696	14	6.8
Spot 31	21	279	305	1.094		3.831	0.047	0.09970	0.00060	1495	16	1618	11	7.6
Spot 33	22	317	301	0.949		3.880	0.043	0.09960	0.00050	1478	15	1616	10	8.5
Spot 36	23	64	49	0.768		3.778	0.061	0.10080	0.00105	1514	22	1638	20	7.6
Spot 37	24	288	290	1.007		3.935	0.058	0.09970	0.00085	1460	19	1618	16	9.8
Spot 38	25	157	119	0.755		3.691	0.042	0.10290	0.00065	1545	15	1677	12	7.8
Spot 41	26	233	246	1.056		3.584	0.084	0.10300	0.00120	1586	33	1678	22	5.5
Spot 43	28	236	188	0.798		3.761	0.045	0.09990	0.00065	1520	16	1622	12	6.3

Sample / Spot I.D.	Grain #	U (ppm)	Th (ppm)	Th/U	$^{206}\text{Pb}/^{204}\text{Pb}$	$^{238}\text{U}/^{206}\text{Pb}$	$^{207}\text{Pb}/^{206}\text{Pb} \pm \sigma$	$^{238}\text{U}/^{206}\text{Pb} \pm \sigma$	$^{207}\text{Pb}/^{206}\text{Pb} \pm \sigma$	Disc. %			
Spot 44	29	163	132	0.808	3.730	0.046	0.10210	0.00065	1531	17	1662	12	7.9
Spot 47	32	153	115	0.749	3.691	0.041	0.10060	0.00065	1545	15	1635	12	5.5
Spot 48	33	156	106	0.680	3.842	0.053	0.09840	0.00075	1491	18	1594	14	6.4
Spot 50	34	282	105	0.371	3.546	0.063	0.10090	0.00085	1601	25	1640	16	2.4
Spot 52	35	171	142	0.831	3.798	0.043	0.10140	0.00060	1507	15	1649	11	8.6
Spot 59	38	198	134	0.674	3.740	0.042	0.10030	0.00055	1528	15	1629	10	6.2
Spot 61	39	243	219	0.901	3.631	0.042	0.09950	0.00055	1568	16	1614	11	2.8
Spot 64	40	133	130	0.976	3.647	0.042	0.10030	0.00060	1562	16	1629	11	4.1
Spot 68	42	170	162	0.951	3.482	0.042	0.09990	0.00060	1628	17	1622	11	-0.3
Spot 69	43	239	343	1.432	3.843	0.058	0.10110	0.00065	1491	20	1644	12	9.3
<b>Sample 3m-ii</b>													
Spot 70	1	235	198	0.844	3.744	0.043	0.10260	0.00060	1526	16	1671	11	8.7
Spot 72	2	462	434	0.939	3.583	0.040	0.10080	0.00075	1587	16	1638	14	3.1
Spot 73	3	196	172	0.878	3.917	0.042	0.09910	0.00070	1466	14	1607	13	8.8
Spot 74	3	145	136	0.937	3.782	0.026	0.09960	0.00050	1512	9	1616	10	6.4
Spot 75	4	304	322	1.061	3.883	0.041	0.10060	0.00065	1477	14	1635	12	9.7
Spot 76	5	187	1	0.004	6.215	0.073	0.07390	0.00065	962	11	1038	18	7.3
Spot 80	9	193	209	1.085	3.630	0.049	0.10310	0.00075	1569	19	1680	14	6.6
Spot 83	7	196	215	1.095	3.702	0.038	0.10150	0.00065	1541	14	1651	12	6.6
<b>Sample 2.5j-i</b>													
Spot 01	1	783	93	0.119	1,400	0.034	0.0935	0.0004	1478	12	1497	9	1.3
Spot 03	3	590	339	0.575	1,720	0.059	0.0948	0.0008	1434	19	1524	16	5.9
Spot 04	5	942	937	0.995	2,800	0.040	0.1081	0.0004	1726	19	1768	7	2.4
Spot 05	4	347	171	0.493	-800	0.031	0.1085	0.0006	1787	16	1774	9	-0.7
Spot 06	4	434	5	0.013	700	0.035	0.1037	0.0005	1684	16	1691	8	0.4
Spot 07	6	741	584	0.788	3,100	0.060	0.0969	0.0007	1438	19	1565	14	8.1



Sample / Spot I.D.	Grain #	U (ppm)	Th (ppm)	Th/U	$^{206}\text{Pb}/^{204}\text{Pb}$	$^{238}\text{U}/^{206}\text{Pb}$	$^{207}\text{Pb}/^{206}\text{Pb} \pm \sigma$	$^{238}\text{U}/^{206}\text{Pb} \pm \sigma$	$^{238}\text{U}/^{206}\text{Pb}$ (Ma)	$^{207}\text{Pb}/^{206}\text{Pb} \pm \sigma$	$^{207}\text{Pb}/^{206}\text{Pb}$ (Ma)	$\pm \sigma$	Disc. %
Spot 08	7	268	76	0.282	1,500	4.165	0.066	0.0009	1387	20	1518	17	8.6
Spot 10	9	423	149	0.352	480	4.032	0.043	0.0006	1428	14	1553	12	8.0
Spot 12	11	609	8	0.012	1,100	3.559	0.033	0.0005	1596	13	1712	9	6.8
Spot 16	15	1104	59	0.054	2,500	3.990	0.041	0.0004	1442	13	1448	10	0.4
Spot 21	19	837	308	0.368	3,700	4.110	0.046	0.0006	1404	14	1520	11	7.6
Spot 24	22	1328	275	0.207	1,500	4.014	0.033	0.0004	1434	11	1447	8	0.9
Spot 28	25	745	22	0.030	2,300	3.837	0.035	0.0005	1493	12	1649	8	9.5
Spot 29	26	994	202	0.203	2,100	3.478	0.056	0.0010	1629	23	1804	16	9.7
Spot 32	28	966	23	0.024	-2,200	3.785	0.034	0.0005	1511	12	1653	8	8.6
Spot 35	31	194	75	0.389	-60	2.822	0.029	0.0006	1955	17	1881	10	-3.9
Spot 37	31	1113	179	0.160	-300	4.027	0.053	0.0006	1430	17	1454	13	1.7
Spot 41	11	178	131	0.736	2,200	3.181	0.036	0.0007	1762	18	1781	12	1.0
Spot 43	32	410	55	0.135	3,700	2.992	0.035	0.0007	1859	19	1872	11	0.7
Spot 44	32	581	8	0.014	100	3.300	0.042	0.0006	1706	19	1678	10	-1.7
Spot 49	35	280	299	1.067	200	4.031	0.047	0.0006	1429	15	1586	12	9.9
Spot 51	37	285	195	0.685	-500	3.170	0.030	0.0005	1768	15	1750	8	-1.0
Spot 52	38	1109	9	0.008	4,800	3.403	0.026	0.0003	1661	11	1676	6	0.9
Spot 54	38	891	5	0.006	1,000	3.392	0.028	0.0004	1665	12	1647	7	-1.1
Spot 58	40	456	222	0.487	2,400	3.107	0.024	0.0005	1799	12	1826	8	1.5
Spot 59	41	611	499	0.817	800	4.029	0.035	0.0004	1429	11	1500	7	4.7
Spot 65	45	846	28	0.033	300	3.807	0.036	0.0005	1504	13	1670	8	10.0
<b>Sample 4g-i</b>													
Spot 01	1	212	168	0.793	-8,900	3.630	0.040	0.0006	1569	15	1597	12	1.8
Spot 02	2	289	410	1.418	100	3.563	0.031	0.0005	1595	12	1592	8	-0.2
Spot 03	3	198	149	0.752	1,420	3.408	0.020	0.0003	1658	9	1588	7	-4.4
Spot 04	4	131	112	0.850	250	3.446	0.020	0.0004	1643	8	1589	7	-3.4
Spot 05	5	192	184	0.959	-1,800	3.241	0.023	0.0004	1733	11	1616	8	-7.3

Sample / Spot I.D.	Grain #	U (ppm)	Th (ppm)	Th/U	$^{206}\text{Pb}/^{204}\text{Pb}$	$^{238}\text{U}/^{206}\text{Pb}$	$^{207}\text{Pb}/^{206}\text{Pb} \pm \sigma$	$^{238}\text{U}/^{206}\text{Pb} \pm \sigma$	$^{207}\text{Pb}/^{206}\text{Pb} \pm \sigma$	$^{207}\text{Pb}/^{206}\text{Pb}$ (Ma)	$\pm \sigma$	Disc. %		
Spot 07	6	189	135	0.712	-200	3.865	0.047	0.0011	0.1001	1483	16	1625	20	8.7
Spot 09	7	163	124	0.761	830	3.509	0.026	0.0005	0.0978	1616	11	1582	9	-2.2
Spot 11	8	232	219	0.944	1,300	3.501	0.025	0.0004	0.0995	1620	10	1615	7	-0.3
Spot 13	9	173	128	0.743	-1,100	3.184	0.023	0.0004	0.1001	1761	11	1625	7	-8.4
Spot 14	10	353	392	1.110	2,900	3.658	0.026	0.0006	0.0994	1558	10	1612	11	3.3
Spot 15	11	155	122	0.790	820	3.388	0.020	0.0005	0.0992	1667	9	1609	9	-3.6
Spot 17	12	262	234	0.894	800	3.512	0.025	0.0005	0.0984	1615	10	1594	8	-1.3
Spot 18	13	203	182	0.897	1,200	3.625	0.041	0.0010	0.0981	1571	16	1588	18	1.1
Spot 20	14	248	296	1.195	1,500	3.482	0.019	0.0004	0.0996	1628	8	1616	9	-0.7
Spot 21	15	238	190	0.800	700	3.457	0.024	0.0004	0.0990	1638	10	1604	7	-2.1
Spot 23	17	268	353	1.317	-1,300	3.782	0.037	0.0005	0.0991	1512	13	1606	8	5.8
Spot 25	18	247	273	1.105	3,600	3.311	0.026	0.0005	0.0983	1701	12	1592	9	-6.9
Spot 26	19	170	189	1.112	800	3.568	0.050	0.0008	0.0980	1593	20	1586	15	-0.4
Spot 27	20	207	191	0.925	1,800	3.547	0.031	0.0006	0.0990	1601	12	1605	10	0.3
Spot 28	21	166	201	1.211	1,300	3.652	0.047	0.0006	0.0992	1560	18	1609	11	3.0
<b>Sample 3b-i</b>														
Spot 31	2	425	294	0.692	-1,700	3.484	0.028	0.0004	0.1038	1627	12	1693	7	3.9
Spot 32	3	521	218	0.418	-1,800	3.241	0.027	0.0003	0.1002	1733	13	1626	5	-6.6
Spot 33	5	948	742	0.783	4,700	3.602	0.034	0.0002	0.1020	1579	13	1660	4	4.9
Spot 35	7	743	307	0.414	200	2.904	0.011	0.0002	0.1077	1908	6	1760	3	-8.4
Spot 41	12	760	125	0.164	-1,600	3.299	0.040	0.0005	0.0976	1707	18	1577	9	-8.2
<b>Sample 3a-v</b>														
Spot 45	2	1132	55	0.048	8,700	3.465	0.017	0.0003	0.0974	1635	7	1575	6	-3.8
Spot 46	3	216	103	0.478	900	3.230	0.031	0.0006	0.1040	1739	15	1696	10	-2.5
Spot 47	3	258	108	0.418	-3,900	3.339	0.024	0.0004	0.1035	1689	11	1688	8	0.0
Spot 48	5	1322	740	0.560	8,600	3.455	0.019	0.0004	0.1040	1639	8	1696	6	3.4

Sample / Spot I.D.	Grain #	U (ppm)	Th (ppm)	Th/U	$^{206}\text{Pb}/^{204}\text{Pb}$	$^{238}\text{U}/^{206}\text{Pb}$	$^{207}\text{Pb}/^{206}\text{Pb} \pm \sigma$	$^{238}\text{U}/^{206}\text{Pb} \pm \sigma$	$^{207}\text{Pb}/^{206}\text{Pb} \pm \sigma$	Disc. %				
Spot 49	6	264	124	0.470	400	3.291	0.020	0.1037	0.0005	1711	9	1692	8	-1.1
<b>Sample 2.5j-iv</b>														
Spot 04	5	672	390	0.580	5,200	3.893	0.028	0.09462	0.00049	1474	9	1520	10	3.0
Spot 05	6	1383	79	0.057	6,000	3.990	0.057	0.09110	0.00080	1442	18	1448	17	0.4
Spot 08	9	709	368	0.519	2,400	3.263	0.027	0.11358	0.00050	1723	12	1857	8	7.2
Spot 10	11	1773	2060	1.162	6,600	3.792	0.045	0.09410	0.00085	1509	16	1510	17	0.1
Spot 11	12	554	779	1.406	700	4.005	0.026	0.09238	0.00038	1437	8	1475	7	2.6
Spot 12	13	2604	2057	0.790	18,300	4.070	0.024	0.09124	0.00026	1416	8	1451	6	2.4
Spot 13	14	494	548	1.109	200	3.542	0.028	0.10330	0.00050	1603	11	1684	9	4.8
Spot 15	15	110	120	1.093	910	3.970	0.042	0.09050	0.00060	1448	14	1436	12	-0.9
Spot 16	17	998	1326	1.329	4,100	4.344	0.024	0.09178	0.00026	1336	7	1462	6	8.6
Spot 17	21	207	110	0.532	1,100	2.582	0.014	0.12206	0.00045	2110	10	1986	7	-6.3
Spot 19	23	981	1299	1.324	800	3.830	0.023	0.09161	0.00024	1495	8	1459	5	-2.5
Spot 22	26	404	444	1.099	2,590	4.034	0.032	0.09479	0.00038	1428	10	1523	8	6.3
Spot 23	27	2403	1890	0.787	10,000	4.407	0.034	0.09007	0.00024	1318	9	1427	5	7.6
Spot 24	31	254	201	0.789	1,100	3.762	0.019	0.09189	0.00030	1519	7	1465	6	-3.7
Spot 27	33	539	102	0.188	2,910	4.008	0.031	0.09538	0.00045	1436	10	1535	9	6.5
<b>Sample 3a-i</b>														
Spot 30	2	316	164	0.519	46,000	3.243	0.027	0.10360	0.00050	1733	13	1689	9	-2.6
Spot 33	5	899	44	0.049	1,800	4.174	0.038	0.09516	0.00048	1385	11	1531	9	9.6
Spot 34	5	159	84	0.526	-80	3.323	0.029	0.10390	0.00070	1696	13	1694	13	-0.1
Spot 35	7	334	201	0.602	4,000	3.210	0.027	0.10551	0.00048	1748	13	1723	8	-1.5
Spot 36	8	375	273	0.728	-100	3.304	0.030	0.10368	0.00031	1705	14	1691	5	-0.8
Spot 37	8	236	117	0.497	400	3.323	0.017	0.10302	0.00032	1696	7	1679	5	-1.0
Spot 38	12	495	521	1.053	4,200	3.348	0.023	0.10880	0.00041	1685	10	1779	7	5.3
Spot 39	13	312	167	0.536	900	3.512	0.026	0.10648	0.00042	1615	11	1740	7	7.2

Sample / Spot I.D.	Grain #	U (ppm)	Th (ppm)	Th/U	$^{206}\text{Pb}/^{204}\text{Pb}$	$^{238}\text{U}/^{206}\text{Pb}$	$^{207}\text{Pb}/^{206}\text{Pb} \pm \sigma$	$^{238}\text{U}/^{206}\text{Pb} \pm \sigma$	$^{207}\text{Pb}/^{206}\text{Pb} \pm \sigma$	$^{238}\text{U}/^{206}\text{Pb}$ (Ma)	$^{207}\text{Pb}/^{206}\text{Pb} \pm \sigma$	Disc. %	
Spot 40	15	208	99	0.476	730	3.617	0.023	0.00036	0.10264	1574	9	6	5.9
Spot 42	16	1050	514	0.490	2,500	3.252	0.041	0.00080	0.10560	1728	19	14	-0.3
Spot 43	19	278	132	0.473		3.310	0.030	0.00040	0.10455	1702	13	7	0.3
Spot 45	21	177	85	0.478	-2,800	3.248	0.013	0.00033	0.10256	1730	6	6	-3.6
Spot 46	25	509	229	0.450	1,700	3.519	0.023	0.00042	0.10532	1612	9	8	6.2
Spot 49	28	363	199	0.546	-1,600	3.222	0.019	0.00040	0.10403	1743	9	7	-2.7
Spot 50	30	992	191	0.192	71,000	3.397	0.020	0.00028	0.10360	1663	8	5	1.5
Spot 52	32	991	417	0.421	6,900	3.484	0.034	0.00065	0.10300	1627	14	12	3.1
Spot 55	35	580	359	0.619	3,700	3.367	0.074	0.00150	0.10530	1676	32	26	2.5
Spot 57	37	446	221	0.496	11,800	3.350	0.022	0.00030	0.10227	1684	10	6	-1.1
Spot 59	40	318	122	0.384	3,500	3.195	0.018	0.00029	0.10219	1755	9	5	-5.5
Spot 60	42	218	121	0.557	-3,000	3.202	0.017	0.00050	0.10320	1752	8	9	-4.2
Spot 62	46	301	146	0.485	2,500	3.375	0.024	0.00044	0.10534	1673	11	7	2.7
Spot 63	48	427	118	0.276	-6,900	3.246	0.022	0.00050	0.10270	1731	10	9	-3.5
Spot 64	50	459	237	0.517	3,300	3.338	0.023	0.00036	0.10313	1689	10	6	-0.5
Spot 65	53	435	176	0.405	-1,200	3.321	0.028	0.00045	0.10270	1697	12	8	-1.4
Spot 66	51	317	134	0.422	1,800	3.126	0.032	0.00055	0.10350	1789	16	10	-6.1
<b>Sample 3a-iii</b>													
Spot 68	8	233	104	0.447	300	3.025	0.014	0.00034	0.10374	1841	9	6	-8.8
Spot 69	9	250	116	0.466		3.141	0.017	0.00034	0.10340	1782	18	6	-5.7
Spot 70	12	231	132	0.571	700	3.278	0.040	0.00070	0.10600	1717	17	12	0.8
Spot 73	14	808	393	0.486	1,700	3.130	0.024	0.00034	0.10679	1787	7	6	-2.4
Spot 75	15	245	126	0.513	2,500	3.243	0.023	0.00060	0.10490	1733	17	11	-1.2
Spot 77	16	274	127	0.463	2,900	3.745	0.028	0.00034	0.09943	1526	9	6	5.4
Spot 78	22	237	110	0.464	-410	3.230	0.020	0.00044	0.10326	1739	9	8	-3.3
Spot 79	23	375	114	0.305	3,400	3.125	0.019	0.00037	0.10360	1790	10	7	-6.0
Spot 80	24	733	346	0.472	7,300	3.055	0.019	0.00030	0.10480	1825	13	5	-6.7

Sample / Spot I.D.	Grain #	U (ppm)	Th (ppm)	Th/U	$^{206}\text{Pb}/^{204}\text{Pb}$	$^{238}\text{U}/^{206}\text{Pb}$	$^{207}\text{Pb}/^{206}\text{Pb} \pm \sigma$	$^{238}\text{U}/^{206}\text{Pb} \pm \sigma$	$^{207}\text{Pb}/^{206}\text{Pb} \pm \sigma$	Disc. %				
Spot 82	27	210	97	0.462	1,600	3.214	0.038	0.00070	0.10520	1746	10	1717	12	-1.7
Spot 83	27	286	152	0.532		3.198	0.021	0.00047	0.10300	1754	12	1678	9	-4.5
Spot 84	28	202	100	0.496	600	3.187	0.025	0.00055	0.10410	1759	7	1698	10	-3.6
Spot 85	29	325	222	0.685	-900	3.191	0.015	0.00029	0.10353	1757	11	1688	5	-4.1
Spot 87	31	394	98	0.249	1,400	2.990	0.026	0.00037	0.10423	1860	11	1700	7	-9.4
Spot 88	32	261	138	0.527	1,700	3.154	0.022	0.00044	0.10337	1776	13	1685	8	-5.4
Spot 89	33	225	105	0.467	-1,600	3.040	0.025	0.00055	0.10370	1833	12	1691	10	-8.4
Spot 90	34	641	155	0.241	-1,000	3.294	0.027	0.00048	0.10388	1709	7	1694	8	-0.9
Spot 91	34	137	120	0.879	70	3.423	0.016	0.00035	0.10703	1652	12	1749	6	5.5
Spot 92	37	269	139	0.518	-1,000	3.107	0.023	0.00044	0.10359	1799	11	1689	8	-6.5
Spot 93	38	300	154	0.514	2,900	3.176	0.022	0.00039	0.10364	1765	14	1690	7	-4.4
Spot 94	36	591	390	0.660	3,700	3.416	0.034	0.00045	0.10498	1655	12	1713	8	3.4
Spot 95	39	432	574	1.328	-400	3.248	0.025	0.00035	0.10414	1730	10	1699	6	-1.8
Spot 96	40	392	471	1.202	3,900	3.493	0.024	0.00037	0.10641	1623	11	1738	7	6.6
Spot 97	43	297	152	0.511	-33,000	3.348	0.026	0.00039	0.10544	1685	13	1722	6	2.2
Spot 99	44	592	339	0.573	2,400	3.675	0.034	0.00070	0.10410	1551	12	1698	12	8.6

## 5 Discussion

### 5.1 Validity of the results

Given the nature of my results, the possibility of exaggerated errors cannot be discounted, both in the field and the laboratory. During fieldwork I focused on tracing the Brobacka-type unit mentioned by Lundqvist et al. (2005; marked in this paper as location 2.5a – sample 4.5a-i) westward into B-Bulan to trace the Hallandian signature and determine the units directly above and below the unit. As a result, I favoured units that closely resembled the composition of sample 4.5a-i (K-feldspar-rich with porphyroblasts) resulting in a degree of sample bias. This explains why, of ten samples chosen for U-Pb analysis, five samples are from two locations of particular interest, location 2.5j and location 3a. It is inevitable that, under time and cost constraints, my samples would be biased towards those that showed a resemblance to the Brobacka sample (4.5a-i) than, for example, typical Idefjorden granodiorites. Nevertheless, sample bias is restricted to the samples I chose for U-Pb analysis, rather than the samples I chose to record and describe (see Appendix 1).

One regrettable mistake was the quality of sampling. Sample size was a problem, as I often didn't take large enough samples for a comprehensive analysis, which affected my ability to produce thin sections and pick zircons for some samples. In the laboratory I aimed to pick 50 zircons per sample, for time reasons, but in some samples I was unable to find more than a dozen. Had I taken a larger sample to begin with, this may have been less of a challenge. Further, when polishing my picked zircons, I did an unsatisfactory job – they could have been polished to a much greater extent – which then made selecting spots for analysis considerably more difficult. When analysing zircons with complex zoning patterns, it was important to be able to distinguish an igneous core from a metamorphic rim.

Some samples showed distinct zoning patterns (such as 4.5a-i), either due to their texture or degree of polishing, whereas others appeared not to show any zoning. In these instances, I decided to analyse an area near the mid-point of the zircon, assuming that it would represent the core (see sample 3b-i in Appendix 10). The presence of inclusions in some zircons also increased the likelihood of erroneous analysis.

Of course, when dealing with complex zircon patterns such as those with Hallandian metamorphic growth patterns, greater complexity leads to a greater potential for error. Rather than just dealing with igneous zircon, you could be analysing a zircon that has experienced new zircon growth during a metamorphic event, possibly with associated Pb loss, and developed complex core-rim zoning that, if not analysed carefully, could produce a mixed age of protolith and later metamorphic growth.

However, despite the challenges listed above, the main sources of error in my results are likely due to calibration issues related to the LA-ICP-MS machine. The problems associated with the secondary standard, 91500, cannot be accounted for by any of the errors listed above, and instead rely either on the quality of

the secondary standard or the calibration of the measuring instrument, the LA-ICP-MS. If the former, the variable  $^{207}\text{Pb}/^{206}\text{Pb}$  (and  $^{238}\text{U}/^{206}\text{Pb}$ ) ratios suggest a mixture of Pb loss and common Pb in the sample, but if the latter then it suggests that the calibration problem is not limited to the secondary standard, but will have affected many of the samples also.

The most plausible explanation is that calibration issues with the LA-ICP-MS were responsible for the discrepancies in the 91500 standard, which were magnified by its low U and Pb count. Because calibration issues were more prevalent in U-Pb analyses than Pb-Pb analyses, U-Pb was used only as a visual representation of the dataset (see Figure 17 and Figure 18), while ages were calculated using Pb-Pb.

Pb-corrected results were not used, as they didn't show an obvious improvement on uncorrected results and produced their fair share of discrepancies. On reflection, sample 4.5a-i, dated to 1450 Ma by Lundqvist et al. (2005) has a weighted mean  $^{207}\text{Pb}/^{206}\text{Pb}$  age of  $1481 \pm 3$  Ma, which is older than previously-recorded Hallandian metamorphism and could be partially explained by the presence of common-Pb, which would make the zircons appear older. As discussed in Section 3.5.3, I decided not to apply a Pb correction to my results, due to the potential for overcorrection.

Results were filtered to show only those with a discordance of less than 10%. As discussed in Section 3.5.4, this was done to draw meaningful conclusions from the results and to avoid diluting the datasets with unreasonably discordant results which would not have given a reliable age. Some outliers that were less than 10% discordant were not factored into age calculations, but these are marked in red on Figure 17 and Figure 18.

Because of the above, these results should be used as guidelines, with general conclusions drawn.

### 5.2 Interpretation of the results

The  $^{207}\text{Pb}/^{206}\text{Pb}$  ages of samples analysed shows the presence of Idefjorden and Eastern Segment signatures, as well as a potential Hallandian signature in a small number of samples. This is interesting because the study area was previously considered to be a part of the Idefjorden terrane, further west of the Eastern Segment and associated Hallandian metamorphism.

At the easternmost sampling location, location 2.5a (revisited on day 4 as location 4.5a), Hallandian-age zircons are recorded in sample 4.5a-i – this is expected, due to the close proximity to the study of Lundqvist et al. (2005). The higher than expected age of  $1481 \pm 3$  Ma is puzzling, as the Hallandian orogeny is defined at 1.47-1.38 Ga (Ulmius et al. 2015). The most plausible reason is that the calibration of my  $^{207}\text{Pb}/^{206}\text{Pb}$  ages is slightly inaccurate, and perhaps with a correction for common Pb the age would come down to below 1.47 Ga. Another possibility is that Hallandian metamorphism is older than previously thought. While it is possible that it could represent something other than a Hallandian age, it is less plausible; other than localised mafic dyke swarms recorded further afield at 1.50 and 1.46 Ga (Åhäll & Connelly 1998; Åhäll & Connelly 2008), the units

closest in age in the surrounding Idefjorden terrane are  $1526 \pm 15$  and  $1530 \pm 18$  Ma (Åhäll 1991; see Table 1), belonging to the Stenungsund granite, which is more than 45 million years older.

At location 2.5j, samples 2.5j-i and 2.5j-iv show multiple zircon populations and complex field relationships which require closer examination. In the field, this location marks a transition zone between Brobacka-type gneiss (sample 4.5a) above and granodiorite gneiss below. A cluster of zircons in each sample show Hallandian signatures (see Table 2), as well as Eastern Segment and perhaps Idefjorden signatures. This is difficult to interpret, especially considering the reliability of the geochronology (the MSWD is high – probably due to geological factors), but is of great interest for future study. The relative lack of alteration in thin section and absence of any evidence of Sveconorwegian zircon growth suggest that this sample avoided high-pressure, high-temperature metamorphism during the Sveconorwegian orogeny. Sample 4f-i shows an Idefjorden signature, as expected. According to Figure 20, it is likely to fall on the border of B-Bulan, very close to the Idefjorden terrane. Given the location, paucity of Eastern Segment dates recorded in the analysis, the general offset in U-Pb ages to the right of the concordia, and the less plausible metamorphic age of  $802 \pm 140$  Ma, it is very unlikely that the discordia intercept (represented on Figure 17) of  $1692 \pm 25$  Ma represents the true protolith age of this sample.

Sample 4g-i, like sample 4f-i, shows an Idefjorden signature, which is unsurprising given its location in the north of my field area. Despite intermediate

alteration and deformation observed in thin section, the lack of recorded metamorphic zircon makes it difficult to determine the timing of metamorphism. Analysis of titanite could give a metamorphic age.

Age data from sample 3m-ii are limited, but some speculative conclusions can be drawn. The lack of good data is likely due to the small sample size (only 13 zircons were analysed, eight of which were less than 10% discordant) and the unreliability of session 2 (see Figure 7). Despite unreliable  $^{207}\text{Pb}/^{206}\text{Pb}$  ages, the thin section shows hornblende, epidote and chlorite, with a distinct lack of K-feldspar (see Appendix 5). This may indicate an Idefjorden protolith, rather than the more felsic Eastern Segment protoliths.

Age data from sample 3b-i are not reliable enough to draw conclusions. The presence of rutile with coronitic texture in thin section is interesting, as it suggests high-pressure and/or high-temperature conditions. The question is: which metamorphic event is responsible for the formation of rutile?

Samples taken at location 3a all show strong Eastern Segment signatures, with no recorded Hallandian metamorphism. The thin section for 3a-i shows intermediate alteration and deformation, but the metamorphic event associated with deformation is not apparent from the U-Pb analysis.

### 5.3 A window into the Eastern Segment?

Eastern Segment ages are recorded at location 3a, in three of the samples analysed (samples 3a-i, 3a-iii and 3a-v), and Eastern Segment-age zircon populations are

*Table 3.* Interpretation of all samples dated in my field area. Green represents a Hallandian-age signature, as seen at 4.5a-i (the Brobacka type locality), red represents a mixed age, brown represents an Idefjorden age, and light blue represents an Eastern Segment age. A visual representation of this is seen in Figure 20.

Sample	Description	Age	Interpretation
4.5a-i	Medium-coarse grained gneiss with an abundance of deformed K-feldspar surrounded by quartz, plagioclase and biotite.	$1481 \pm 8$ Ma (dated by Lundqvist et al. (2005) to 1450 Ma)	Hallandian signature, and represents both the igneous protolith and the subsequent metamorphism.
2.5j-i	Medium-grained granitic gneiss made up of K-feldspar, plagioclase and quartz with abundant biotite. Less deformed than other samples in the area.	Mixed; at least three distinct zircon populations	Transition zone between Brobacka-type gneiss (4.5a-i) above and granodiorite gneiss below.
2.5j-iv	Medium-coarse grained granitic gneiss consisting of K-feldspar, quartz, minor plagioclase and biotite. Mica content varies; contains K-feldspar megacrysts.	Mixed; at least three distinct zircon populations	May suggest the presence of Eastern Segment, Idefjorden and Hallandian populations within one sample. Alternatively, the Idefjorden signature could be a mixed age due to careless polishing and analysis.
4f-i	Medium-grained granitic gneiss rich in plagioclase with notable quantities of quartz and K-feldspar.	$1625 \pm 10$ Ma	Idefjorden signature, and represents the igneous protolith.
4g-i	Medium-grained granitic gneiss, consisting of plagioclase, quartz and K-feldspar with abundant biotite.	$1603 \pm 6$ Ma	Idefjorden signature, and represents the igneous protolith.
3m-ii	Fine- to medium-grained granodioritic gneiss rich in plagioclase, with quartz and K-feldspar.	$1641 \pm 25$ Ma	Idefjorden, upper limit, with an error bar large enough to be an Eastern Segment age. Requires further attention.
3b-i	Medium-grained granitic-granodioritic gneiss with plagioclase, quartz, minor K-feldspar and abundant biotite.	-	N/A - analyses are too discordant
3a-v	Fine- to medium-grained granitic gneiss consisting of quartz, plagioclase and K-feldspar.	$1693 \pm 12$ Ma	Eastern Segment signature, and represents the igneous protolith.
3a-iii	Fine- to medium- grained granitic gneiss consisting of K-feldspar, abundant mafic minerals, quartz and maybe plagioclase.	$1692 \pm 12$ Ma	Eastern Segment signature, and represents the igneous protolith.
3a-i	Fine- to medium-grained granitic gneiss consisting of K-feldspar porphyroclasts with a dark, sugary matrix of quartz.	$1705 \pm 9$ Ma	Eastern Segment signature, and represents the igneous protolith.

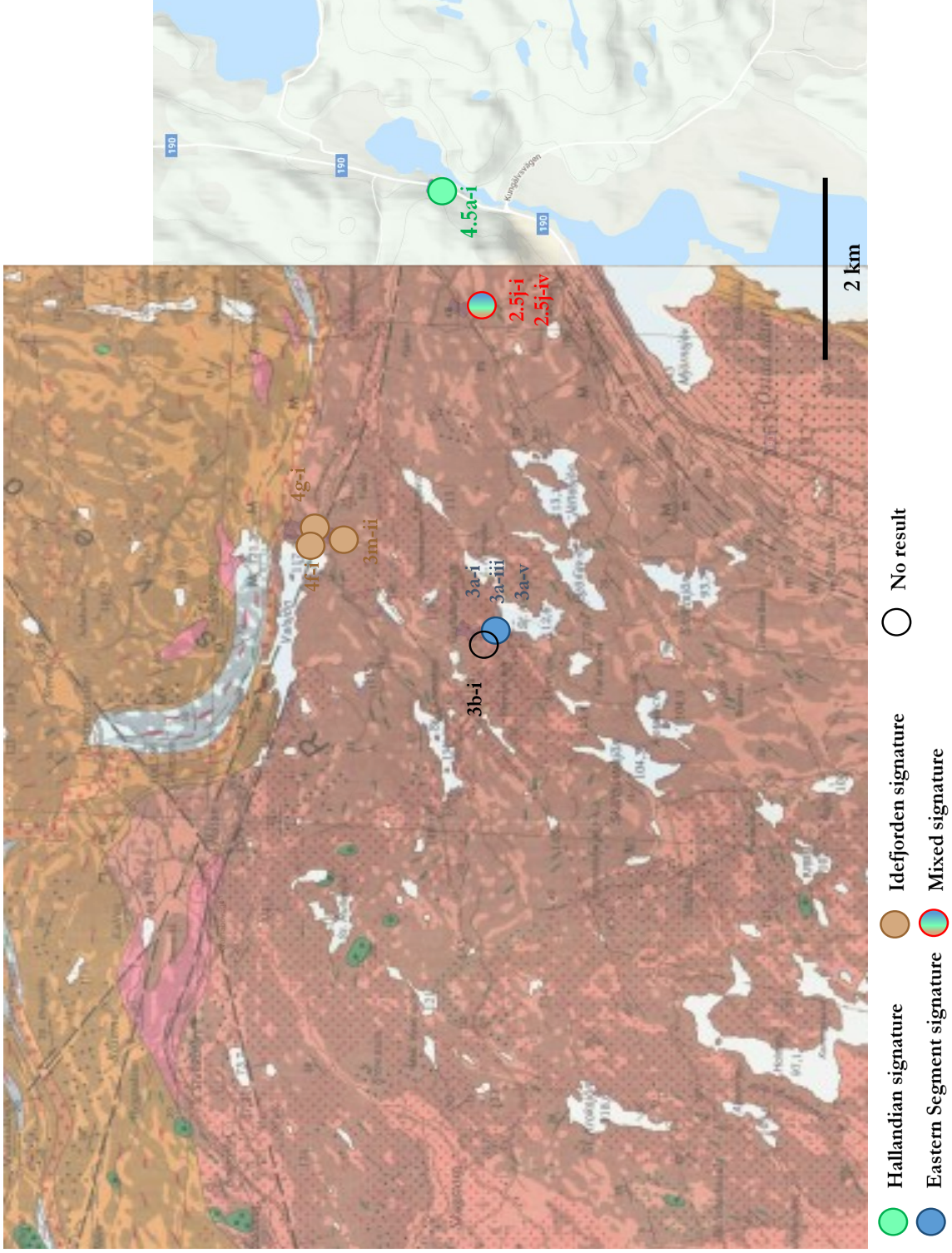


Figure 19. A visual representation of Table 3 showing the location of the samples dated overlain onto Samuelsson's (1982) Swedish Geological Survey map - refer to Appendix 12 for legend. The map, not the equivalent map to the east, doesn't cover location 4.5a-i (the Brobacka location), so a terrain map has been used. Map data © 2019 Google.



recorded at location 2.5j (sample 2.5j-i and 2.5j-iv). This study shows the presence of Eastern Segment-aged units within B-Bulan, something which has not been previously observed.

Evidence of Eastern Segment signatures further west than previously recorded requires an explanation that this study alone is unable to provide. One possibility may be that part of B-Bulan provides a tectonic window into the Eastern Segment, possibly emplaced in its current position through faulting and erosion. Given that this area lies between the Mylonite Zone and the Göta Alv Shear Zone (GÄSZ), which records movement at 0.97 Ga (Austin Hegardt 2010), it is likely that these two shear zones have played an important role in the emplacement of Eastern Segment units and the architecture of B-Bulan. Further, the lack of evidence for metamorphic zircon growth dating to the Sveconorwegian orogeny and relative lack of deformation at location 3a may point to this area being in a pressure shadow during the Sveconorwegian orogeny. Without further study, this is just speculation.

#### 5.4 Evidence of a common pre-Sveconorwegian history?

Hallandian metamorphism outside of B-Bulan within the Idefjorden terrane has not been recorded. And within B-Bulan, the presence of Hallandian-aged zircons, indicated by 1.47-1.38 Ga signatures, is confined to an east-west trending transect between location 2.5a and 2.5j. Evidence of Hallandian-age zircon signatures is not recorded at any locations visited on day 3 or day 4 (location 3a to location 4g).

One possible reason why the Hallandian-age unit has not been observed to continue further west is because it has been folded, and follows the general shape of B-Bulan – as the magnetic anomaly in Figure 4 would suggest. If this is the case, I would expect to observe the unit to the south of 2.5j, rather than to the west.

While evidence of Hallandian metamorphism within the Idefjorden terrane has not been clearly outlined, the presence of Idefjorden- and Hallandian-age populations at location 2.5j is of great interest. Whether the populations represent Idefjorden-age zircons, are merely a mixed age consisting of Eastern Segment and Hallandian signatures, or are just a result of common-Pb in the sample providing a deceptively high age is yet to be determined.

If Hallandian metamorphism can be linked to Idefjorden protoliths, which at the moment it is not clear that it can be, the implications for the evolution of SW Sweden would be significant. It would suggest that the Idefjorden terrane and Eastern Segment were together around 1.47 Ga, long before the Sveconorwegian orogeny, and therefore that the Sveconorwegian orogeny would have had a major phase of accretion, rather than collision between the Idefjorden terrane and the Eastern Segment, because both terranes had been together for at least 350 million years.

However, the only definitive result of this study is the presence of Eastern Segment protoliths further west than previously defined. Other suggestions are just speculation.

## 6 Conclusions

- Eastern Segment protolith ages are recorded in five samples at two locations (2.5j and 3a). At location 3a, samples show weighted mean  $^{207}\text{Pb}/^{206}\text{Pb}$  ages of  $1693 \pm 12$  Ma (3a-v),  $1692 \pm 3$  Ma (3a-iii) and  $1705 \pm 3$  Ma (3a-i). At location 2.5j, zircon populations of Eastern Segment age are observed between 1850 and 1650 Ma (2.5j-i) and around 1685 Ma (2.5j-iv). All of these locations are within B-Bulan.
- Hallandian signatures are recorded in three samples at two locations (2.5a and 2.5j). At location 2.5a, sample 4.5a (location revisited on day 4, hence the discrepancy) shows a weighted mean  $^{207}\text{Pb}/^{206}\text{Pb}$  age of  $1481 \pm 3$  Ma, which is slightly older than recorded Hallandian ages, but is interpreted to be Hallandian in origin due to its similarity to the sample analysed by Lundqvist et al. (2005); the discrepancy is possibly due to either a calibration inaccuracy or the presence of common Pb, both of which could account for the slightly older date. At location 2.5j, zircon populations of approximately Hallandian age are observed around 1500 to 1450 Ma (2.5j-i) and 1480 to 1430 Ma (2.5j-iv).
- Idefjorden signatures are recorded in three samples at three locations (4f-i, 4g-i and 3m-ii). They show weighted mean  $^{207}\text{Pb}/^{206}\text{Pb}$  ages of  $1625 \pm 5$  Ma (4f-i),  $1603 \pm 4$  Ma (4g-i) and  $1641 \pm 11$  Ma (3m-ii).
- Eastern Segment protoliths and Hallandian signatures are present further west than previously acknowledged.
- B-Bulan, showing Eastern Segment, Idefjorden and Hallandian signatures, is more complex than current maps suggest.
- Evidence of Sveconorwegian zircon growth is lacking in B-Bulan, even in Eastern Segment units.
- Knowledge of B-Bulan needs to be improved to determine its structural relationship to the Idefjorden terrane. It is bounded by shear zones on all sides.

## 7 Future studies

- A structural study at the margins of B-Bulan to constrain the extent of the shear zones and characterise the nature and structural relations of the Mylonite Zone and Göta Alv Shear Zone.
- Undertake dating in other areas of B-Bulan, such as the western and southern areas, to determine the extent of Hallandian and Eastern Segment signatures.
- More detailed mapping of the vicinity of location 2.5j to determine structural relationships. Further dating of samples at location 2.5j to investigate the possibility of Hallandian signatures associated with Idefjorden protoliths.
- Focus on samples with metamorphic alteration and/or deformation but no record of metamorphic zircon. Perhaps U-Pb dating in titanite will preserve the age of metamorphism at locations 2.5j, 4g and 3m. Rutile coronas at

location 3b may provide more information about the P-T conditions of metamorphism in the region

## Acknowledgements

I am very grateful to my supervisor, Anders Scherstén, for his support, guidance and patience over the course of the project. I would also like to thank Lena Lundqvist from SGU in Gothenburg for giving me advice and helping me with my field work, Jenny Andersson and Lotta Möller for helping me get acquainted with the region when I first started, and Tomas Næraa for assisting me with my LA-ICP-MS analyses and subsequent data reduction. I would also like to thank the Lunds Geologiska Fältklubb (LGF) for providing me with a research grant to help cover the costs of the project.

## References

- Åhäll, K.-I., 1991: An investigation of the Proterozoic Stenungsund granitoid intrusion, southwest Sweden; conflicting geochronological and field evidence. In: Gower, G. F., Rivers, T. & Ryan, B. (eds.): Mid-Proterozoic Laurentica-Baltica Geological Association Canada Special Paper 38, 117-129.
- Åhäll, K.I. & Schöberg, H. 1999: The 963 Vinga intrusion and postcompressional deformation in the Sveconorwegian orogen, SW Sweden. *GFF* 121, 101-106.
- Åhäll, K.I., Persson, P.O. & Skiöld, T. 1995: Westward accretion of the Baltic Shield: implications from the 1.6 Åmål-Horred Belt, SW Sweden. *Precambrian Research* 70, 235-251.
- Åhäll, K.I., Samuelsson, L. & Persson, P.-O., 1997: Geochronology and structural setting of the 1.38 Ga Torpa granite; implications for the charnockite formation in SW Sweden. *GFF* 119, 37-43.
- Åhäll, K.I., Cornell, D.H., Armstrong, R., 1998: Ion probe zircon dating of three metasedimentary units bordering the Oslo Rift; new constraints for early Meso-proterozoic growth of the Baltic Shield. *Precambrian Research* 87, 117-134.
- Åhäll, K.I. & Connelly, J.N. 1998: Intermittent 1.53-1.13 Ga magmatism in western Baltica; age constraints and correlations within a postulated supercontinent. *Precambrian Research* 92, 1-20.
- Åhäll, K.I., Connelly, J.N., 2008: Long-term convergence along SW Fennoscandia: 330m.y. of Proterozoic crustal growth. *Precambrian Research* 163, 402-421.
- Åhäll, K.I., Daly, J.S., 1989: Age, tectonic setting and provenance of Östfold-Marstrand belt supracrustals: westward crustal growth of the Baltic Shield at 1760 Ma. *Precambrian Research* 45, 45-61.
- Ahlin, S., Austin Hegardt, E. & Cornell, D., 2006: Nature and stratigraphic position of the 1614 Ma Delsjön augen granite-gneiss in the Median Segment of south-west Sweden. *GFF* 128, 21-32.
- Andersson, J., Söderlund, U., Cornell, D., Johansson, L. & Möller, C., 1999: Sveconorwegian (-Grenvillian) deformation, metamorphism and leucosome formation in SW Sweden, SW Baltic Shield: Constraints from a Mesoproterozoic granite intrusion. *Precambrian Research* 98, 151-171.
- Andersson, J., Möller, C., Johansson, L., 2002: Zircon geochronology of migmatite gneisses along the Mylonite Zone (SW Sweden): a major Sveconorwegian terrane boundary in the Baltic Shield. *Precambrian Research* 114, 121-147.
- Austin Hegardt, E., Cornell, D.H., Claesson, L., Simakov, S., Stein, H.J. & Hannah, J.L., 2005: Eclogites in the central part of the Sveconorwegian Eastern Segment of the Baltic Shield: support for an extensive eclogite terrane. *GFF* 127, 221-232.
- Austin Hegardt, E., Cornell, D.H., Hellström, F.A. & Lundqvist, I., 2007: Emplacement ages of the mid-Proterozoic Kungsbacka Bimodal Suite, SW Sweden. *GFF* 129, 227-234.
- Austin-Hegardt, E., (Doctoral Thesis A134) 2010: Pressure, Temperature and Time Constraints on Tectonic Models for Southwestern Sweden. Earth Sciences Centre, Gothenburg, 33 pp.
- Austin Hegardt, E., Cornell, D., Claesson, L., Simakov, S., Stein, H. & Hannah, J., 2005: Eclogites in the central part of the Sveconorwegian Eastern Segment of the Baltic Shield: Support for an extensive eclogite terrane. *GFF* 127, 221-232.
- Austin Hegardt, E., Cornell, D.H., Hellström, F.A. & Lundqvist, I., 2007: Emplacement ages of the mid-Proterozoic Kungsbacka Bimodal Suite, SW Sweden. *GFF* 129, 227-234.
- Berthelsen, A., 1980: Towards a palinspastic analysis of the Baltic Shield. In: Cogné, J., Slansky, M. (Eds.), *Geology of Europe from Precambrian to post-Hercynian Sedimentary Basins*. International Geological Congress Colloque C6, 5-21.
- Berglund, J., 1997: Mid-Proterozoic evolution in southwestern Sweden. (Ph.D. thesis). A16. Earth Sciences Centre, Göteborg University, 1-132.
- Bingen, B., Skår, Ø., Marker, M., Sigmond, E.M.O., Nordgulen, Ø., Ragnhildstveit, J., Mansfeld, J., Tucker, R.D., Liégeois, J.P., 2005: Timing of continental building in the Sveconorwegian orogen, SW Scandinavia. *Norwegian Journal of Geology* 85, 87-116.
- Bingen, B., Stein, H.J., Bogaerts, M., Bolle, O. & Mansfeld, J. 2006: Molybdenite Re-Os dating constrains gravitational collapse of the Sveconorwegian orogen, SW Scandinavia. *Lithos* 87, 328-346.
- Bingen, B., Andersson, J., Söderlund, U., Möller, C., 2008a: The Mesoproterozoic in the Nordic countries. *Episodes* 31, 29-34.
- Bingen, B., Nordgulen, Ø., Viola, G., 2008b: A four-phase model for the Sveconorwegian orogeny, SW Scandinavia. *Norwegian Journal of Geology* 88, 43-72.
- Brander, L., Appelqvist, K., Cornell, D., Andersson, U.B., 2012: Igneous and metamorphic geochronologic evolution of granitoids in the central Eastern Segment, southern Sweden. *International Geology Review* 54, 505-546.
- Brewer, T.S., Daly, J.S. & Åhäll, K.I. 1998: Contrasting magmatic arcs in the Palaeoproterozoic of the south-western Baltic Shield. *Precambrian*

- Research 92, 297-315.
- Christoffel, C.A., Connelly, J.N. & Åhäll, K.I. 1999: Timing and characterization of recurrent pre-Sveconorwegian metamorphism and deformation in the Varberg–Halmstad region of SW Sweden. *Precambrian Research* 98, 173-195.
- Connelly, J.N., Berglund, J. & Larson, S.Å., 1996: Thermotectonic evolution of the Eastern Segment of southwestern Sweden: tectonic constraints from U-Pb geochronology. Geological Society, London, Special Publications 112, 297-313.
- Cornell, D.H. & Austin Hegardt, E. 2004: Abstract. When, where and how did the Sveconorwegian terranes of Sweden meet? *GFF* 126, 20.
- Egerton, R.F., 2005: Physical principles of electron microscopy: An introduction to TEM, SEM, and AEM. Springer, New York. 202 pp.
- Eliasson, T. & Schöberg, H., 1991: U-Pb dating of the post-kinematic Sveconorwegian (Grenvillian) Bohus granite, SW Sweden: evidence of restitic zircon. *Precambrian Research* 51, 337-350.
- Faure, G., Mensing, T.M., 2005: Principles of isotope geology, 3rd edition. John Wiley & Sons, Hoboken. 589 pp.
- Finch, R.J., Hanchar, J.M., 2003: Structure and chemistry of zircon and zircon-group minerals. In J.M Hanchar & P.W.P Hoskin (eds.): *Zircon. Reviews in Mineralogy and Geochemistry* 53, 1-25.
- Frei, D. & Gerdes, A., 2009: Precise and accurate in situ U-Pb dating of zircon with high sample throughput by automated LA-SF-ICP-MS. *Chemical Geology* 261, 261-270.
- Hellström, F.A. & Persson P.-O., 2009: U-Pb baddeleyite age of a post-collisional Sveconorwegian dolerite dyke in the western part of the Idefjorden Terrane, SW Sweden. Manuscript, 11 pp. In: Hellström, F., 2009. Lic. thesis A121, Univ. Of Gothenburg.
- Haeggman, R., 2015: Zircon dating of the Lake Horsika migmatite. Master of Science thesis B875, University of Gothenburg Department of Earth Sciences, 26 pp
- Hageskov, B., 1987: Tholeiitic dykes and their chemical alteration during amphibolite facies metamorphism: the Kattsund-Koster dyke swarm, SE Norway-W Sweden. *SGU ser. C* 817, 1-61.
- Horn, I., Rudnick, R. L. & McDonough, W. F., 2000: Precise elemental and isotope ratio determination by simultaneous solution nebulization and laser ablation-ICP-MS; application to U-Pb geochronology. *Chemical Geology* 164, 281-301.
- Jackson, S., Dunning, G. R., Horn, I. & Longerich, H., 1997: The application of laser ablation microprobe (LAM)-ICP-MS to in situ zircon and monazite U-Pb geochronology. Program with Abstracts - Geological Association of Canada; Mineralogical Association of Canada: Joint Annual Meeting 22, 73.
- Jarl, L.G., 2002: U-Pb zircon ages from the Vaggeryd syenite and the adjacent Hagshult granite, southern Sweden, *GFF* 124, 211-216
- Johansson, L., Lindh, A. & Möller, C. 1991: Late Sveconorwegian (Grenville) high-pressure granulite facies metamorphism in southwest Sweden. *Journal of Metamorphic Geology* 9, 283-292.
- Johansson, L., Johansson, Å. 1993: U-Pb age of titanite in the Mylonite Zone, southwestern Sweden. *Geologiska Föreningens i Stockholm Förhandlingar* 11, 1-7.
- Johansson, L., Möller, C. & Söderlund, U. 2001: Geochronology of eclogite facies metamorphism in the Sveconorwegian Province of SW Sweden. *Precambrian Research* 106, 261-275.
- Jonason, D., 2016: U-Pb radiometric dating and trace element characteristics of columbite from the Högsbo pegmatite quarry, south-western Sweden. Master of Science thesis B937, University of Gothenburg Department of Earth Sciences, 25 pp.
- Kiel, H., Cornell, D. & Whitehouse, M., 2003: Age and emplacement conditions of the Chalmers mafic intrusion deduced from contact melts. *GFF* 125, 213-220.
- Kosler, J. & Sylvester, P. J., 2003: Present trends and the future of zircon in geochronology; laser ablation ICPMS. *Reviews in Mineralogy and Geochemistry* 53, 243-275.
- Larson, S.Å., Cornell, D.H. & Armstrong, R.A. 1999: Emplacement ages and metamorphic overprinting of granitoids in the Sveconorwegian Province in Värmland, Sweden - an ion probe study. *Norsk Geologisk Tidsskrift* 79, 87-96.
- Lee, J. K.W., Williams, I.S., Ellis, D.J., 1997: Pb, U and Th diffusion in natural zircon. *Nature* 390, 159-163.
- Lewerentz, A., 2011: Experimental zircon alteration and baddeleyite formation in silica saturated systems: implications for dating hydrothermal events. *Dissertations in Geology at Lund University, Master's Thesis, No. 293*, 56 pp.
- Linders, W., 2016: U-Pb geochronology and geochemistry of host rocks to the Bastnäs-type REE mineralization in the Riddarhyttan area, west central Bergslagen, Sweden. *Dissertations in Geology at Lund University, Master's Thesis* 466, 1-60.
- Long, J.V.P., 1995: Microanalysis from 1950 to the 1990s. In Potts, P.J., Bowles, J.F.W., Reed, S.J.B., & Cave, M.R. (eds.): *Microprobe Techniques in the Earth Sciences. Mineralogical Society Series* 6, 1-48.
- Ludwig, K.R., 2012: User's manual for Isoplot 3.75. A geochronological toolkit for Microsoft Excel. *Berkeley Geochronology Center Special Publications* 5, 1-75.
- Lundqvist, I., Skioöld, T., 1993: U-Pb zircon dating of the Åmål Group, western Sweden. In: Lundqvist, T. (Ed.), *Radiometric dating results, Division of Bedrock Geology, Geological Survey of Sweden*, 823. *Sver. Geol. Unders. C*, pp. 24-31.
- Lundqvist, Antal Lundin, Andersson, Bergström, Hellström, 2005: Delin (ed) *SGU Rapport och Meddelanden* 120, 36-51.
- Lundqvist, L., Andersson, J. & Hellström, F., 2012: U-Pb igneous protolith zircon age of a granitic migmatitic gneiss in the Eastern Segment of the Sveconorwegian orogen, Alingsås area. In: Andersson, J. (ed.) *U-Pb zircon geochronology of granitic and syenitoid rocks across the southern*

- part of the Sveconorwegian orogen. Geological Survey of Sweden, SGU-rapport 2012:14, 13-18.
- Möller, C., 1998: Decompressed eclogites in the Sveconorwegian (-Grenvillian) orogen of SW Sweden: petrology and tectonic implications. *Journal of Metamorphic Geology* 16, 641-656.
- Möller, C., 1999: Sapphirine in SW Sweden: a record of Sveconorwegian (-Grenvillian) late-orogenic tectonic exhumation. *Journal of Metamorphic Geology* 17, 127-141.
- Möller, C. & Söderlund, U. 1997: Age constraints on the regional deformation within the Eastern Segment, S Sweden: Late Sveconorwegian granite dyke intrusion and metamorphic deformational relations. *GFF* 119, 1-12.
- Möller, C., Andersson, J., Lundqvist, I., Hellström, F.A., 2007: Linking deformation, migmatite formation and zircon U-Pb geochronology in polymetamorphic gneisses, Sveconorwegian province, Sweden. *Journal of Metamorphic Geology* 25, 727-750
- Möller, C., Andersson, J., Dyck, B. & Antal Lundin, I., 2015: Exhumation of an eclogite terrane as a hot migmatitic nappe, Sveconorwegian orogen. *Lithos* 226, 147-168.
- Olsson, A., 2016: Metamorphic record of monazite in aluminous migmatitic gneisses at Stensjöstrand, Sveconorwegian orogen. *Dissertations in Geology at Lund University, Master's Thesis* 467, 1-43
- Österlund, E., 2015: An investigation of the Landvetter intrusion based on geochemical and petrographic analysis and LA-ICP-MS zircon dating. Bachelor of Science thesis, University of Gothenburg Department of Earth Sciences, 28 pp.
- Primer, 2005: Inductively Coupled Plasma Mass Spectrometry, a Primer. USA, Agilent Technologies. 84 pp.
- Persson, P.O., Wahlgren, C.H. & Hansen, B.T.. 1983: U-Pb ages of Proterozoic metaplutonics in the gneiss complex of southern Värmland, southwestern Sweden. *Geologiska Föreningens i Stockholm Förhandlingar* 105, 1-8.
- Petersson, A., Scherstén, A., Andersson, J., Möller, C., 2013: Zircon U-Pb and Hf — isotopes from the eastern part of the Sveconorwegian Orogen, SW Sweden: implications for the growth of Fennoscandia. *Geological Society of London, Special Publications* 389.
- Petersson, A., Scherstén, A., Bingen, B., Gerdes, A., Whitehouse, M.J., 2015: Mesoproterozoic continental growth: U-Pb-Hf-O zircon record in the Idefjorden terrane, Sveconorwegian Orogen. *Precambrian Research* 261, 75-95
- Richter, M., 2013: Evaluation of U-Th-Pb dating of monazite by LA-ICP-MS. Mainz, Johannes Gutenberg-Universität. 191 pp.
- Robin, P.Y.F. & Cruden, A.R. 1994: Strain and vorticity patterns in ideally ductile transpression zones. *Journal of Structural Geology*, 16, 447-466.
- Samuelsson, L. 1982: Bedrock map 7B Göteborg NO. Scale 1:50,000. Swedish Geological Survey Af 136.
- Scherstén, A., Årebäck, H., Cornell, D., Hoskin, P., Åberg, A., Armstrong, R., 2000: Dating mafic-ultramafic intrusions by ion-microprobing contact-melt zircon: examples from SW Sweden. *Contributions to Mineralogy and Petrology* 139, 115-125
- Scherstén, A., Larson, S.-Å., Cornell, D.H., Stigh, J., 2004: Ion probe dating of a migmatite in SW Sweden: the fate of zircon in crustal processes. *Precambrian Research* 130, 251-266.
- Schoene, B., 2014: U-Th-Pb Geochronology, In H.D. Holland & K.K. Turekian (eds.): *Treatise on Geochemistry* vol. 4, 341-378. Elsevier, Oxford.
- Söderlund, U., Jarl, L.G., Persson, P.O., Stephens, M.B., Wahlgren, C.-H., 1999: Protolith ages and timing of deformation in the eastern, marginal part of the Sveconorwegian orogen, southwestern Sweden. *Precambrian Research* 94, 29-48.
- Söderlund, U., Möller, C., Andersson, J., Johansson, L., Whitehouse, M., 2002: Zircon geochronology in polymetamorphic gneisses in the Sveconorwegian orogen, SW Sweden: ion microprobe evidence for 1.46-1.42 and 0.98-0.96 Ga reworking. *Precambrian Research* 113, 193-225.
- Söderlund, P., Söderlund, U., Möller, C., Gorbatshev, R., Rodhe, A., 2004: Petrology and ion microprobe U-Pb chronology applied to a metabasic intrusion in southern Sweden: a study on zircon formation during metamorphism and deformation. *Tectonics* 23, 1-16.
- Söderlund, U., Isachsen, C.E., Bylund, G., Heaman, L.M., Patchett, P.J., Vervoort, J.D. & Andersson, U.B., 2005: U-Pb baddeleyite ages, and Hf, Nd isotope chemistry constraining repeated mafic magmatism in the Fennoscandian Shield from 1.6 to 0.9 Ga. *Contributions to Mineralogy and Petrology* 150, 174-194.
- Söderlund, U. & Ask, R. 2006: Mesoproterozoic bimodal magmatism along the Protogine Zone, S Sweden: three magmatic pulses at 1.56, 1.22 and 1.205 Ga, and regional implications. *GFF* 128, 303-310.
- Söderlund, U., Hellström, F.A. & Kamo, S.L., 2008: Geochronology of high-pressure mafic granulite dykes in SW Sweden: tracking the P-T-t path of metamorphism using Hf isotopes in zircon and baddeleyite. *Journal of Metamorphic Geology* 26, 539-560.
- Stephens, M.B., Wahlgren, C.-H., Weijermars, R., Cruden, A.R., 1996: Left-lateral transpressive deformation and its tectonic implications, Sveconorwegian orogen, Baltic Shield, southwestern Sweden. *Precambrian Research* 79, 261-279
- Ulmius, J., Andersson, J. & Möller, C., 2015: Hallandian 1.45 Ga high-temperature metamorphism in Baltica: P-T evolution and SIMS U-Pb zircon ages of aluminous gneisses, SW Sweden. *Precambrian Research* 265, 10-39.
- Vander Auwera, J., Bolle, O., Bingen, B., Liégeois, J.-P., Bogaerts, M., Duchesne, J.C., De Waele, B., & Longhi, J., 2011: Sveconorwegian massif-type anorthosites and related granitoids result from post-collisional melting of a continental arc root. *Earth Science Reviews* 107, 375-397.
- Vermeesch, P., 2018: IsoplotR: a free and open toolbox for geochronology. *Geoscience Frontiers*,

v. 9, pp. 1479-1493

- Viola, G. & Henderson, I.C. 2010: Inclined transpression at the toe of an arcuate thrust: an example from the Precambrian 'Mylonite Zone' of the Sveconorwegian orogen. *Geological Society, London, Special Publications*, 335, 715-737.
- Viola, G., Henderson, I.H.C., Bingen, B., Hendriks, B.W.H., 2011: The Grenvillian-Sveconorwegian orogeny in Fennoscandia: back thrusting and extensional shearing along the "Mylonite Zone". *Precambrian Research* 189, 368-388.
- Welin, E., Lindh, A. & Kähr, A.M. 1981: The radiometric age of the Proterozoic granite at Sandsjön, western Värmland, Sweden. *Geologiska Föreningens i Stockholm Förhandlingar* 103, 514-518.
- Welin, E. & Samuelsson, L. 1987: Rb-Sr and U-Pb isotope studies of granitoid plutons in the Göteborg region, southwestern Sweden. *Geologiska Föreningens i Stockholm Förhandlingar* 109, 39-45.
- Wahlgren, C.H., Cruden, A.R., Stephens, M.B., 1994: Kinematics of a major fan-like structure in the eastern part of the Sveconorwegian Orogen, Baltic Shield, south-central Sweden. *Precambrian Research* 70, 67-91.
- Wahlgren, C.H., Heaman, L.M., Kamo, S. & Ingvold, E., 1996: U-Pb baddeleyite dating of dolerite dykes in the eastern part of the Sveconorwegian orogen, south-central Sweden. *Precambrian Research* 79, 227-237.
- Wiedenbeck, M., Alle, P., Corfu, F., Griffin, W.L., Meier, M., Oberli, F., von Quadt, A., Roddick, J.C., Spiegel, W., 1995: Three natural zircon standards for U-Th-Pb, Lu-Hf, trace element and REE analyses. *Geostandards Newsletter* 19, 1-23.

## Appendix

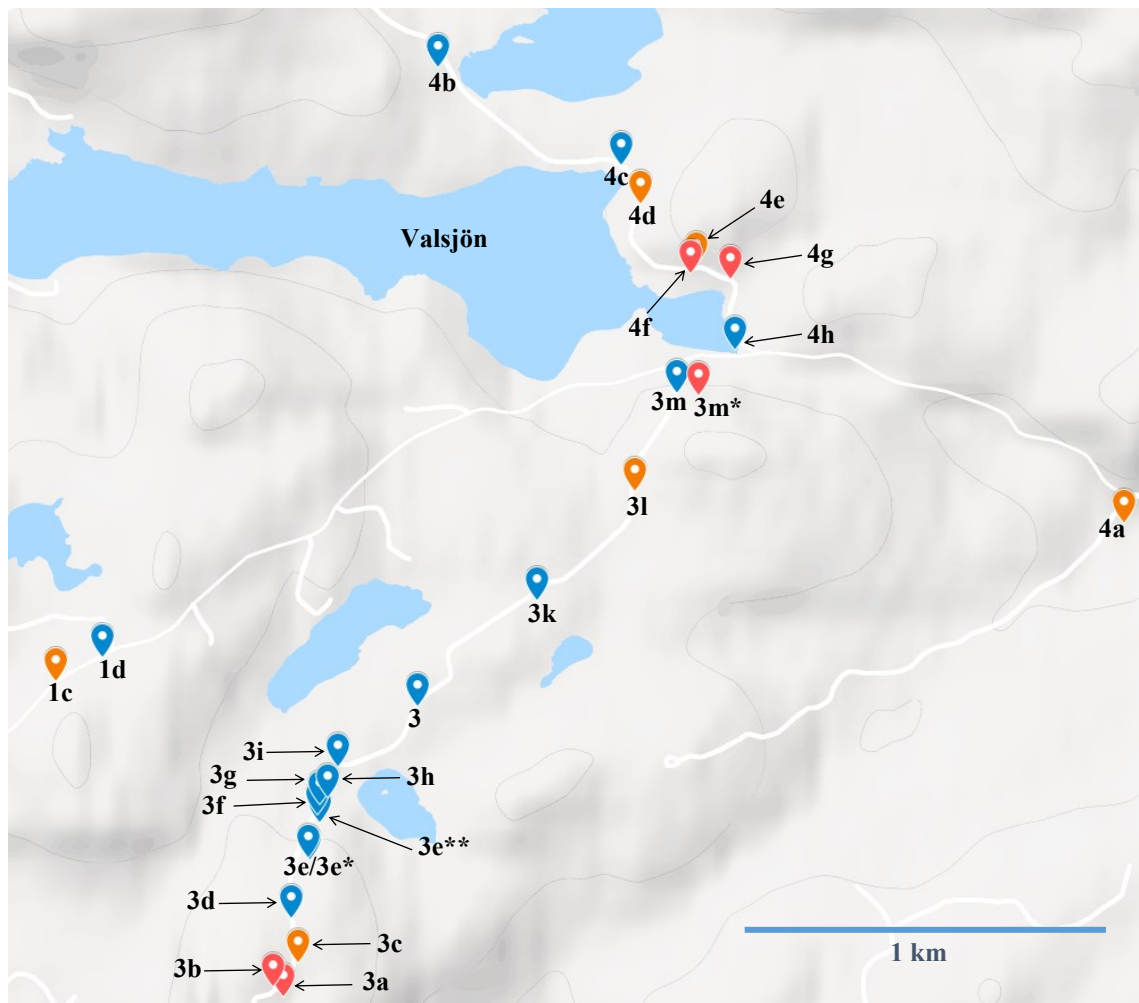
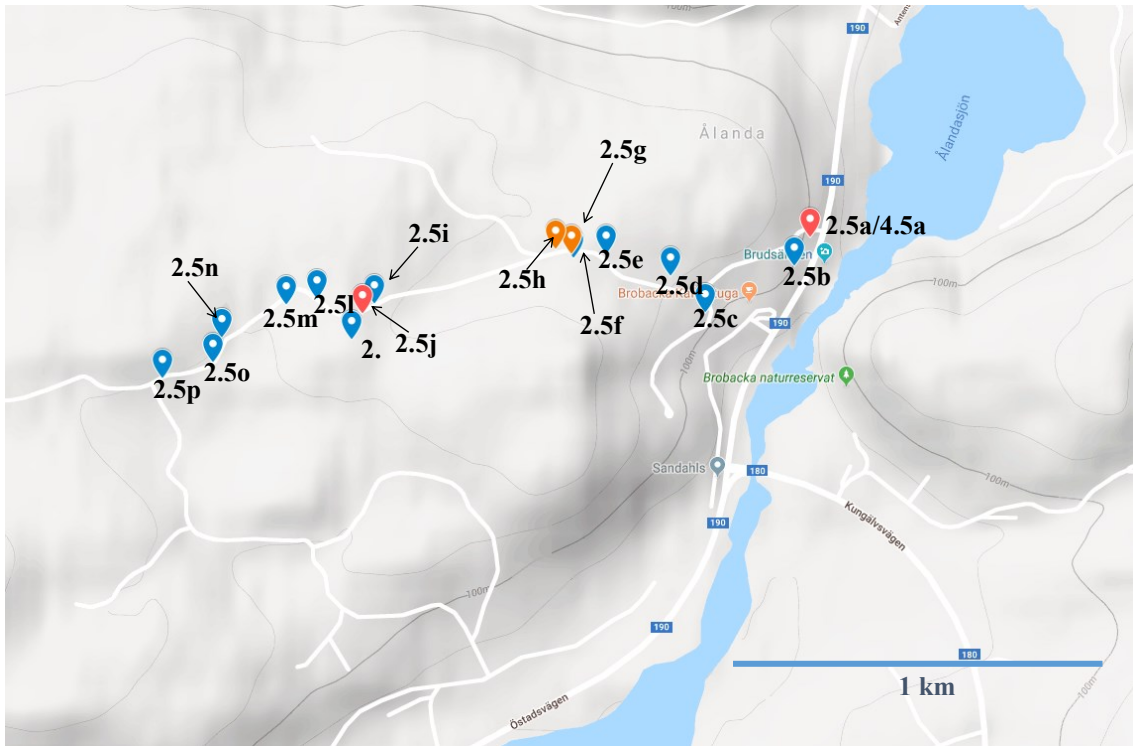
Appendix 1. A condensed version of the field trip notes from each locality visited. Localities marked in bold indicate samples taken. Localities in green represent rock types that look similar to the Brobacka type-locality (2.5a/4.5a), and therefore may allow Hallandian metamorphism to be traced into the Idefjorden terrane. Yellow represents samples that are worth a closer look, but that I am not sure are similar to Brobacka.

Locality	Longitude, Latitude	Rock type	Sample (Y/N)	Description/Composition	Texture/Structure	Brobacka (Y/N)	Notes	Structural data
1a	Not recorded	Granite-Granodiorite	N	Eastern Segment gneiss - k-fsp + plag + qz + bt + hbl; Mafic lense/xenolith and mafic dyke	Strongly banded; dyke further down is undeformed	N	N of Allingsås	
1b	Not recorded	Granite	N	Augen gneiss - w/ microcline porphyroclasts + grey qz		?	7 min drive from Loc. 1a; within MZ	
1c	<b>N57°51.106, E012°21.477</b>	<b>Granite-Granodiorite</b>	Y	<b>Different composition to 1a, but similar texture; less fsp + qz, more hbl + bt. Qz is dark grey</b>	<b>Gneissose banding; migmatization</b>	N	Near Välsjön	
1d	N57°58.985, E012°19.774	Granite	N	K-fsp porphyroclasts + qz ribbons; k-fsp rich		Y		32°030 (Lin), 20°322 (Lin)
1d	N57°58.952, E012°19.507	Granodiorite	N	Grey gneiss; k-fsp poor	Possible folding	Some slithers	Vertically dipping, N-S trending	
1e	<b>N57°58.764, E012°19.506</b>	<b>Granite</b>	Y	<b>K-fsp megacrysts + qz ribbons (grey) + plag</b>	<b>Stretching lineations</b>	?	<b>SGU sample 006 is nearby</b>	<b>022°338 (Lin)</b>
1f	N57°58.328, E012°17.262	Granite	Y	K-fsp, but more diffuse/less euhedral than Brobacka	L-tectonite on sample 1f <sub>i</sub>	N		
1g	N57°55.379, E012°17.595	Gabbro	Y	Amphibolite - dominated by mafics; plagioclase defines the banding; no presence of garnet	Pronounced lineation	N	Use for thin section	
1h	Outside Lena's house	Granodiorite (?)	Y	Grey w/ some felsic and mafic areas; pegmatites present	Heavily strained; flattened w/ leucosomes	N	B-Bulan border zone; outside Lena's house	
2.5a	<b>N57°58.840, E012°26.142</b>	<b>Granite</b>	*	Augen gneiss w/ microcline porphyroclasts		Y	<b>Brobacka gneiss type locality (+ some pegmatite)</b>	<b>50°NW/253</b>
4.5a <sup>o</sup>	<b>N57°58.858, E012°26.164</b>	<b>Granite</b>	Y*	Augen gneiss (k-fsp rich) w/ bt + plag + qz + hbl	K-fsp megacrysts are augen + qz ribbons are elongated, suggesting ~ 600°C	Y	This is Brobacka-type locality	
2.5b	N57°58.828, E012°26.115	Granite	N	Augen gneiss w/ microcline porphyroclasts		Y	This is also Brobacka	32°N/260
2.5c	N57°58.779, E012°25.882	Granite-Granodiorite	N	Micaceous, granodioritic; traces of k-fsp, but mainly dark (bt + hbl) and pale (plag + qz) minerals		N	This is only a boulder within a thick forest covering - unreliable!	
2.5d	N57°58.804, E012°25.829	Granite	N	Augen gneiss w/ microcline porphyroclasts		Y	Brobacka gneiss	

2.5e	N57°58.832, E012°25.667	Granite	N	Augen gneiss w/ microcline porphyroclasts		Y	Brobacka gneiss	
2.5f	N57°58.829, E012°25.589	Granite	N	Hybrid gneiss; plag (w/ some k-fsp) + hbl + bt	Strongly deformed; possibly migmatitised	N		
2.5g	N57°58.839, E012°25.565	Mylonitised	Y	Mylonitised gneiss - can't make out composition	Strongly foliated; fissile	N		
2.5h	N57°58.839, E012°25.540	Mylonitised	Y	Mylonitised gneiss - plag/k-fsp clasts; dark matrix	Veining + migmatitisation	?		40° N250
2.5i	N57°58.763, E012°25.069	Granite	N	Augen gneiss w/ microcline porphyroclasts		Y		
2.5j	N57°58.759, E012°25.035	Granite + Granodiorite	Y, Y, Y	Augen gneiss; granodiorite	Strongly banded, foliated and folded	Y/N		38° N268
2.5k	(10m from 2j, road side)	Pegmatite	N	Plag + qz-rich, coarse-grained pegmatite	Massive	N		
2.5l	N57°58.715, E012°25.008	Pegmatite	N	Plag + qz-rich, coarse-grained pegmatite, w/ some k-fsp	Massive	N		
2.5m	N57°58.757, E012°24.840	Granodiorite/ Pegmatite	N	Meta-granodiorite w/ plag, qz, hbl, bt, ms; pegmatite w/ plag + qz		N		
2.5n	N57°58.717, E012°24.676	Tonalite	N	Meta-tonalite w/ plag + qz	Obvious fabric on weathered surface	N		
2.5o	N57°58.685, E012°24.649	Granite-Granodiorite	N	Grey gneiss w/ k-fsp ribbons + some mica	Ribbons; gradational k-fsp (more at the bottom)	N		
2.5p	N57°58.664, E012°24.525	Granodiorite	N	Micaceous granodiorite w/ veins + k-fsp pegmatite	Granodiorite = foliated (like pancakes); cut by veins	N		
2a	N57°56.772, E012°14.495	Granite	Y	Gneiss w/ microcline porphyroclasts + qz + plag + bt	Strongly deformed; elongated porphyroclasts; veined k-fsp + plag	?		Is this SGU 025006?
2b	N57°56.833, E012°12.653	Granite	N	Gneiss w/ k-fsp porphyroclasts + qz + plag + bt (basically same as 2a)	Strongly deformed; elongated porphyroclasts	?		SGU 015004
2c	N57°55.540, E012°12.777	Granite	N	Gneiss w/ k-fsp porphyroclasts; pale matrix (plag + qz)	Clear foliation + possible lineation	?		
2d	N57°55.170, E012°12.748	Granite	N	Gneiss w/ k-fsp porphyroclasts, some recrystallised	Possible recrystallisation	Y		
2e	N57°54.871, E012°08.672	Granite-Granodiorite	N	Peraluminous, garnet-bearing gneiss; muscovite-rich	Slickenlines on the surface - typical of Idejorden shear zone	N		
2f	N57°55.370, E012°04.460	Granite	N	Augen gneiss - large k-fsp crystals (weathered white) w/ dark grey matrix; peraluminous, but less micaceous than 2e		?		May have similar to this north of Brobacka
3a	N57°58.703, E012°21.843	Granite	Y, Y, Y, Y, Y	K-fsp porphyroclasts w/ dark matrix		?		
3b	N57°58.711, E012°21.858	Granite-Granodiorite	Y	K-fsp + plag + qz + hbl + bt (Brobacka hybrid)		?		

3c	N57°58.738, E012°21.909	Granite	Y	Plag + qz + k-fsp in a dark matrix (quite micaceous)		N	Definitely out of Brobacka	
3d	N57°58.785, E012°21.909	Granodiorite-Tonalite	N	Plag + qz; micaceous	Deformed plagioclase; biotite defines fabric	N		
3e	N57°58.866, E012°21.939	Granite	N	Augen gneiss w/ microcline porphyroclasts	Strongly deformed and very steeply dipping; dull qz ribbons; mylonitised	?	Brobacka gneiss. Nearby = heavy strain - mylonite	68NE318
3f	N57°58.920, E012°21.957	Granodiorite-Tonalite	N	Micaceous granodiorite w/ k-fsp + plag veins; K-fsp + qz-rich gneiss		?	Seems to be a transition between Brobacka and micaceous gneiss	
3g	N57°58.929, E012°21.963	Granite	N	Micaceous granite w/ k-fsp (little quartz)		N		40W174
3h	N57°58.939, E012°21.982	Granite	N	K-fsp + plag w/accessory hbl + qz. Not micaceous		?		
3i	N57°58.978, E012°22.002	Granite	N	K-fsp rich gneiss; looks like Brobacka	Foliated w/veining	?		28NW240
3j	N57°58.703, E012°21.852	Pegmatite	N	K-fsp pegmatite		N		
3k	N57°59.044, E012°22.184	Granite	N	K-fsp rich gneiss w/more mafic minerals		N	Not as red as Brobacka	
3l	N57°59.314, E012°22.677	Granite/Syenite	Y	Very k-fsp rich gneiss (very red); matrix is sugary, neither micaceous or non-micaceous		?	Very red gneiss; redder than Brobacka	
3m	N57°59.420, E012°22.776	Granite	N	K-fsp rich gneiss; quartz is less obvious (matrix is dark, but not micaceous)	Heavily strained; feldspar behaving plastically	?	Probably Brobacka; quartz may not be obvious due to the amount of deformation	
3m <sup>o</sup>	N57°59.414, E012°22.816	Granite	N	K-fsp rich gneiss w/ qz + plag + hbl + bt	Heavily foliated weathered surface	?	Unsure whether this is a more deformed Brobacka gneiss or a different gneiss altogether	
4a	N57°59.270, E012°23.788	Granite	Y	K-fsp rich gneiss (very red); fissile	Forms distinct beds	N	Looks like sample 3l-i	42N256
4b	N57°59.815, E012°22.236	Granite-Granodiorite	N	Micaceous gneiss w/ dark, al-rich bt + hbl + ms; occasional patches of k-fsp		N	Outcrop mostly covered in moss; appears to be typical Idefforden gneiss	20W170
4c	N57°59.695, E012°22.641	Granite	N	K-fsp and mafic-rich gneiss; bt + some plag + qz		N	Not enough quartz to be Brobacka	
4d	N57°59.651, E012°22.693	Granite-Granodiorite	Y	Plag + mafic-rich gneiss; very bt-rich	Clear banding of mafics	N	Topographically 10m higher than 4c; this is the overlying unit	28NW220
4e	N57°59.628, E012°22.685	Granite-Granodiorite	Y (?)	K-fsp veins; otherwise micaceous (sh) w/ plag + qz		N	Looks like Loc 4c; Loc 4e ~ 1.5m higher than 4d, but dip suggests it could easily fall below it on the opposite side of the path	22N260
4f	N57°59.579, E012°22.793	Granite	Y	K-fsp rich gneiss w/ bt + hbl + ms + plag/qz	Heavily foliated weathered surface	?	Looks like sample 4c	
4g	N57°59.568, E012°22.796	Granite	Y	K-fsp rich gneiss		?	Less micaceous than Loc 4f, but not Brobacka	32NNW250
4h	N57°59.491, E012°22.916	Granite-Granodiorite	N	Bt-rich gneiss w/ less k-fsp		N	Rubbish sampling location	

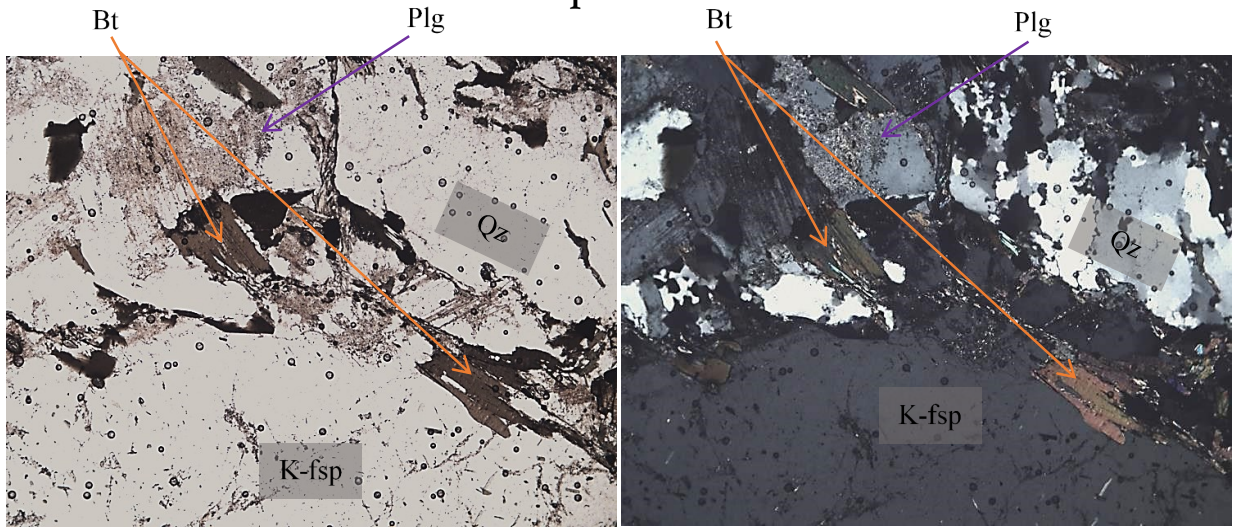




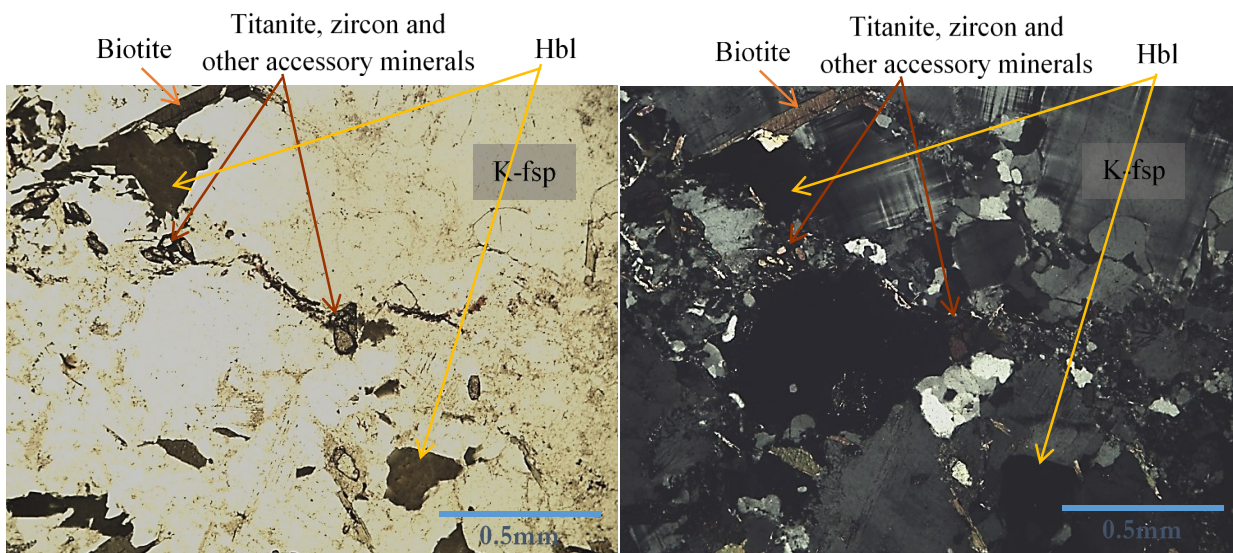
Appendix 2. Terrain maps showing all locations visited on days 2, 3 and 4. See Figure 5 for context. Map data © 2019 Google.

<b>Laboratory &amp; Sample Preparation</b>	
Laboratory name	LA-ICP-MS lab at Lund University
Sample type / mineral	Zircon
Sample preparation	Conventional mineral separation, 1 inch resin mount, 1 $\mu\text{m}$ polish to finish
Imaging	BSE-imaging, CL-imaging, TESCAN Mira 3, 10kV, 18nA, 15 mm working distance
<b>Laser ablation system</b>	
Make, Model & type	Teledyne Photon Machines, Analyte G2
Ablation cell & volume	HelEx II Active 2-volume
Laser wavelength	193 nm
Pulse width	>4 ns
Fluence	3.5 J/cm <sup>2</sup>
Repetition rate	10 Hz
Spot size	20 x 20, 24 x 17, 29 x 14 $\mu\text{m}$
Sampling mode / pattern	20 $\mu\text{m}$ single spot analyses
Carrier gas	He 0,8 L/min, N <sup>2</sup> 4 ml/min, Ar make-up gas combined using a Y-connector close to sample cell
Pre-ablation laser warm-up (background collection)	20 seconds
Ablation duration	20 seconds
Wash-out delay	7 seconds
Cell carrier gas flow	0.8 l/min He
<b>ICP-MS Instrument</b>	
Make, Model & type	Bruker Aurora M90 ICP-MS
Sample introduction	Via conventional tubing
RF power	1100-1300 W
Make-up gas flow	1.0 l/min Ar
Detection system	Single collector secondary electron multiplier
Masses measured	202, 204, 206, 207, 208, 232, 238
Integration time per peak	4 ms
Total integration time per reading	Approx. 1 sec
Sensitivity	20000 cps/ppm Pb
Dead time	16 ns
<b>Data Processing</b>	
Gas blank	40 second on-peak
Calibration strategy	GJ-1 used as primary reference material, 91500 used as secondary reference material
Reference Material info	GJ-1 (Jackson et al. 2004) 91500 (Weidenbeck et al. 1995)
Data processing package used / Correction for LIEF	Iolite Software, baseline correction and downhole correction
Mass discrimination	Standard-sample bracketing with <sup>207</sup> Pb/ <sup>206</sup> Pb and <sup>206</sup> Pb/ <sup>238</sup> U normalised to reference material GJ-1
Uncertainty level & propagation	Ages are quoted at 2 sigma internal errors
Quality control / Validation	GJ-1: Wtd ave <sup>207</sup> Pb/ <sup>206</sup> Pb Age = 605 $\pm$ 5 Ma 91500: Wtd ave <sup>207</sup> Pb/ <sup>206</sup> Pb Age = 1068 $\pm$ 4 Ma
<b>Other information</b>	Detailed method description reported by Frei & Gerdes (2009)

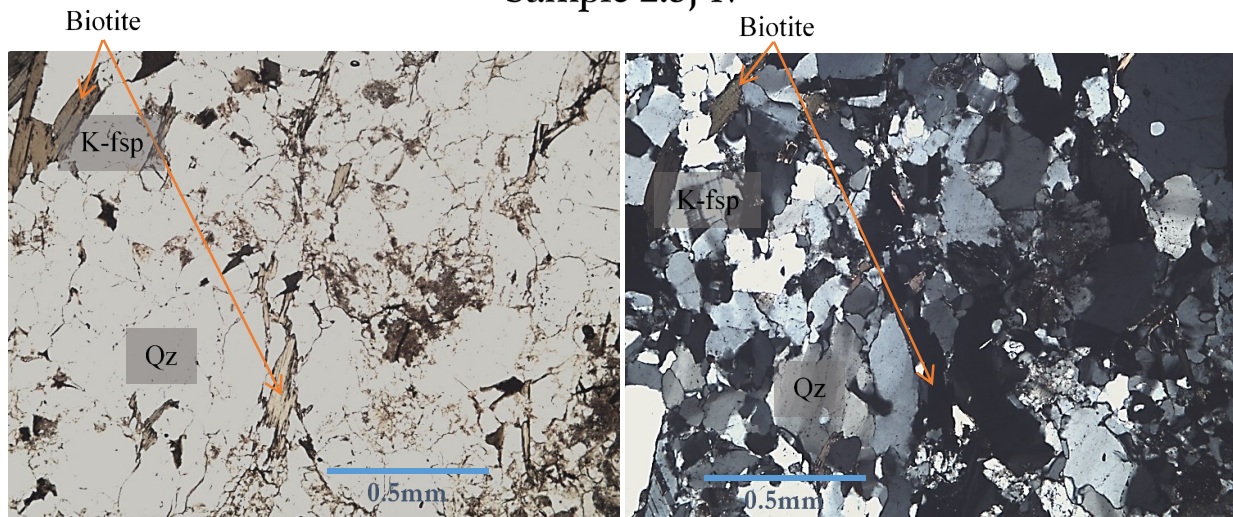
Sample 4.5a-i



Sample 2.5j-i

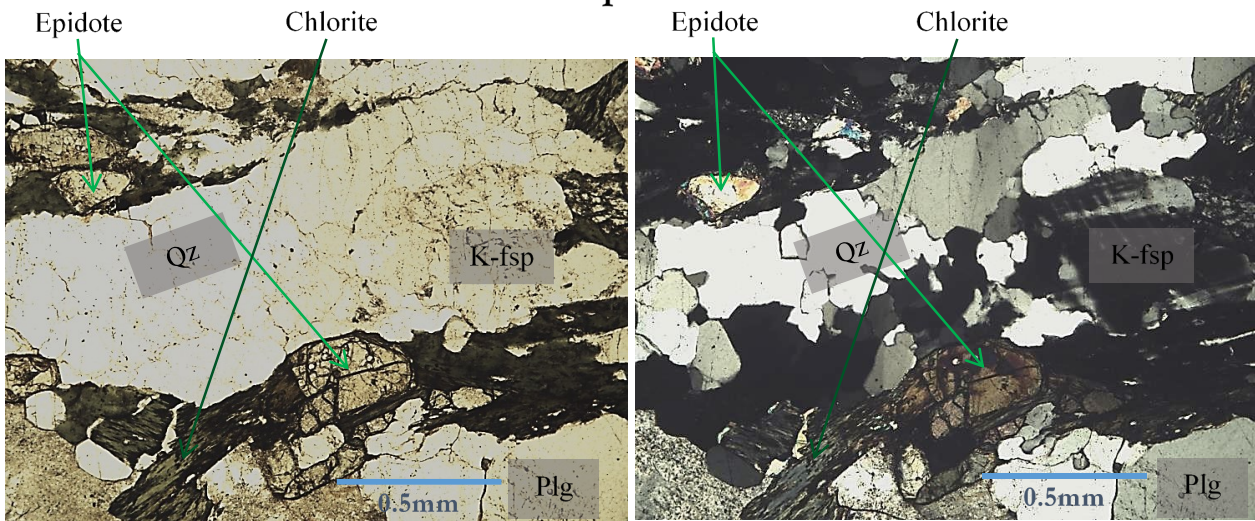


Sample 2.5j-iv

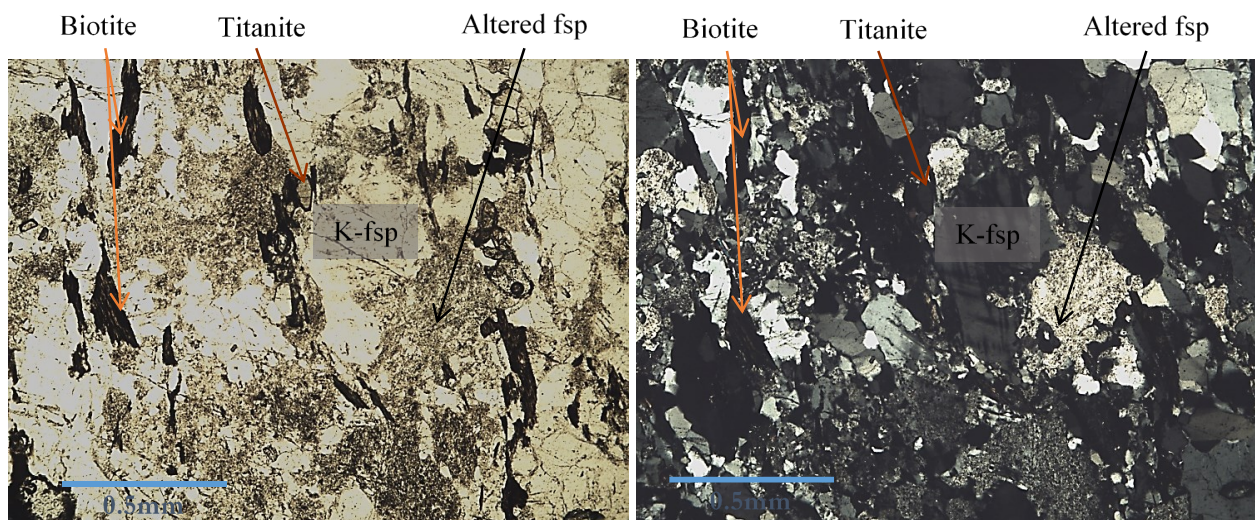


Appendix 4. Thin sections of samples 4.5a-i, 2.5j-i and 2.5j-iv. (Right): plane-polarised light; (Left): cross-polarised light. Bt = biotite, Plg = plagioclase, Qz = quartz, K-fsp = K-feldspar, Hbl = hornblende.

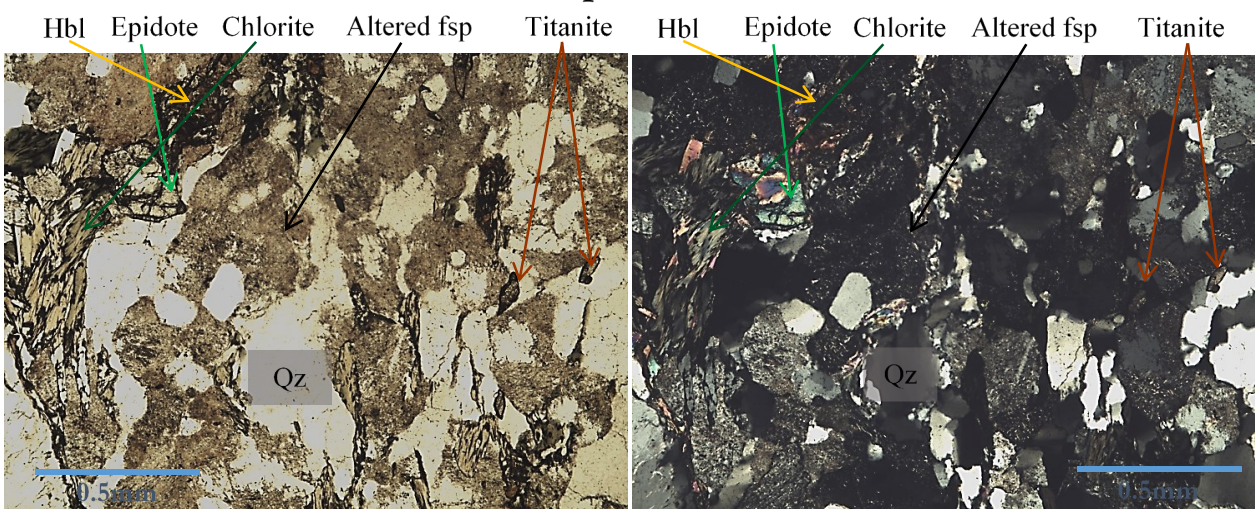
### Sample 4f-i



### Sample 4g-i

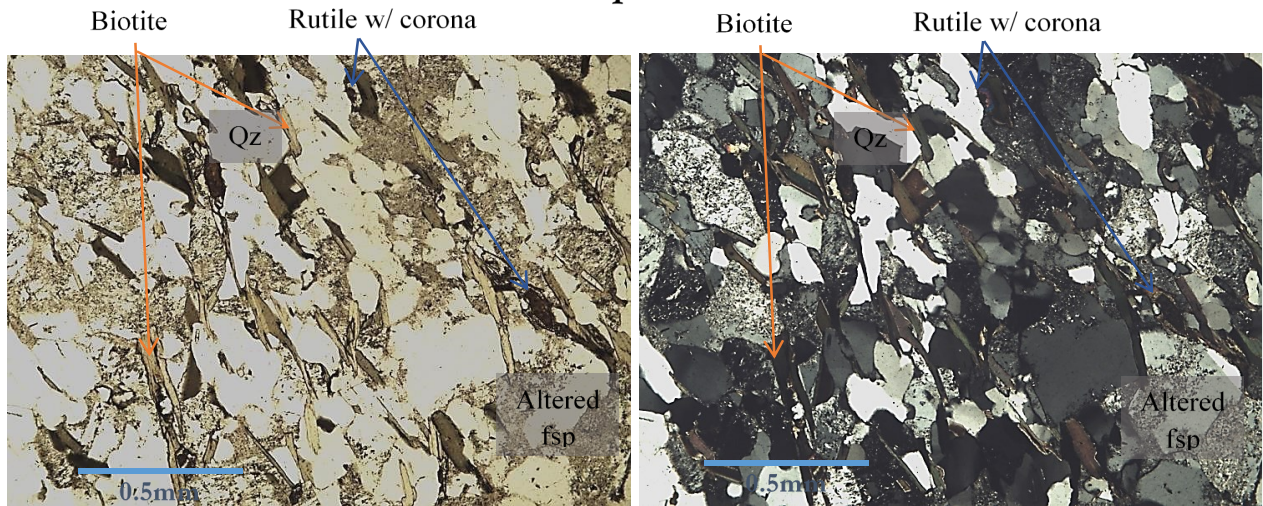


### Sample 3m-ii

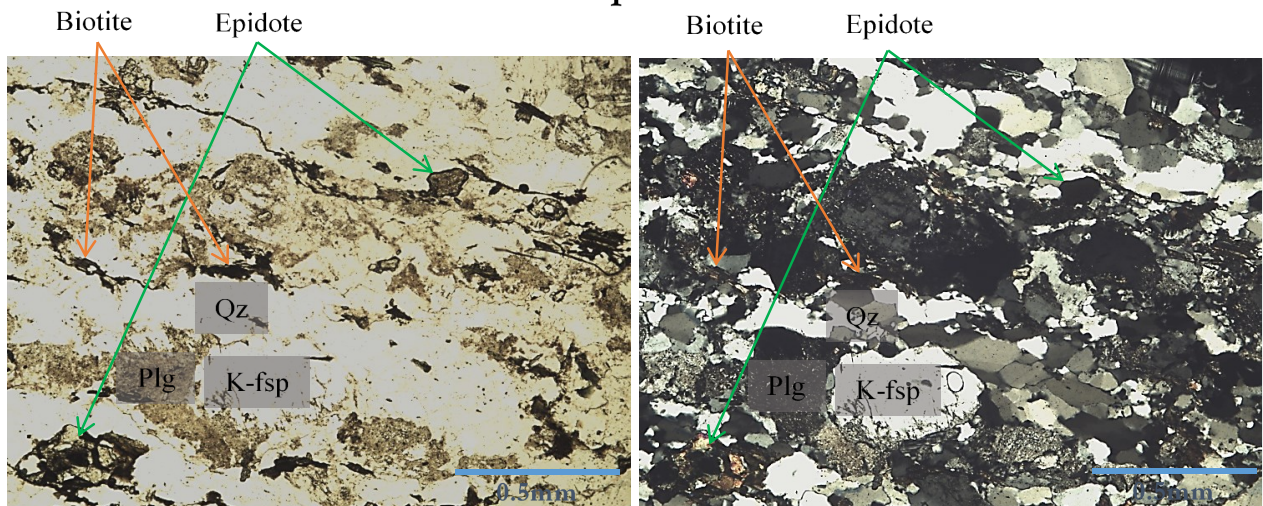


Appendix 5. Thin sections of samples 4f-i, 4g-i and 3m-ii. (Right): plane-polarised light; (Left): cross-polarised light. Plg = plagioclase, Qz = quartz, K-fsp = K-feldspar.

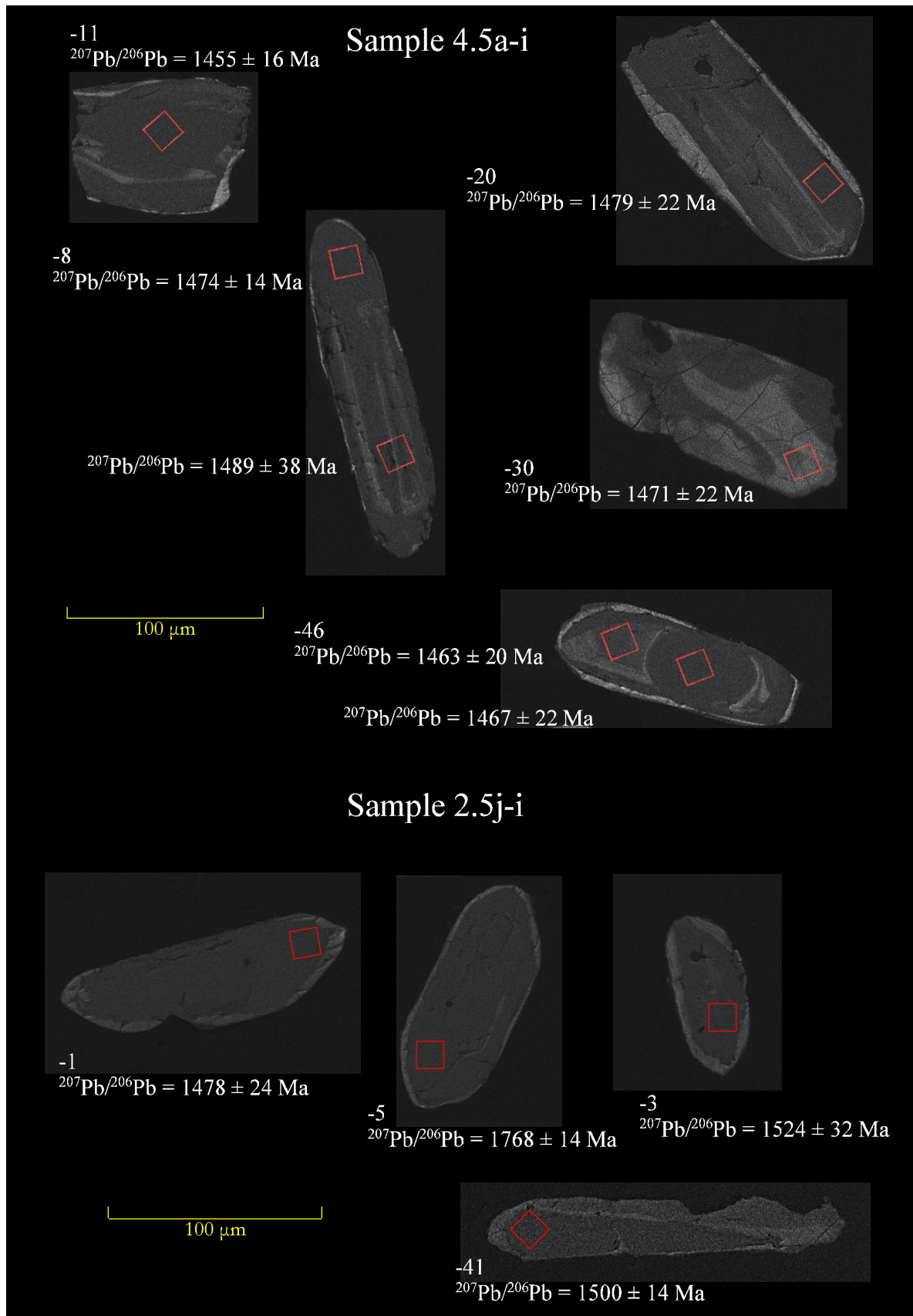
### Sample 3b-i



### Sample 3a-i

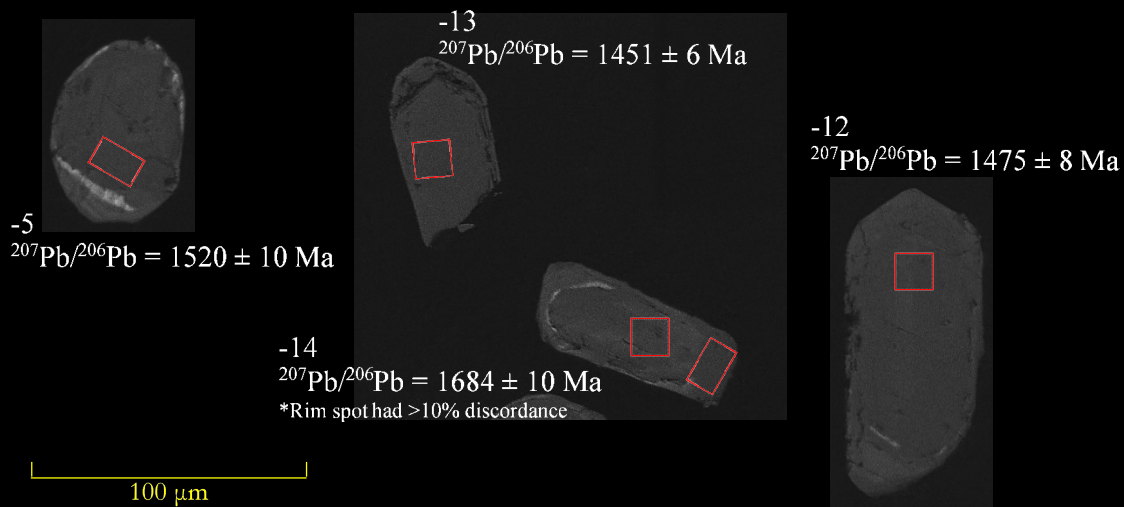


Appendix 6. Thin sections of samples 3b-i and 3a-i. (Right): plane-polarised light; (Left): cross-polarised light. Plg = plagioclase, Qz = quartz, K-fsp = K-feldspar.

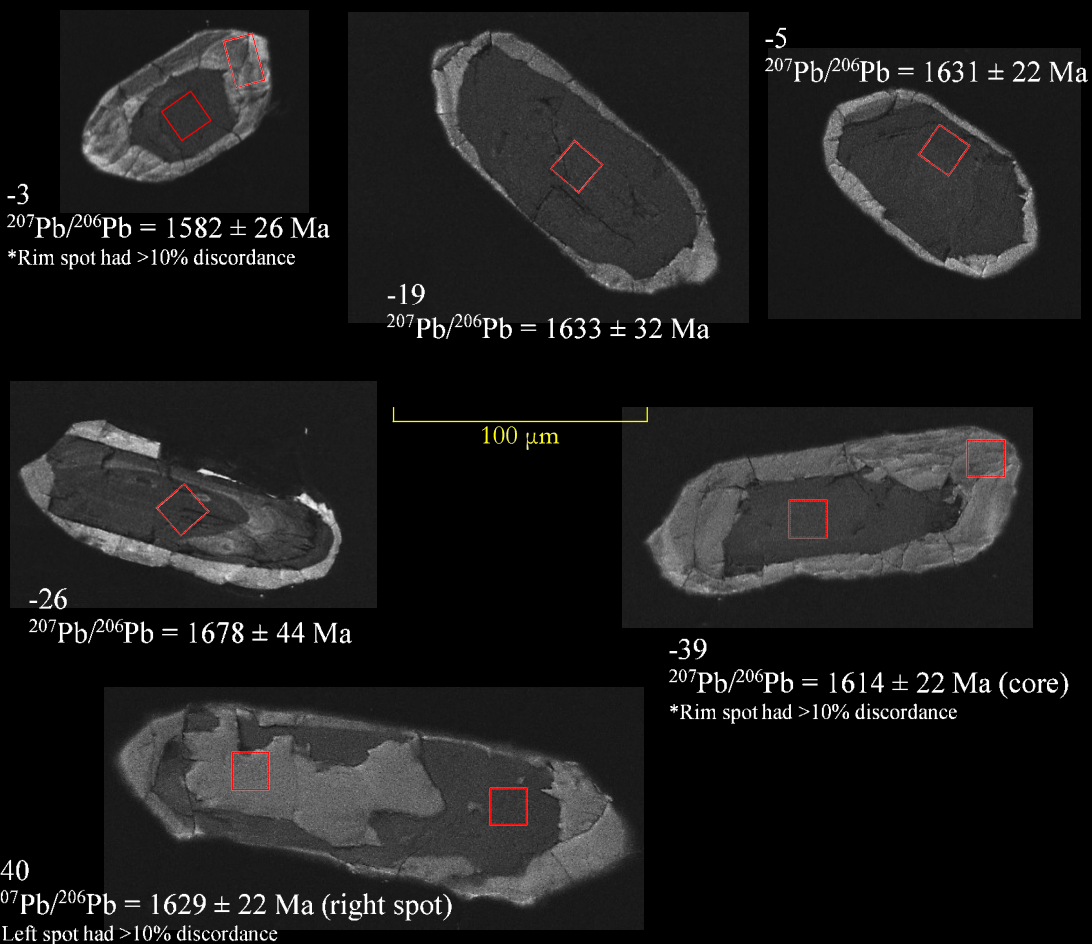


Appendix 7. Cathodoluminescence (CL) images of representative zircon grains from Sample 4.5a-i and Sample 2.5j-i that are  $\leq 10\%$  discordant. Each number corresponds with the grain # in Table 2.

## Sample 2.5j-iv

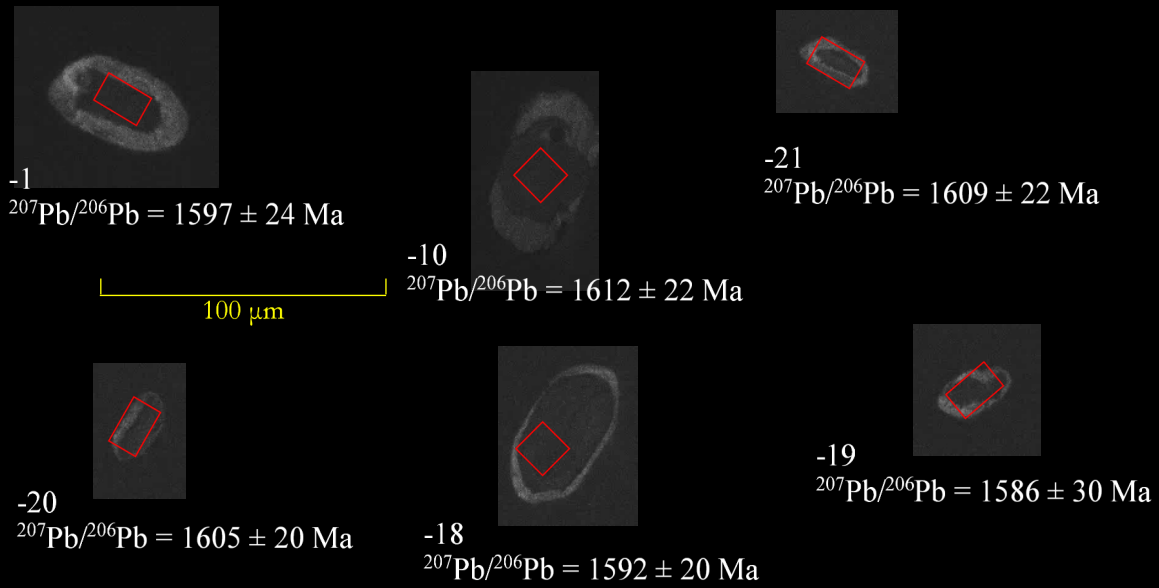


## Sample 4f-i

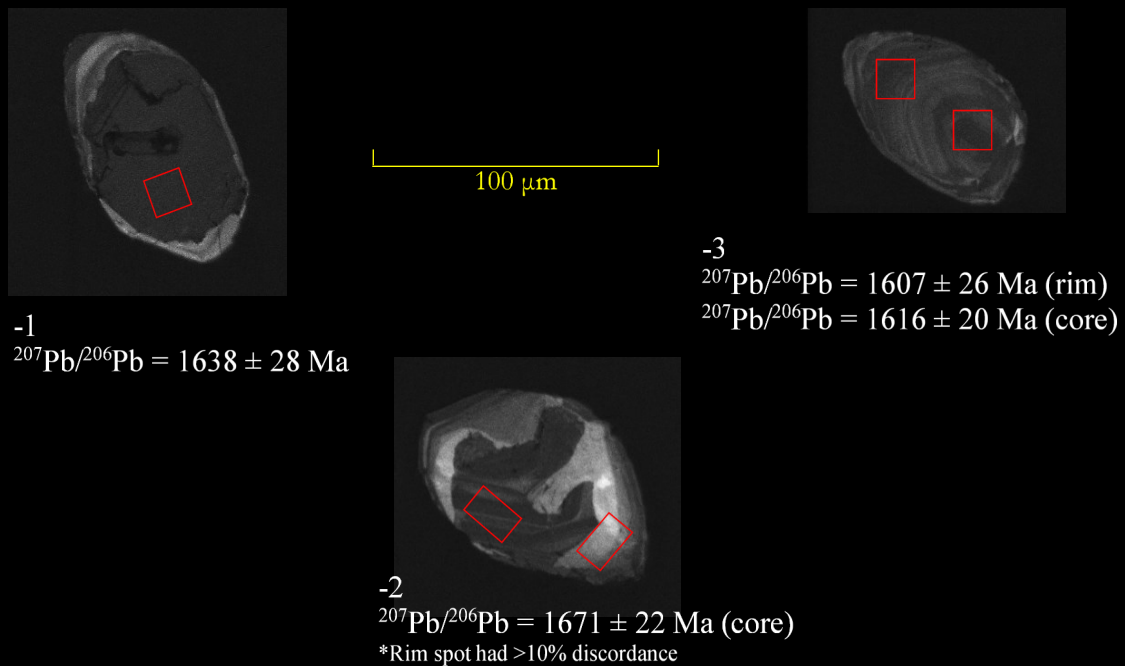


Appendix 8. Cathodoluminescence (CL) images of representative zircon grains from Sample 2.5j-iv and Sample 4f-i that are  $\leq 10\%$  discordant. Each number corresponds with the grain # in Table 2.

## Sample 4g-i



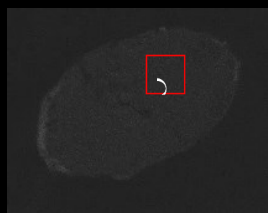
## Sample 3m-ii



Appendix 9. Cathodoluminescence (CL) images of representative zircon grains from Sample 4g-i and Sample 3m-ii that are  $\leq 10\%$  discordant. Each number corresponds with the grain # in Table 2.



### Sample 3b-i

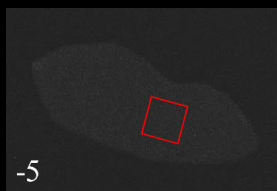


-1  
 $^{207}\text{Pb}/^{206}\text{Pb} = 1677 \pm 12 \text{ Ma}$

100  $\mu\text{m}$



-2  
 $^{207}\text{Pb}/^{206}\text{Pb} = 1693 \pm 14 \text{ Ma}$



-5  
 $^{207}\text{Pb}/^{206}\text{Pb} = 1660 \pm 10 \text{ Ma}$

### Sample 3a-v

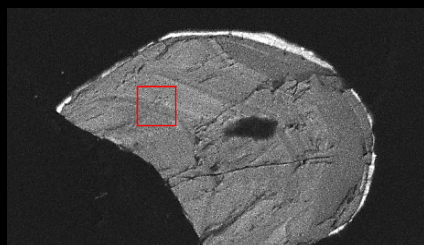
-2  
 $^{207}\text{Pb}/^{206}\text{Pb} = 1575 \pm 12 \text{ Ma}$



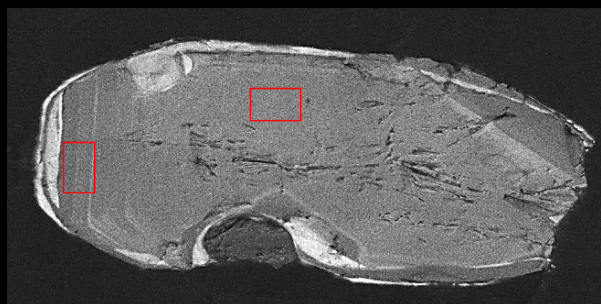
100  $\mu\text{m}$



-5  
 $^{207}\text{Pb}/^{206}\text{Pb} = 1696 \pm 12 \text{ Ma}$



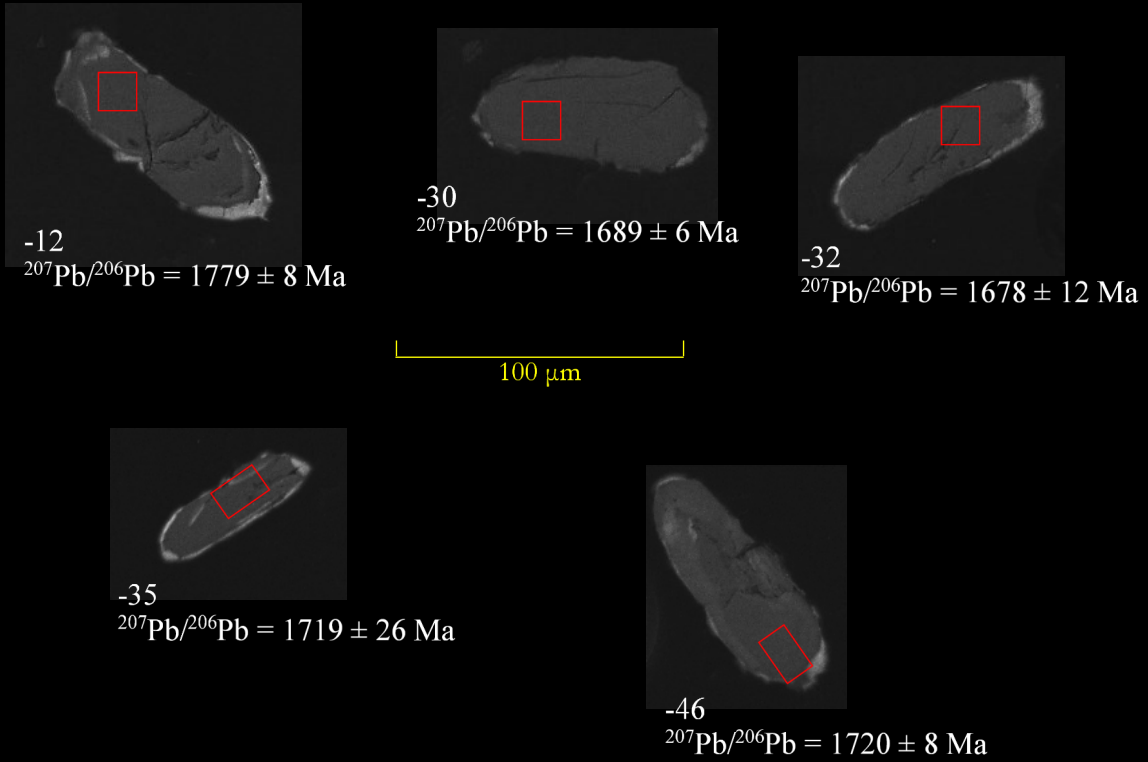
-6  
 $^{207}\text{Pb}/^{206}\text{Pb} = 1692 \pm 16 \text{ Ma}$



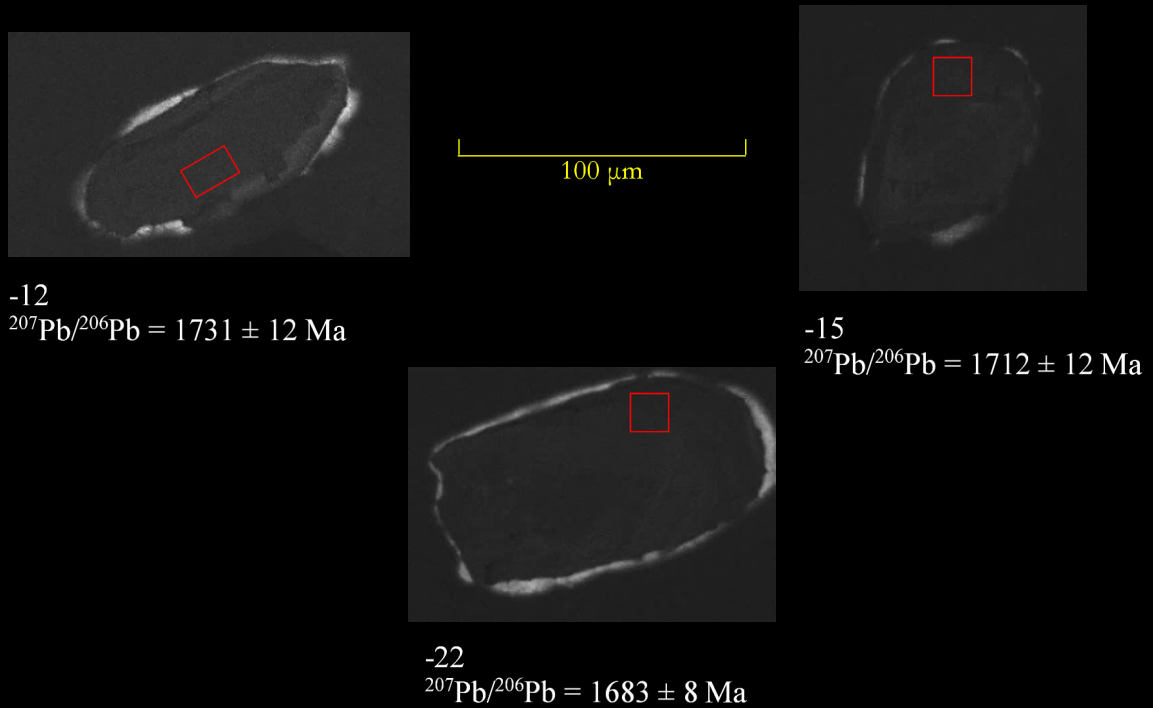
-3  
 $^{207}\text{Pb}/^{206}\text{Pb} = 1696 \pm 20 \text{ Ma}$  (core)  
 $^{207}\text{Pb}/^{206}\text{Pb} = 1688 \pm 16 \text{ Ma}$   
 (transition/rim)

Appendix 10. Cathodoluminescence (CL) images of representative zircon grains from Sample 3b-i and Sample 3a-v that are  $\leq 10\%$  discordant. Each number corresponds with the grain # in Table 2.







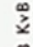


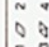


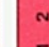
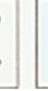




### Sample 3a-iii



### Sample 3a-i



Appendix 11. Cathodoluminescence (CL) images of representative zircon grains from Sample 3a-iii and Sample 3a-i that are  $\leq 10\%$  discordant. Each number corresponds with the grain # in Table 2.

	Häll Outcrop		Granit, fint medelkornig och något gnejsig Granite, finely medium-grained, slightly foliated
	Stenbrott, nedlagt Quarry, abandoned		Omkrystalliserat till apatit granit av ursprungligen medel- till grovkornig intrusiv bergart Recrystallization to apatite granite of primarily medium- to coarse-grained intrusive rocks
	Stänglighet med gradtal för stupning Lineation, plunge in degrees		Mikroklinozon med diameter < 2 cm Microcline augen with diameter < 2 cm
	Veckaxel med gradtal för stupning Fold axis, plunge in degrees		Mikroklinozon med diameter > 2 cm Microcline augen with diameter > 2 cm
	Skiffrighet med gradtal för stupning Foliation, dip in degrees		Stark migmatitisering Strong migmatization
	Skiffrighet med vertikal stupning Foliation, dip vertical		Ådergångsvandring Veined gneiss
	Sandstensgångar Sandstone dikes		Gnejs, rödgrå, med mikroklinozon Gneiss, reddish grey with microcline augen
	Tektonisk zon med gradtal för stupning och med observerad förkastningsriktning Tectonic zone, dip in degrees, with observed strike-slip direction		Granit och ljus granodiorit, gnejsiga, äldre Granite and light granodiorite, gneissic, older
	B = tektonisk breccia, KVB = kvartslikt breccia, M = mylonit B = tectonic breccia, KVB = breccia cemented by quartz, M = mylonite		Granodiorit och ljus tonalit, gnejsiga, äldre Granodiorite and light tonalite, gneissic, older
	Starkt skiffrad berggrund Strongly foliated rocks		Tonalit, gnejsig, äldre Tonalite, gneissic, older
	Inneslutningar av 1, ospecifierade bergarter, 2, finkornig gnejs, 3, intrusiva bergarter, 4, basiska bergarter Inclusions of 1, unspecified rocks, 2, fine-grained gneiss, 3, intrusive rocks, 4, basic rocks		Metabasit (amfibolit) som tunna skikt, skivor och linser Metabasite (amphibolite) in thin layers, sheets and lenses
	Muskovit i relativt riklig mängd Muscovite in considerable amounts		Metabasit, ultramafisk Metabasite, ultramafic
	Granit, pegmatit och apatit som gångar i granit (t.h.), i andra bergarter (t.v.) Dikes of granite, pegmatite and apatite in granite (right), in other rocks (left)		Metagabbro och metadiorit Metagabbro and metadiorite
	Pegmatit Pegmatite		Metabasit (amfibolit), fin- till medelkornig Metabasite (amphibolite), fine- to medium-grained
	Graniter, ögonförande och gnejsiga, 1, rödgrå, granatirik, äldst, 2, röd, gammastrålning > 30µR, 3, grårod, yngst Granites, porphyritic and foliated, 1, reddish-grey, garnet rich, oldest, 2, red, γ-radiation > 30µR, 3, greyish-red, youngest		Skarn, mindre förekomst Skarn, minor occurrence
	Metabasit (amfibolit), medelkornig, oftast med relict diabasstruktur Metabasite (amphibolite), medium-grained, mostly with relict diabasic texture		Gnejs, grå till rödgrå, plagioklas-kvartsbiotitrik, fin- till medelkornig Gneiss, grey to reddish-grey, plagioclase-quartz-biotite-rich, fine- to medium-grained
	Granit och ljus granodiorit, gnejsiga, yngre Granite and light granodiorite, gneissic, younger		Gnejs, röd till grårod, mikroklino-kvartsrik, fin- till medelkornig Gneiss, red to greyish-red, microcline-quartz-rich, fine- to medium-grained
	Granodiorit och ljus tonalit, gnejsiga, yngre Granodiorite and light tonalite, gneissic, younger		Tonalit, gnejsig, yngre Tonalite, gneissic, younger

Appendix 12. Detailed legend from Samuelsson's (1982) map of the region NE of Gothenburg.



**Tidigare skrifter i serien  
”Examensarbeten i Geologi vid Lunds  
universitet”:**

530. Balija, Fisnik, 2018: Stratigraphy and pyrite geochemistry of the Lower–Upper Ordovician in the Lerhamn and Fågelsång -3 drill cores, Scania, Sweden. (45 hp)
531. Höglund, Nikolas, 2018: Groundwater chemistry evaluation and a GIS-based approach for determining groundwater potential in Mörbylånga, Sweden. (45 hp)
532. Haag, Vendela, 2018: Studie av mikrostrukturer i karbonatslagkägglor från nedslagsstrukturen Charlevoix, Kanada. (15 hp)
533. Hebrard, Benoit, 2018: Antropocen – vad, när och hur? (15 hp)
534. Jancsak, Nathalie, 2018: Åtgärder mot kusterosion i Skåne, samt en fallstudie av erosionsskydden i Löderup, Ystad kommun. (15 hp)
535. Zachén, Gabriel, 2018: Mesosideriter – redogörelse av bildningsprocesser samt SEM-analys av Vaca Muertameteoriten. (15 hp)
536. Fägersten, Andreas, 2018: Lateral variability in the quantification of calcareous nannofossils in the Upper Triassic, Austria. (15 hp)
537. Hjertman, Anna, 2018: Förutsättningar för djupinfiltration av ytvatten från Ivösjön till Kristianstadbassängen. (15 hp)
538. Lagerstam, Clarence, 2018: Varför svalde svanödlor (Reptilia, Plesiosauria) stenar? (15 hp)
539. Pilser, Hannes, 2018: Mg/Ca i bottenlevande foraminiferer, särskilt med avseende på temperaturer nära 0°C. (15 hp)
540. Christiansen, Emma, 2018: Mikroplast på och i havsbotten - Utbredningen av mikroplaster i marina bottensediment och dess påverkan på marina miljöer. (15 hp)
541. Staahlnacke, Simon, 2018: En sammanställning av norra Skånes prekambriska berggrund. (15 hp)
542. Martell, Josefin, 2018: Shock metamorphic features in zircon grains from the Mien impact structure - clues to conditions during impact. (45 hp)
543. Chitindingu, Tawonga, 2018: Petrological characterization of the Cambrian sandstone reservoirs in the Baltic Basin, Sweden. (45 hp)
544. Chonewicz, Julia, 2018: Dimensionerande vattenförbrukning och alternativa vattenkvaliteter. (15 hp)
545. Adeen, Lina, 2018: Hur lämpliga är de geofysiska metoderna resistivitet och IP för kartläggning av PFOS? (15 hp)
546. Nilsson Brunlid, Anette, 2018: Impact of southern Baltic sea-level changes on landscape development in the Verkeån River valley at Haväng, southern Sweden, during the early and mid Holocene. (45 hp)
547. Perälä, Jesper, 2018: Dynamic Recrystallization in the Sveconorwegian Frontal Wedge, Småland, southern Sweden. (45 hp)
548. Artursson, Christopher, 2018: Stratigraphy, sedimentology and geophysical assessment of the early Silurian Halla and Klinteberg formations, Altajme core, Gotland, Sweden. (45 hp)
549. Kempengren, Henrik, 2018: Att välja den mest hållbara efterbehandlingsmetoden vid sanering: Applicering av beslutsstödsverktyget SAMLA. (45 hp)
550. Andreasson, Dagnija, 2018: Assessment of using liquidity index for the approximation of undrained shear strength of clay tills in Scania. (45 hp)
551. Ahrenstedt, Viktor, 2018: The Neoproterozoic Visingsö Group of southern Sweden: Lithology, sequence stratigraphy and provenance of the Middle Formation. (45 hp)
552. Berglund, Marie, 2018: Basaltkuppen - ett spel om mineralogi och petrologi. (15 hp)
553. Hernnäs, Tove, 2018: Garnet amphibolite in the internal Eastern Segment, Sveconorwegian Province: monitors of metamorphic recrystallization at high temperature and pressure during Sveconorwegian orogeny. (45 hp)
554. Halling, Jenny, 2019: Characterization of black rust in reinforced concrete structures: analyses of field samples from southern Sweden. (45 hp)
555. Stevic, Marijana, 2019: Stratigraphy and dating of a lake sediment record from Lyngsjön, eastern Scania - human impact and aeolian sand deposition during the last millennium. (45 hp)
556. Rabanser, Monika, 2019: Processes of Lateral Moraine Formation at a Debris-covered Glacier, Suldenferner (Vedretta di Solda), Italy. (45 hp)
557. Nilsson, Hanna, 2019: Records of environmental change and sedimentation processes over the last century in a Baltic coastal inlet. (45 hp)
558. Ingered, Mimmi, 2019: Zircon U-Pb constraints on the timing of Sveconorwegian migmatite formation in the Western and Median Segments of the Idefjorden terrane, SW Sweden. (45 hp)
559. Hjorth, Ingeborg, 2019: Paleomagnetisk undersökning av vulkanen Rangitoto, Nya Zeeland, för att bestämma dess ut-

- brottshistoria. (15 hp)
560. Westberg, Märta, 2019: Enigmatic worm-like fossils from the Silurian Waukesha Lagerstätte, Wisconsin, USA. (15 hp)
561. Björn, Julia, 2019: Undersökning av påverkan på hydraulisk konduktivitet i förorenat område efter in situ-saneringsförsök. (15 hp)
562. Faraj, Haider, 2019: Tolkning av georadarprofiler över grundvattenmagasinet Verveln - Gullringen i Kalmar län. (15 hp)
563. Bjermo, Tim, 2019: Eoliska avlagringar och vindriktningar under holocen i och kring Store Mosse, södra Sverige. (15 hp)
564. Langkjaer, Henrik, 2019: Analys av Östergötlands kommande grundvattenresurser ur ett klimtperspektiv - med fokus på förstärkt grundvattenbildning. (15 hp)
565. Johansson, Marcus, 2019: Hur öppet var landskapet i södra Sverige under Atlantisk tid? (15 hp)
566. Molin, Emmy, 2019: Litologi, sedimentologi och kolisotopstratigrafi över krita-paleogen-gränsvärdet i borrhölen Limhamn-2018. (15 hp)
567. Schroeder, Mimmi, 2019: The history of European hemp cultivation. (15 hp)
568. Damber, Maja, 2019: Granens invandring i sydvästra Sverige, belyst genom pollenanalys från Skottenesjön. (15 hp)
569. Lundgren Sassner, Lykke, 2019: Strandmorfologi, stranderosion och stranddeposition, med en fallstudie på Tylösandstrand, Halland. (15 hp)
570. Greiff, Johannes, 2019: Mesozoiska konglomerat och Skånes tektoniska utveckling. (15 hp)
571. Persson, Eric, 2019: An Enigmatic Cerapodian Dentary from the Cretaceous of southern Sweden. (15 hp)
572. Aldenius, Erik, 2019: Subsurface characterization of the Lund Sandstone – 3D model of the sandstone reservoir and evaluation of the geoenery storage potential, SW Skåne, South Sweden. (45 hp)
573. Juliusson, Oscar, 2019: Impacts of subglacial processes on underlying bedrock. (15 hp)
574. Sartell, Anna, 2019: Metamorphic paragenesis and P-T conditions in garnet amphibolite from the Median Segment of the Idefjorden Terrane, Lilla Edet. (15 hp)
575. Végvári, Fanni, 2019: Vulkanisk inverkan på klimatet och atmosfärcirkulationen: En litteraturstudie som jämför vulkanism på låg respektive hög latitud. (15 hp)
576. Gustafsson, Jon, 2019: Petrology of platinum-group element mineralization in the Koillismaa intrusion, Finland. (45 hp)
577. Wahlquist, Per, 2019: Undersökning av mindre förkastningar för vattenuttag i sedimentärt berg kring Kingelstad och Tjutebro. (15 hp)
578. Gaitan Valencia, Camilo Esteban, 2019: Unravelling the timing and distribution of Paleoproterozoic dyke swarms in the eastern Kaapvaal Craton, South Africa. (45 hp)
579. Eggert, David, 2019: Using Very-Low-Frequency Electromagnetics (VLF-EM) for geophysical exploration at the Albertine Graben, Uganda - A new CAD approach for 3D data blending. (45 hp)
580. Plan, Anders, 2020: Resolving temporal links between the Högberget granite and the Wigström tungsten skarn deposit in Bergslagen (Sweden) using trace elements and U-Pb LA-ICPMS on complex zircons. (45 hp)
581. Pilser, Hannes, 2020: A geophysical survey in the Chocaya Basin in the central Valley of Cochabamba, Bolivia, using ERT and TEM. (45 hp)
582. Leopardi, Dino, 2020: Temporal and genetical constraints of the Cu-Co Vena-Dampetorp deposit, Bergslagen, Sweden. (45 hp)
583. Lagerstam Lorien, Clarence, 2020: Neck mobility versus mode of locomotion – in what way did neck length affect swimming performance among Mesozoic plesiosaurs (Reptilia, Sauropterygia)? (45 hp)
584. Davies, James, 2020: Geochronology of gneisses adjacent to the Mylonite Zone in southwestern Sweden: evidence of a tectonic window? (45 hp)



# LUNDS UNIVERSITET

Geologiska institutionen  
Lunds universitet  
Sölvegatan 12, 223 62 Lund